AD-A273 723

DTIC
S ELECTE
DEC 16 1993
A

AN APPROXIMATE SOLUTION FOR THE
SPINUP DYNAMICS OF NEAR AXISYMMETRIC AXIAL
GYROSTATS USING THE METHOD OF MULTIPLE SCALES

THESIS
Stewart J Kowall
Captain, USAF

AFIT/GA/ENY/93D-5

93-30473

Approved for public release; distribution unlimited

93 12 15 083
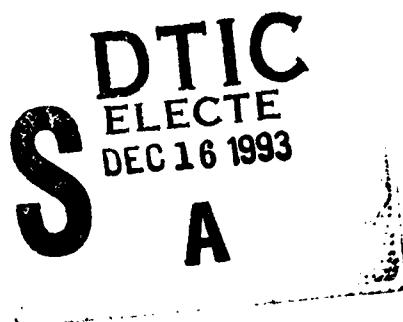
AFIT/GA/ENY/93D-5

AN APPROXIMATE SOLUTION FOR THE SPINUP DYNAMICS OF NEAR AXISYMMETRIC AXIAL GYROSTATS USING THE METHOD OF MULTIPLE SCALES

THESIS

Presented to the Faculty of the Graduate School of Engineering

of the Air Force Institute of Technology

Air University

In Partial Fulfillment of the

Requirements for the Degree of

Master of Science in Astronautical Engineering

Stewart J Kowall, B.S. Aeronautical Engineering

Captain, USAF

December, 1993

Accesion For		
NTIS CRA&I	☑	
DTIC TAB	☐	
Unannounced	☐	
Justification		
By		
Distribution /		
Availability Codes		
Dist	Avail and / or Special	
A-1		

Acknowledgements

Table of Contents

iv

List of Figures

List of Tables

AFIT/GA/ENY/93D-5

Abstract

Approximate solutions for the spinup of a near axisymmetric dual-spin gyrostat are derived using the straightforward expansion method and the method of multiple scales. Two method of multiple scale solutions are presented. The first is derived using cartesian coordinates while the second is derived using cylindrical coordinates. The multiple scales solutions are compared to numerically integrated results for oblate and prolate configurations. A comparison for flat spin recovery is also accomplished. Excellent results are obtained for oblate configurations. Trajectory separatrix crossings hindered the results for prolate configurations and flat spin recoveries.

AN APPROXIMATE SOLUTION FOR THE SPINUP DYNAMICS OF NEAR AXISYMMETRIC AXIAL GYROSTATS USING THE METHOD OF MULTIPLE SCALES

I. Introduction

In 1958, the United States of America launched Explorer I into orbit as its answer to the Soviet Unions' Sputnik. The great space race between the two nations began, and unfortunately, the United States' entry suffered a serious flaw. Explorer I was shaped like a missile and was designed to rotate about its minimum moment of inertia axis. Ninety minutes after insertion into its orbit, Explorer I was tumbling end-over-end and the engineers at the Jet Propulsion Laboratory did not know why (9:129). In the following years, U.S. engineers learned a great deal about rotational dynamics.

By 1960, engineers accepted the idea that internal energy dissipation, caused by spacecraft flexibility, violated the assumptions of the classical analyses of Euler. The result was the belief that all spin stabilized satellites must be shaped like "tuna cans" so that spin stabilization could be achieved through spin about the maximum moment of inertia axis. As satellite design progressed, the idea of an inertial platform became increasingly attractive. With such a platform, sensors could be continuously pointed at a source rather than rely on scanned coverage. The first satellite to employ such a platform was launched in 1962 and was called the Orbiting Solar Observatory, OSO-1(13:761). This satellite was still designed to spin about its maximum moment of inertia axis, but the concept of an inertial platform was flown (9:131).

As satellites progressed even further, however, they were designed to accomplish more tasks and as a result, became bigger. The constraint to such large satellites

was the size of the payload shroud used to protect them during assent to orbit. The aerodynamics of rocket design dictated a long slender shape which conflicted with the short squat shape required for spin stability. The lessons of Explorer I, however, were firmly entrenched in the minds of our satellite designers. Surprisingly, Mr. Vernon Landon, an employee at RCA, deduced the instability about the minimum moment of inertia axis due to energy dissipation as early as 1957. Further, by 1962, Mr. Landon knew that stable spin about the minimum moment of inertia axis was possible if enough angular momentum was stored in a rigid rotor aligned with the spin axis of the spacecraft (9:130). Unfortunately, his efforts went unrecognized for many years.

In 1965, Mr. Tony Iorillo of Hughes Aircraft Company, found that by putting a damper on the platform section of a dual-spin spacecraft, spin stabilization for spacecraft of any inertia distribution was possible. By using an *energy sink* analysis, it was shown that if the energy dissipation rate of the platform is much greater than the energy dissipation rate of the rotor, spin stabilization could be achieved for a spacecraft spinning about its minor moment of inertia axis (14:151-154).

The advantages of dual-spin spacecraft are many and it is used on many of todays satellites. There is an important problem in the dynamics of dual-spin spacecraft to which this thesis addresses itself. That problem is concerned with the spinup of the rotor such that spin stability can be achieved. The spinup maneuver can occur at two different instances in the spacecrafts lifespan. The first is when a satellite is initially deployed. As the satellite is inserted into its orbit, the rotor and platform are both spinning at the same rate and their relative angular velocity is zero. In order to give the platf rm an essentially inertial reference, a torque motor is incorporated to spinup the rotor and thereafter maintain the desired relative rotation rate. The initial spinup causes the angular momentum of the platform to be transferred to the rotor which, in turn, causes the platform to despin. The second instance occurs if the torque motor used to maintain a specified spin rate between the rotor and

platform fails. Internal friction will eventually reduce the relative spin rate between the rotor and platform to zero. Continued energy dissipation will cause the satellite to seek its maximum moment of inertia axis. Should failure of the torque motor be corrected, the relative spin rate between the rotor and platform and the satellite's attitude could be reestablished by spinning up the rotor.

1.1 Problem Statement

The objective of this thesis is to derive an approximate solution to the equations of motion that describe the spinup dynamics of near axisymmetric dual-spin satellites. Specifically, the method of multiple scales perturbation technique will be used to develop these approximate solutions valid for dual-spin satellites with small differences in transverse inertias being spun up with a non-zero axial torque. There are several benefits associated with the development of approximate solutions. The first is the reduction of computational time. If the attitude of a spacecraft is desired for a particular time in the future, the equations of motion must be integrated from the initial state to the time in question. If an approximate solution is available, the time need only be placed in the equation to determine the future attitude. Second, approximate solutions provide valuable insight into the dynamics of a rotating body as its trajectory passes through a separatrix. Third, with an increased level of understanding of the spinup dynamics attained, weight savings for future spacecraft may be realized since torque values for spinup motors can be more accurately predicted. Finally, development of approximate solution techniques further enhance the body of knowledge available for the design of future space systems (3:860).

1.2 Related Work

Four different groups of researchers have completed work in approximate solutions that is most closely related to the type of dual-spin satellite modelled in this thesis. Sen and Bainum (13) derived an approximate solution for the spinup of an oblate satellite. Using a perturbation technique, they developed dimensional

equations for a near axisymmetric gyrostat model of the Small Astronomy Satellite (SAS-A). Their results only included the transverse components of angular momentum. While they were able to capture the amplitude of the system, they were not able to account for the increase in frequency during the spinup maneuver.

The work of Gebman and Mingori (3) was completed in 1976 and was concerned with an approximate solution for a flat spin recovery. Their solution incorporated the use of a multiple scales method in which their initial conditions were fixed at the exact equilibrium point for flat spin recovery. Their solution proved satisfactory for this one particular case.

A method by which the spinup dynamics of a dual-spin satellite in an external torque free environment could be analyzed has recently been developed by Hall (5). By plotting the energy of the satellite versus the angular momentum of the rotor, he was able to capture the dynamics of three distinct spinup problems. The first two problems were oblate and prolate spinup which are associated with the initial satellite deployment. The terms "oblate" and "prolate" refer to the inertia distribution of the satellite. The third problem was termed transverse spinup and is associated with the satellite attitude recovery problem should the torque motor fail. This problem is commonly referred to as flat spin recovery. Hall took the four first order differential equations that describe the dynamics of a rigid dual-spin satellite and reduced them to a single first-order non-autonomous ordinary differential equation for the slow evolution of kinetic energy during spinup. This reduction was made possible by using the conservation of angular momentum and the method of averaging. Previous studies of spin-up dynamics had been restricted to particular classes of gyrostats or particular regions of phase space. Hall, however, provides a unified treatment for all gyrostats with his discovery of a symmetry relating oblate and prolate gyrostats which reduce the number of cases to be investigated. A significant difference in notation between this thesis and Hall's work is in the use of the variable "ε". Hall used "ε" to denote the non-dimensional torque applied by the platform on the rotor.

This thesis used the variable "g" to denote this value while "ε" is used as the small parameter in the perturbation methods.

Kinney (8) linearized the equations of motion for the spinup of an ideal axial gyrostat about the oblate and prolate equilibrium points. He then applied the WKB (Wentzel, Krammers, and Brillouin) approximation method for the linearized equations of motion. Because the equations of motion were linearized about the equilibrium points, his approximate solutions were forced to stay very close to these points. While obtaining good results for oblate spinup, the WKB solution failed for prolate spinup due to its inherent inability to adapt to the bifurcations associated with the prolate equilibrium point.

1.3 Outline of Thesis

The thesis begins with a review of the dynamics of a dual-spin spacecraft. Chapter 2 first develops the equations of motion for the spinup maneuver and then transforms them to a non-dimensional system of equations. The boundary conditions for the spinup maneuver are discussed and a numerical value for the end of spinup is derived. In order to provide a treatment for all types of dual-spin spacecraft, the dynamical shape of the spacecraft in terms of its non-dimensional moments of inertia is discussed. Finally, a review of the three types of spinup problems (oblate, prolate, and transverse) is presented.

Chapter 3 employs the straightforward expansion method to the equations of motion. While this method fails in general, it provides insight for the development of an approximate solution using the method of multiple scales. Results for an oblate spacecraft are presented to show the inadequacy of this expansion.

Chapter 4 employs the method of multiple scales to derive another approximate solution. Excellent results are obtained for oblate spacecraft. Results for prolate spacecraft and transverse spinup are also presented and discussed.

Chapter 5 also employs the method of multiple scales, but, applies the method to the equations of motion after they are transformed to cylindrical coordinates. Comparison between the two multiple scales approximate solutions are presented for the three spinup problems.

II. Dynamics of the Dual-Spin Spacecraft

The spacecraft to be modelled is as shown in Fig 2.1 (5:26). The model consists of a rigid body free to rotate in space. The relative motion of the platform ($\mathcal{P}$) and rotor ($\mathcal{R}$), however, is constrained to rotation about a rigid frictionless shaft aligned with a principal axis ($\hat{e}_i$). This model accommodates an asymmetric spacecraft through the assumption that the platform is asymmetric, but the rotor is axisymmetric about a principal axis which is also the relative rotation axis. This assumption leads to a constant moment of inertia tensor for the modelled spacecraft, and therefore, by definition is also known as a *gyrostat*. The vector h represents the total angular momentum of the gyrostat. Because the assumption of no external torques is made, the magnitude of the angular momentum vector must be conserved and the angular momentum vector is fixed in an inertial reference frame.

$$h^2 = h_1^2 + h_2^2 + h_3^2 = \text{constant} \tag{2.1}$$

In order to derive the equations of motion of the gyrostat, the angular velocities, torque, moments of inertia, and angular momentum of the rotor and platform must first be defined (5:28).

- $h_1 = I_1\omega_1 + I_s\omega_s$ = angular momentum of $\mathcal{P} + \mathcal{R}$ about $\hat{e}_1$

- $h_i = I_i\omega_i$ = angular momentum of $\mathcal{P} + \mathcal{R}$ about $\hat{e}_i$, i=2,3

- $h_a = I_s(\omega_s + \omega_1)$ = angular momentum of $\mathcal{R}$ about $\hat{e}_1$

- I_i = moment of inertia of $\mathcal{P} + \mathcal{R}$ about $\hat{e}_i$, i = 1,2,3

- I_s = axial moment of inertia of $\mathcal{R}$ about $\hat{e}_1$

- $I_p = I_1 - I_s$ = axial moment of inertia of $\mathcal{P}$ about $\hat{e}_1$

- ω_i = angular velocity of $\mathcal{P}$ about $\hat{e}_1$, i=1,2,3

- ω_s = angular velocity of $\mathcal{R}$ about $\hat{e}_1$ relative to $\mathcal{P}$
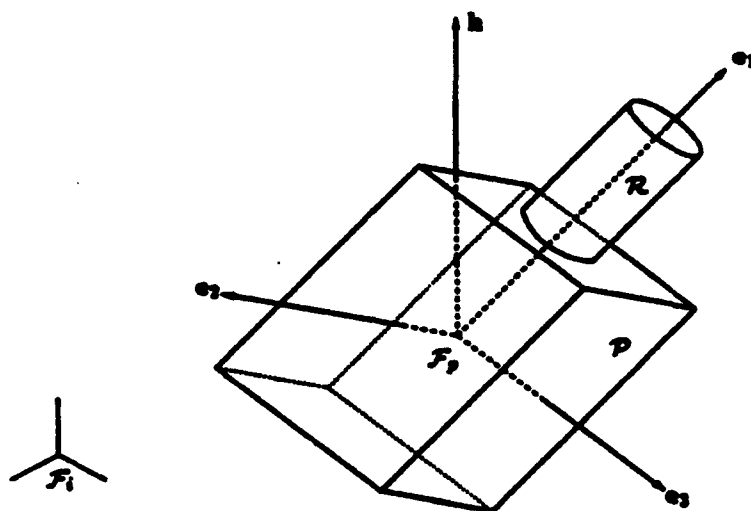
Figure 2.1. Model of axial gyrostat. The asymmetric platform is denoted as $\mathcal{P}$ while the axisymmetric rotor is denoted as $\mathcal{R}$. The body frame $\mathcal{F}_p$ is aligned with the principle axis and rotates relative to the inertial frame $\mathcal{F}_i$. The total angular momentum vector is denoted as **h** and is constant in direction and magnitude.

- g_a = torque applied by $\mathcal{P}$ on $\mathcal{R}$ about $\hat{e}_1$

- $\hat{e}_i$ = principal axes of $\mathcal{P} + \mathcal{R}$, i = 1,2,3

- $\tilde{t}$ = time

Note that the angular velocity vector is relative to an inertial reference frame and that the transverse moments of inertia of the rotor are embodied in I_2 and I_3. A motor is incorporated in the gyrostat for the spinup maneuver to provide torque to both bodies. While the transverse torques between the two bodies are present, they are not required for the equations of motion. As noted, h_a is the angular momentum of the $\mathcal{R}$ about $\hat{e}_1$. Therefore the time derivative of this angular momentum is the axial torque applied by the platform on the rotor.

$$\frac{dh_a}{d\tilde{t}} = g_a \qquad (2.2)$$

The angular momentum components of the gyrostat may now be written.

$$\mathbf{h} = \mathbf{h}_\mathcal{P} + \mathbf{h}_\mathcal{R} \qquad (2.3)$$

$$\mathbf{h} = \begin{bmatrix} h_1 \\ h_2 \\ h_3 \end{bmatrix} = \begin{bmatrix} I_1 & 0 & 0 \\ 0 & I_2 & 0 \\ 0 & 0 & I_3 \end{bmatrix} \begin{bmatrix} \omega_1 \\ \omega_2 \\ \omega_3 \end{bmatrix} + \begin{bmatrix} I_s & 0 & 0 \\ 0 & 0 & 0 \\ 0 & 0 & 0 \end{bmatrix} \begin{bmatrix} \omega_s \\ 0 \\ 0 \end{bmatrix} \qquad (2.4)$$

$$\mathbf{h} = \begin{bmatrix} I_1\omega_1 + I_s\omega_s \\ I_2\omega_2 \\ I_3\omega_3 \end{bmatrix} \qquad (2.5)$$

In order to get the time rate of change of the angular momentum of the gyrostat in an inertial frame, the derivative of the angular momentum vector is taken via the standard convention.

$$\frac{^i d}{d\tilde{t}}\mathbf{h} = \frac{^e d}{d\tilde{t}}\mathbf{h} + \vec{\omega}^{ei} \times \mathbf{h} \qquad (2.6)$$

This yields

$$\frac{^id}{dt}\mathbf{h} = \begin{bmatrix} \dot{h}_1 - \omega_3 h_2 + \omega_2 h_3 \\ \dot{h}_2 + \omega_3 h_1 - \omega_1 h_3 \\ \dot{h}_3 - \omega_2 h_1 + \omega_1 h_2 \end{bmatrix} = \begin{bmatrix} 0 \\ 0 \\ 0 \end{bmatrix} \tag{2.7}$$

The derivative of the angular momentum vector is set equal to zero since the gyrostat is modelled in an external torque free environment. From Eq. 2.5 we see $h_1 = I_1\omega_1 + I_s\omega_s$ which can be solved for ω_1 to yield

$$\omega_1 = \frac{h_1 - I_s\omega_s}{I_1} \tag{2.8}$$

By using the moment of inertia of $\mathcal{P}$ about $\hat{e}_1$ ($I_p = I_1 - I_s$) and the angular momentum of $\mathcal{R}$ about $\hat{e}_1$ ($h_a = I_s(\omega_s + \omega_1)$) Eq. 2.8 can be rearranged to yield

$$\omega_1 = \frac{h_1 - h_a}{I_p} \tag{2.9}$$

The components of $\frac{d}{dt}\mathbf{h}$ can now be written in terms of angular momentum and moments of inertia. From Eq. 2.7

$$\begin{aligned} \frac{^ed}{dt}h_1 &= \omega_3 h_2 - \omega_2 h_3 \\ &= \omega_3 I_2\omega_2 - \omega_2 I_3\omega_3 \\ &= (I_2 - I_3)\omega_2\omega_3 \end{aligned}$$

finally

$$\frac{^ed}{dt}h_1 = \frac{(I_2 - I_3)}{I_2 I_3} h_2 h_3 \tag{2.10}$$

Similarly

$$\frac{^ed}{dt}h_2 = -\omega_3 h_1 + \omega_1 h_3 \tag{2.11}$$

using Eq. 2.9

$$\frac{^ed}{dt}h_2 = -\omega_3 h_1 + \left(\frac{h_1 - h_a}{I_p}\right) h_3 \tag{2.12}$$

$$\frac{{}^e d}{dt} h_2 = \left[\frac{I_3 - I_p}{I_3 I_p} h_1 - \frac{h_a}{I_p} \right] h_3 \qquad (2.13)$$

and

$$\frac{{}^e d}{dt} h_3 = \omega_2 h_1 - \omega_1 h_2 \qquad (2.14)$$

$$\frac{{}^e d}{dt} h_3 = \left[\frac{I_p - I_2}{I_2 I_p} h_1 + \frac{h_a}{I_p} \right] h_2 \qquad (2.15)$$

Equations 2.2, 2.10, 2.13 and 2.15 represent the complete system of equations that describe the spinup dynamics of the gyrostat. The cone angle (also known as the *nutation* angle) is the angle between the angular momentum vector and the symmetry axis of the gyrostat. In terms of Euler angles it is defined as (5:28)

$$\eta = \cos^{-1} \left(\frac{\mathbf{h} \cdot \hat{e}_1}{h} \right) = \cos^{-1} \left(\frac{h_1}{h} \right) \qquad (2.16)$$

2.1 Dimensionless Equations

In order to simplify the equations of motion further, the variables are non-dimensionalized using the following transformations first developed by Guelman (4:111) and refined by Hall (5:30).

- $x_i = h_i / h$ - dimensionless component of angular momentum, $i = 1, 2, 3$

- $\mu = h_a / h$ - dimensionless angular momentum of $\mathcal{R}$ about $\hat{e}_1$

- $t = h\tilde{t} / I_p$ - dimensionless time

- $g = (g_a I_p)/h^2$ - dimensionless torque applied by the $\mathcal{P}$ to the $\mathcal{R}$ about $\hat{e}_1$

The non-dimensional equations will now be with respect to the non-dimensional time t and denoted as $(\dot{\ }) = d()/dt$. Further, the moments of inertia are non-dimensionalized using the following definition by Hall (5:30)

$$i_j = 1 - \frac{I_p}{I_j}; \; j = 1, 2, 3 \qquad (2.17)$$

Simple substitution into Eqs. 2.10 2.13 and 2.15 yields the following set of dimensionless equations on which the rest of the analysis follows

$$\dot{x}_1 = (i_2 - i_3)x_2 x_3 \tag{2.18}$$

$$\dot{x}_2 = (i_3 x_1 - \mu)x_3 \tag{2.19}$$

$$\dot{x}_3 = -(i_2 x_1 - \mu)x_2 \tag{2.20}$$

$$\dot{\mu} = g \tag{2.21}$$

Note that there has been no change in the angular momentum integral (Eq. 2.1) which now becomes

$$x_1^2 + x_2^2 + x_3^2 = 1 \tag{2.22}$$

Also note that the cone angle is reduced to

$$\eta = \cos^{-1}(x_1) \tag{2.23}$$

2.2 SpinUp Boundary Conditions

The spinup problem in this analysis usually begins with the gyrostat operating such that the relative velocity between the platform and rotor is close to zero. This would be the case in both the initial satellite deployment or a satellite that has degraded to a flat spin for an extended period of time. The spinup maneuver begins when a small constant torque g is applied to increase the angular momentum of the rotor to a value near $\mu = 1$. The value of $\mu = 1$ is apparent if you recognize that for an inertially fixed platform, ω_1 (angular velocity of $\mathcal{P}$ about $\hat{e}_1$) $= 0$. Substituting μ into Eq. 2.9 yields

$$\omega_1 = \frac{(1 - \mu)}{I_P/h} \tag{2.24}$$

If $\omega_1 = 0$ then $\mu = 1$ for the spun up condition (5:58-59).

Since $\dot{\mu} = g$ implies $\mu = gt + \mu_0$, the lower boundary for μ is not necessarily 0. Having $\mu_0 \neq 0$ implies that the rotor is spinning relative to the platform with some initial angular velocity condition. This only affects the amount of time required to complete the spinup maneuver since

$$t_{final} = \frac{\mu_{final} - \mu_0}{g} = \frac{1 - \mu_0}{g} \qquad (2.25)$$

2.3 The Dynamical Shape of the Gyrostat

(5:33-35) It can be seen from Eq. 2.17 that the three dimensionless inertia parameters retain their relative values with respect to the original moments of inertia. Mathematically,

$$I_j > I_k \iff i_j > i_k; \; j, k = 1, 2, 3 \qquad (2.26)$$

Further, the sign of i_2 and i_3 are determined by the relationship between I_p and I_2 or I_3.

$$I_p > I_k \iff i_k < 0$$
$$I_p < I_k \iff i_k > 0$$
$$k = 2, 3$$

Since only i_2 and i_3 appear in Eqs. 2.18 - 2.21, these parameters define the dynamical shape of the gyrostat. Using the standard definitions for satellite shape, the following possibilities are available.

- if $i_3 < i_2 < 0 \Rightarrow$ Oblate gyrostat

- if $i_2 > i_3 > 0 \Rightarrow$ Prolate gyrostat

- if $i_2 > 0 > i_3 \Rightarrow$ Intermediate gyrostat

The assumption is made that $i_2 > i_3$. The other non-dimensional inertia parameter simplifies to $i_1 = I_s/I_1$ which is the ratio of the axial inertia of $\mathcal{R}$ to the axial inertia
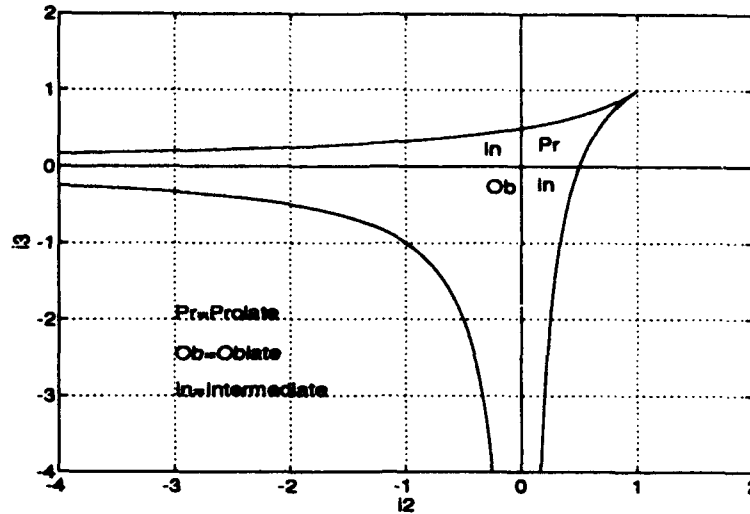
Figure 2.2. Allowable values of i_2 and i_3 for a gyrostat with a rod shaped rotor ($i_1 = 0$). Oblate gyrostats have negative values of i_2 and i_3. Prolate gyrostats have positive values of i_2 and i_3.

of $\mathcal{P} + \mathcal{R}$. This implies that $0 < i_1 < 1$ which has the limiting physical shape of a rod shaped rotor ($i_1 = 0$) to a rod shaped platform ($i_1 = 1$). The effect of i_1 on the gyrostats dynamics are described in Hall's work (5:33-35). He shows that by using the triangle inequalities for the moments of inertia, i_1 limits the physically possible values of i_2 and i_3 through the following relations.

$$
i_3 = \begin{cases}
(1 - 2i_1 + i_1 i_2)/(i_2 - i_1) & (I) \\
(2i_2 - i_1 i_2 - 1)/(i_2 - i_1) & (II) \\
(1 - i_1 i_2)/(2 - i_1 - i_2) & (III)
\end{cases}
$$

A graphical presentation is shown in Figure 2.2 for a gyrostat that has $i_1 = 0$. In accordance with the relations given above, oblate gyrostats will have negative i_2 and i_3 values while prolate gyrostats will have positive values of i_2 and i_3. Intermediate gyrostats will not be discussed in this thesis.

2-8

Hall also demonstrates that i_1 impacts the dynamics of the gyrostat through its effect on the initial conditions. Note that the definition of oblate and prolate do not involve i_1. Because spinup typically begins with the platform and rotor spinning as a single rigid body ($\omega_s = 0$), the following relations hold.

$$h_1 = I_1\omega_1 + I_s\omega_s = I_1\omega_1$$

$$h_a = I_s\omega_s + I_s\omega_1 = I_s\omega_1$$

Since

$$x_1 = \frac{h_1}{h} = \frac{I_1\omega_1}{h} \tag{2.27}$$

and

$$\mu = \frac{h_a}{h} = \frac{I_s\omega_1}{h} \tag{2.28}$$

using Eq. 2.27

$$\mu = \frac{I_s}{h}\frac{h}{I_1}x_1 = \frac{I_s}{I_1}x_1 = i_1x_1 \tag{2.29}$$

This initial spin can be about either the major or minor moment of inertia axis of the gyrostat. For example, an all spun prolate spacecraft can be represented by two possibilities (6:644).

- if $i_1 > i_2 > i_3 > 0$ then $\hat{e}_1$ is the major axis and the state is $x_1 = 1$, $x_2 = x_3 = 0$, $\mu = 1$.

- if $i_2 > i_1 > i_3 > 0$ then $\hat{e}_2$ is the major axis and the state is $x_2 = 1$, $x_1 = x_3 = \mu = 0$. This is commonly referred to as a flat spin condition.

The reader is referred to reference (5) for an in-depth discussion of the dimensionless parameters.

2.4 Spinup Problems

To describe the nature of the different spinup problems, an understanding of the system dynamics when $g = 0$ is first required. As can be seen from Eq. 2.21, setting $g = 0$ implies that the angular momentum of $\mathcal{R}$ about $\hat{e}_1$ is a constant value. Because the angular momentum first integral cannot be violated in a torque free environment, the motion of the gyrostat is confined to one dimensional curves on the momentum sphere defined by Eq. 2.22. Hall (5:Chapter 5) demonstrated that when $g = 0$, Eqs. 2.18-2.20 reduce to a single integral which is solved using Jacobi's elliptic functions. In Hall's development of the reduction of quadrature for $g = 0$, he derives an energy like constant, y, which defines lines of constant "energy" on the momentum sphere (5:39-42). The "energy" term, y, represents a functional combination of the three integrals of motion when $g = 0$. The three integrals are total angular momentum, axial angular momentum, and rotational kinetic energy.

$$y = \frac{1}{2}\left\{(i_2 + i_3)x_1^2 - (i_2 - i_3)(x_2^2 - x_3^2) - 4\mu x_1 - (i_2 + i_3)\right\} \qquad (2.30)$$

Because this constant is only valid for $\mu =$ constant, the momentum sphere has a different topology for each value of μ. Figure 2.3 depicts a progression of momentum spheres for a near axisymmetric gyrostat as μ increases. This is essentially a graphical presentation of a spinup maneuver for either an oblate or prolate gyrostat. In Section 2.3, we discussed the non-dimensional moments of inertia i_2 and i_3. If both these values are negative, the gyrostat is oblate and its energy for a particular value of μ is associated with a polhode that lies in the upper (northern) half of the momentum sphere (note: "upper" and "lower" are in reference to the spheres shown in Figure 2.3 regardless of the coordinate axis). If i_2 and i_3 are both positive, the gyrostat is prolate and its energy is associated with polhodes that lie in the lower (southern) half of the momentum sphere. Note that the number of equilibrium points on the momentum sphere vary as the values of μ change. Hall's work demonstrates that for μ less than the smaller of $|i_2|$ or $|i_3|$, there are six equilibrium points. The six

Table 2.1. Equilibrium Points

Equilibrium Pts	Validity
$(\pm 1, 0, 0)$	$\forall$ g
$\left(\dfrac{\mu}{i_3}, 0, \pm\sqrt{1 - (\mu/i_3)^2}\right)$	g=0
$\left(\dfrac{\mu}{i_2}, \pm\sqrt{1 - (\mu/i_2)^2}, 0\right)$	g=0

equilibrium points are listed in Table 2.1 and were first published in Guelman's work (4:112).

The points O_μ and P_μ in Figure 2.3 are centers for an oblate and prolate gyrostat respectively. The two points U_μ indicate the unstable equilibria for unstable flat spin motion. The two points labeled F_μ located within the unstable flat spin separatrix correspond to the centers of stable flat spin motion. As μ increases, the separatrices associated with flat spin motion migrate to the prolate equilibrium point. At μ equal to the smaller of $|i_2|$ or $|i_3|$, the two saddles of the unstable flat spin motion converge to form a single saddle at the south pole and, as a result, with the smaller of $|i_2|$ or $|i_3| < \mu <$ the larger of $|i_2|$ or $|i_3|$, there are only four equilibrium points. Finally, at μ equal to the larger of $|i_2|$ or $|i_3|$, the two stable flat spin centers converge with the saddle at the south pole to form a center. For μ greater than the larger of $|i_2|$ or $|i_3|$ only two equilibrium points remain and no further bifurcations occur. It is important not to visualize the polhodes as circular disks. The momentum sphere contains separatrices which affect all the polhodes on the sphere. A more realistic concept of what is seen as circles is a surface of a hyperboloid or a "Pringles potato chip".

Unfortunately, the spinup problem involves the case when $g \neq 0$. When $g \neq 0$, there are no polhodes defined by Eq. 2.30 since μ is no longer constant. Further, the separatrices which separate the different kinds of motion in a $g = 0$ system no longer
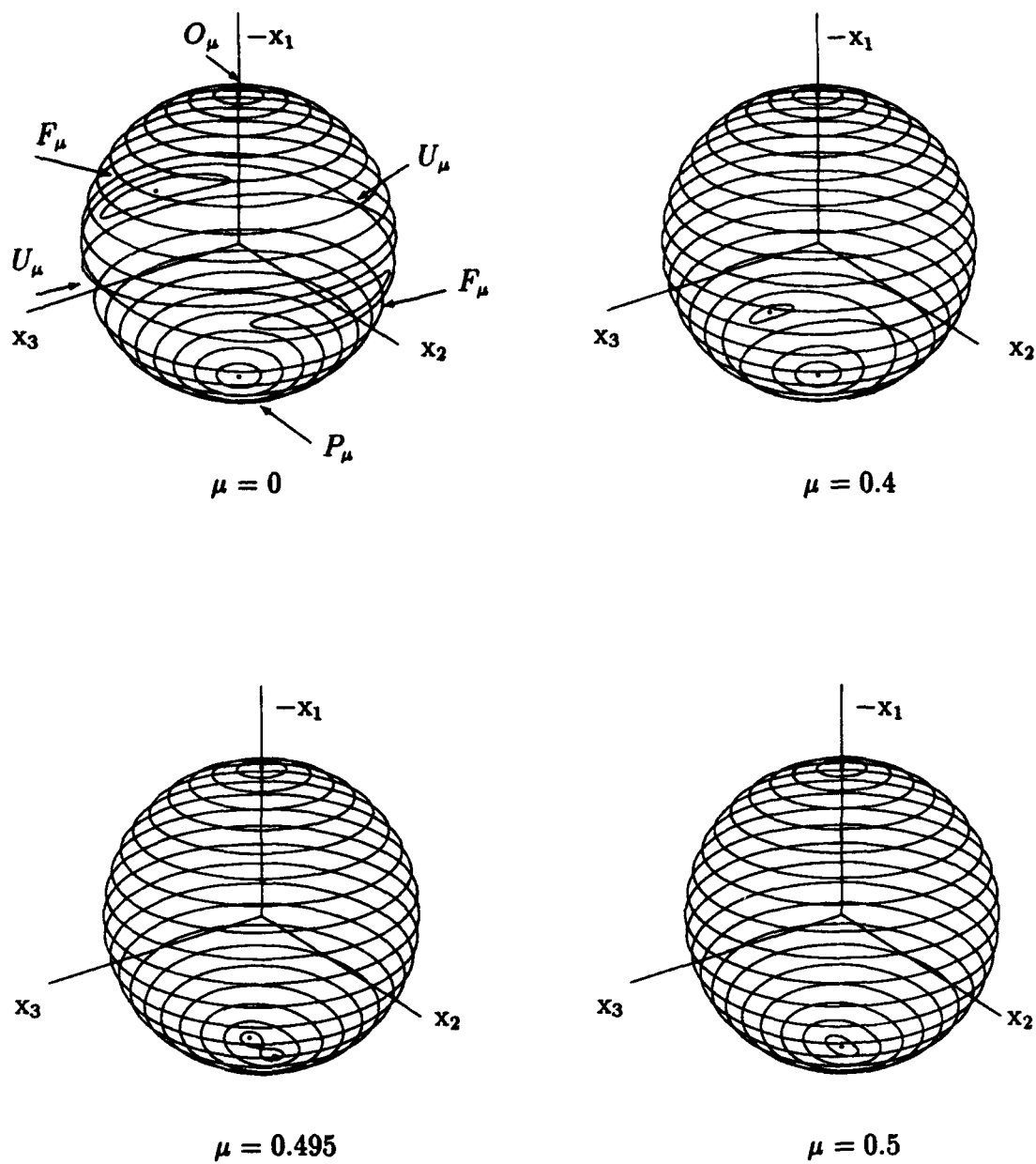
Figure 2.3. Momentum spheres for a near axisymmetric gyrostat with a one percent difference in transverse inertias and a range of μ's.

separate different regions of phase space. It is entirely possible for a trajectory to cross the "instantaneous" separatrix as μ is increasing. The term "instantaneous" is used since at each value of μ, there exists a range of energy values which can be plotted as instantaneous polhodes on the momentum sphere. One way to envision the dynamics is to think of the trajectory moving on the momentum sphere as the instantaneous separatrices migrate to P_μ. An important conceptual point is to realize that for near axisymmetric gyrostats, the trajectory will not move towards the oblate or prolate equilibrium points. In fact, without a significant asymmetry in the transverse moments of inertia, the x_1 component of angular momentum will stay at approximately the same value. This implies that the cone angle at the end of spinup is not going to vary significantly from . initial value.

As mentioned earlier, trajectories for oblate gyrostats will begin in the northern hemisphere. The instantaneous separatrices on the momentum sphere will migrate toward the south pole, so the oblate trajectory will not experience any separatrix crossings. Prolate gyrostats begin spinup in the southern hemisphere. As the spinup progresses, the trajectory is influenced by the instantaneous separatrices. Specifically, as the trajectory crosses an instantaneous separatrix, its frequency decreases until the second bifurcation occurs. At this point, the trajectory paths look similar to those present before the separatrix crossing and the frequency should increase again. Transverse spinup of a prolate gyrostat begins spinup near one of the stable flat spin equilibrium points. In order to keep the trajectory near the equilibrium point, the gyrostat must have an extremely small torque or substantial asymmetry. Since this thesis deals with near axisymmetric gyrostats, the second option is not considered. If the gyrostat has too much torque, the trajectory will cross the instantaneous separatrix. Obviously, with a higher torque, this will happen quicker.

Motion near a separatrix is highly non-linear and, therefore, difficult to approximate. As a result, we expect to experience some difficulties associated with prolate and transverse spinup. As mentioned above, the problem of defining exactly where

the instantaneous separatrix crossing occurs is extremely difficult. The reason is the constantly changing nature of the instantaneous separatrices as the spinup maneuver progresses. To define the separatrix crossing, the rate at which the instantaneous separatrices are moving on the momentum sphere along with the exact position and rate of movement of the angular momentum vector on the momentum sphere would have to be known. Given the extremely non-linear nature of the motion in this region along with an infinite number of initial conditions; the difficulty of the problem can be appreciated.

2.5 Summary

In this chapter, we have derived the non-dimensional equations of motion that describe the spinup of an axial gyrostat. The spinup boundary conditions have been specified and a discussion of the three types of spinup problems in terms of their trajectories' relationship to the nonlinear effects of separatrices has been presented. In the next chapter, the straightforward expansion method is used to outline the general flow of an approximate solution for the governing equations.

III. The Straightforward Expansion

We begin the analysis using the straightforward expansion method as a possible perturbation technique. The rationale behind using this approach is twofold. First, by employing the straightforward expansion method, a general flow of the solution using perturbation theory is presented. Second, the method is employed to determine if valid solutions can be obtained for larger torque values. A well known limitation of the straightforward expansion method is that it produces terms which are proportional to the independent variable, t. These terms, commonly referred to as *secular* terms, invalidate an approximate solution at large values of the independent variable because they grow without bound. However, for larger values of g, Eq. 2.25 shows that the amount of time required for the spinup problem is reduced.

We wish to derive an approximate solution for the spinup of a near axisymmetric gyrostat which have the following equations of motion (Eqs. 2.18-2.21).

$$
\begin{aligned}
\dot{x}_1 &= (i_2 - i_3)x_2 x_3 \\
\dot{x}_2 &= (i_3 x_1 - \mu)x_3 \\
\dot{x}_3 &= -(i_2 x_1 - \mu)x_2 \\
\dot{\mu} &= g
\end{aligned}
$$

This system is subject to the following initial conditions.

$$
\mathbf{x}(0) = \begin{bmatrix} x_1(0) \\ x_2(0) \\ x_3(0) \\ \mu(0) \end{bmatrix}
\tag{3.1}
$$

3-1

The small parameter which we use in the approximation is the difference in transverse inertias

$$i_2 - i_3 = \alpha \epsilon \qquad (3.2)$$

where α is $\mathcal{O}(1)$. We begin with the assumption that each component of angular momentum has a solution of the form

$$x_i = x_{i0} + \epsilon x_{i1} + \epsilon^2 x_{i2} + \mathcal{O}(\epsilon^3); \quad i = 1, 2, 3 \qquad (3.3)$$

Further, the time derivative of each component takes the form

$$\dot{x}_i = \dot{x}_{i0} + \epsilon \dot{x}_{i1} + \epsilon^2 \dot{x}_{i2} + \mathcal{O}(\epsilon^3); \quad i = 1, 2, 3 \qquad (3.4)$$

Note that x_i refers to the total component of angular momentum while x_{ij} refers to the terms which make up the solution for x_i. Substituting Eqs. 3.3 and 3.4 into Eqs. 2.18-2.20 and collecting terms of ϵ yields the following system of equations.

$$\mathcal{O}(1): \quad \dot{x}_{10} = 0 \qquad (3.5)$$

$$\dot{x}_{20} = -(\mu - i_3 x_{10}) x_{30} \qquad (3.6)$$

$$\dot{x}_{30} = (\mu - i_3 x_{10}) x_{20} \qquad (3.7)$$

$$\mathcal{O}(\epsilon): \quad \dot{x}_{11} = \alpha x_{20} x_{30} \qquad (3.8)$$

$$\dot{x}_{21} = -(\mu - i_3 x_{10}) x_{31} + i_3 x_{11} x_{30} \qquad (3.9)$$

$$\dot{x}_{31} = (\mu - i_3 x_{10}) x_{21} - \alpha x_{10} x_{20} - i_3 x_{11} x_{20} \qquad (3.10)$$

Notice the important contribution of selecting the difference in transverse inertias as the small parameter. Equations 2.18-2.20 are transformed from a set of non-linear differential equations to systems of linear differential equations in each power of ϵ. Solving the $\mathcal{O}(1)$ system of equations first, we immediately see that

x_{10} = constant, leaving a set of coupled linear differential equations of the form

$$\dot{\mathbf{X}} = A(t)\mathbf{X} \tag{3.11}$$

where

$$A(t) = \begin{bmatrix} 0 & -(\mu - i_3 x_{10}) \\ (\mu - i_3 x_{10}) & 0 \end{bmatrix} \tag{3.12}$$

$$\mu = gt + \mu_0 \tag{3.13}$$

This system has the solution

$$\mathbf{X} = \Phi(t, 0)\mathbf{X_0} \tag{3.14}$$

where $\mathbf{X_0}$ are the initial conditions and Φ is the state transition matrix. While coupled systems of differential equations with time varying coefficients are typically difficult to solve, this system of equations contains a simple property which permits a simple solution. We make use of the following relation (7:p. 600)

$$\text{If } A(t_1)A(t_2) = A(t_2)A(t_1); \text{ then } \Phi(t, \tau) = \exp \int_\tau^t A(\sigma)d\sigma \tag{3.15}$$

The A matrix in this system of equations satisfies the commutative property and so the integration is easily done:

$$\int_0^t (g\sigma + \mu_0 - i_3 x_{10})d\sigma = \frac{gt^2}{2} + (\mu_0 - i_3 x_{10})t \tag{3.16}$$

We now make the following definitions.

$$k = \mu_0 - i_3 x_{10} \tag{3.17}$$

$$f(t) = \frac{gt^2}{2} + kt \tag{3.18}$$

3-3

The resulting state transition matrix is

$$\Phi(t,0) = \exp \begin{bmatrix} 0 & -f(t) \\ f(t) & 0 \end{bmatrix} = \begin{bmatrix} \cos f(t) & -\sin f(t) \\ \sin f(t) & \cos f(t) \end{bmatrix} \quad (3.19)$$

Note that if we were to stop the expansion right here, we would be deriving an exact solution to the equations of motion for a completely axisymmetric gyrostat (i.e. $\varepsilon = 0$). Application of the initial conditions to the $\mathcal{O}(1)$ system solutions yields the following result.

$$x_{10} = x_1(0) \quad (3.20)$$

$$x_{20} = x_2(0)\cos f(t) - x_3(0)\sin f(t) \quad (3.21)$$

$$x_{30} = x_2(0)\sin f(t) + x_3(0)\cos f(t) \quad (3.22)$$

We now proceed to the $\mathcal{O}(\varepsilon)$ system of equations shown here again for convenience.

$$\dot{x}_{11} = \alpha\, x_{20}x_{30}$$

$$\dot{x}_{21} = -(\mu - i_3 x_{10})x_{31} + i_3 x_{11} x_{30}$$

$$\dot{x}_{31} = (\mu - i_3 x_{10})x_{21} - \alpha x_{10}x_{20} - i_3 x_{11} x_{20}$$

Starting with the x_{11} term

$$x_{11} = \int_0^t \{\alpha x_{20}x_{30}\}\, d\sigma \quad (3.23)$$

$$\int_0^t \alpha \left\{ x_2(0)x_3(0)\cos^2 f(\sigma) + (x_3^2(0) - x_2^2(0))\cos f(\sigma)\sin f(\sigma) \right.$$
$$\left. - x_2(0)x_3(0)\sin^2 f(\sigma) \right\}\, d\sigma \quad (3.24)$$

The result, using the symbolic manipulation program *Mathematica 2.0* for SPARC by Wolfram Research Inc. (15), is

$$x_{11} = S\left[\frac{\sqrt{2/\pi}(k+gt)}{\sqrt{g}}\right]b_1 + C\left[\frac{\sqrt{2/\pi}(k+gt)}{\sqrt{g}}\right]b_2$$

$$- C\left[k\frac{\sqrt{2/\pi}}{\sqrt{g}}\right]b_2 - S\left[k\frac{\sqrt{2/\pi}}{\sqrt{g}}\right]b_1 \qquad (3.25)$$

with

$$b_1 = \alpha\sqrt{\frac{\pi}{8g}}\left(x_2(0)^2\cos\frac{k^2}{g} - x_3(0)^2\cos\frac{k^2}{g} + 2x_2(0)x_3(0)\sin\frac{k^2}{g}\right)$$

$$b_2 = \alpha\sqrt{\frac{\pi}{8g}}\left(-x_2(0)^2\sin\frac{k^2}{g} + x_3(0)^2\sin\frac{k^2}{g} + 2x_2(0)x_3(0)\cos\frac{k^2}{g}\right)$$

The Fresnel Sine, denoted by "S", and Fresnel Cosine, denoted by "C", are functions that are defined as (1:300)

$$C(x) = \int_0^x \cos\left(\pi\frac{t^2}{2}\right)dt$$

$$S(x) = \int_0^x \sin\left(\pi\frac{t^2}{2}\right)dt$$

Figure 3.1 depicts both of these functions. Note that as $t \to \infty$, both functions asymptotically approach $\frac{1}{2}$. The Fresnel Sine and Fresnel Cosine can be approximated using the following functions.

$$C(x) = \frac{1}{2} + p\sin\left(\frac{\pi}{2}x^2\right) - q\cos\left(\frac{\pi}{2}x^2\right)$$

$$S(x) = \frac{1}{2} - q\sin\left(\frac{\pi}{2}x^2\right) - p\cos\left(\frac{\pi}{2}x^2\right)$$

where

$$p = \frac{1 + .926x}{2 + 1.729x + 3.104x^2} \qquad (3.26)$$
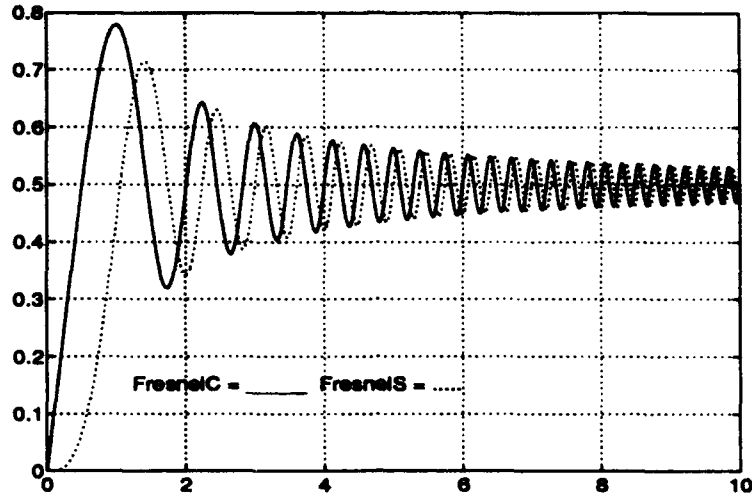
Figure 3.1. Fresnel Sine and Fresnel Cosine Functions.

$$q = \frac{1}{2 + 4.124x + 3.429x^2 + 6.670x^3} \tag{3.27}$$

These approximations are valid to 2×10^{-3} for $0 \leq x \leq \infty$ (1:302). An important consideration is the singularity at $x = -0.4932$ in Eq. 3.27. This inconvenience can be accommodated by using the following symmetry relations (1:301).

$$C(-x) = -C(x)$$
$$S(-x) = -S(x)$$

With x_{11} determined, we now proceed to the set of coupled differential equations for x_{21} and x_{31}. Eqs. 3.9 and 3.10 form a system that has the form

$$\dot{\mathbf{X}} = A(t)\mathbf{X} + B\mathbf{u}(t) \tag{3.28}$$

3-6

where A(t) is the same as Eq. 3.12, B is the identity matrix and

$$\mathbf{u}(t) = \begin{bmatrix} x_{30}i_3x_{11} \\ -\alpha x_{10}x_{20} - i_3x_{11}x_{20} \end{bmatrix} \tag{3.29}$$

This is simply the $\mathcal{O}(1)$ system of equations (cf. Eq. 3.11) with a forcing function u. This system has a solution of the form

$$\mathbf{X}(t) = \Phi(t,0)\mathbf{X}(0) + \Phi(t,0)\int_0^t \Phi^{-1}(\sigma)\mathbf{u}(\sigma)d\sigma \tag{3.30}$$

The state transition matrix Φ is defined by Eq. 3.19. The first term of the solution must be set to zero since the initial conditions were matched in the $\mathcal{O}(1)$ system of equations. The multiplication of the integrand results in

$$\Phi^{-1}\mathbf{u} = \begin{bmatrix} x_3i_3x_{11} - \frac{1}{2}\sin{(2f)}x_{10}\alpha\ x_2 + \frac{1}{2}x_3\alpha\ x_{10} - \frac{1}{2}\cos{(2f)}x_3\alpha\ x_{10} \\ -x_2i_3x_{11} + \frac{1}{2}\sin{(2f)}x_{10}\alpha\ x_3 - \frac{1}{2}x_2\alpha\ x_{10} - \frac{1}{2}\cos{(2f)}x_2\alpha\ x_{10} \end{bmatrix} \tag{3.31}$$

Recall that $f = f(t)$ which is defined by Eq. 3.18 and x_i are the initial conditions. The first and third terms in each row of the integrand will produce *secular* terms, but the second and fourth terms will not. Integrating each row of Eq. 3.31 and multiplying the resulting matrix by Φ yields the following results (secular terms are over-bracketed). The terms a_k and b_k; $k = 1,2,3,4$ are located in Appendix A. Further, the terms x_2 and x_3 are defined as $x_2(0)$ and $x_3(0)$ respectively.

$$\begin{aligned} x_{21} &= \overbrace{\frac{1}{2}\alpha\ x_{10}tx_3\cos{(f)}}^{} - \frac{1}{4g}\alpha\ i_3x_3(x_2^2 - x_3^2)\cos{(f)} \\ &+ \frac{1}{4g}\alpha\ i_3x_3(x_2^2 - x_3^2)\cos{(f)}\cos{2f} + \overbrace{\frac{1}{2}\alpha\ x_{10}tx_2\sin{(f)}}^{} \\ &- \frac{1}{4g}\alpha\ i_3x_2(x_3^2 - x_2^2)\sin{(f)} - \frac{1}{4g}\alpha\ i_3x_2(x_3^2 - x_2^2)\cos{(2f)}\sin{(f)} \\ &+ S\left[\frac{k\sqrt{2/\pi}}{\sqrt{g}}\right]\cdot a1 + C\left[\frac{k\sqrt{2/\pi}}{\sqrt{g}}\right]\cdot a2 \end{aligned}$$

$$+ \quad S\left[\frac{\sqrt{2/\pi}(k+gt)}{\sqrt{g}}\right] \cdot a3 + C\left[\frac{\sqrt{2/\pi}(k+gt)}{\sqrt{g}}\right] \cdot a4$$

$$- \quad \frac{1}{2g}\alpha \; i_3 x_2 x_3^2 \cos(f)\sin(2f) - \frac{1}{2g}\alpha \; i_3 x_2^2 x_3 \sin(f)\sin(2f) \qquad (3.32)$$

$$x_{31} \quad = \quad \overbrace{-\frac{1}{2}\alpha \; t x_{10} x_2 \cos(f)} - \frac{1}{4g}\alpha \; i_3 x_2 (x_3^2 - x_2^2)\cos(f)$$

$$+ \quad \frac{1}{4g}\alpha \; i_3 x_2 (x_3^2 - x_2^2)\cos(f)\cos(2f) + \overbrace{\frac{1}{2}\alpha \; t x_{10} x_3 \sin(f)}$$

$$- \quad \frac{1}{4g}\alpha \; i_3 x_3 (x_2^2 - x_3^2)\sin(f) + \frac{1}{4g}\alpha \; i_3 x_3 (x_2^2 - x_3^2)\cos(2f)\sin(f)$$

$$+ \quad S\left[\frac{k\sqrt{2/\pi}}{\sqrt{g}}\right] \cdot b1 + C\left[\frac{k\sqrt{2/\pi}}{\sqrt{g}}\right] \cdot b2$$

$$+ \quad S\left[\frac{\sqrt{2/\pi}(k+gt)}{\sqrt{g}}\right] \cdot b3 + C\left[\frac{\sqrt{2/\pi}(k+gt)}{\sqrt{g}}\right] \cdot b4$$

$$+ \quad \frac{1}{2g}\alpha \; i_3 x_2^2 x_3 \cos(f)\sin(2f) - \frac{1}{2g}\alpha \; i_3 x_2 x_3^2 \sin(f)\sin(2f) \qquad (3.33)$$

Notice that there are no *secular* terms in the x_{11} solution while they do appear in the x_{21} and x_{31} solutions.

3.1 Straightforward Expansion Results

Because we know that secular terms are present in the solution, we test the solution on an oblate gyrostat to avoid any problems with instantaneous separatrix crossings. Figures 3.2 through 3.5 depict the validity of this solution with the numerical integration of the equations of motion. The numerical integration is done using a 4th order Runge-Kutta subroutine in the computer program *Matlab 4.0a* by the Mathworks Inc. (10). The initial conditions will always be written at the top of the graph as the "state vector." The state vector is interpreted as $[x_1(0); x_2(0); x_3(0); \mu(0)]$. Further, the x axis is represented as μ and is essentially a

time axis from the beginning to the end of spinup. As can be seen, the solution for the x_1 component of angular momentum is very good. However, as the amount of time required for spinup increases with smaller values of g, the approximate solution begins to get out of phase with the numerical solution (see Figure 3.3). The x_2 component of angular momentum captures the increasing frequency of the spinup maneuver but, as g decreases the *secular* terms become dominant and invalidate the solution. Figure 3.6 and 3.7 depict the maximum error seen throughout spinup for different t_{final} or g values. The x_2 and x_3 components of angular momentum show a large divergence in error as the spinup times increases. As a result, this approximate solution is invalid for $g < 0.1$. The x_1 component of angular momentum displays very little error as the spinup time is increased. This is due to the fact that there are no secular terms in the x_1 solution. It is interesting to note that the x_1 approximate solution does capture the decreasing amplitude as spinup time increases. The error seen in Figure 3.6 is due to the out of phase condition that develops. However, because the scale of the x_1 component is so small, (i.e. increments as small as 0.0005), the error would still be less then one percent even if the approximate solution were completely out of phase with the numerical solution. For smaller values of g (for example $g = 0.001$), the approximate solution does get completely out of phase with the numerical solution about half way through the spinup maneuver. However, when $\mu \rightarrow 1$, the approximate solution is back in phase with the numerical solution. Further, the amplitude error is minimal throughout spinup. With such small error in the x_1 component of angular momentum, the cone angle described by Eq. 2.23 is useful at any time during the spinup maneuver. Note that the example in this analysis began spinup relatively close to the oblate equilibrium point located at the north pole of the momentum sphere. The region of validity of the x_1 approximate solution will be explored further in Chapter 4.
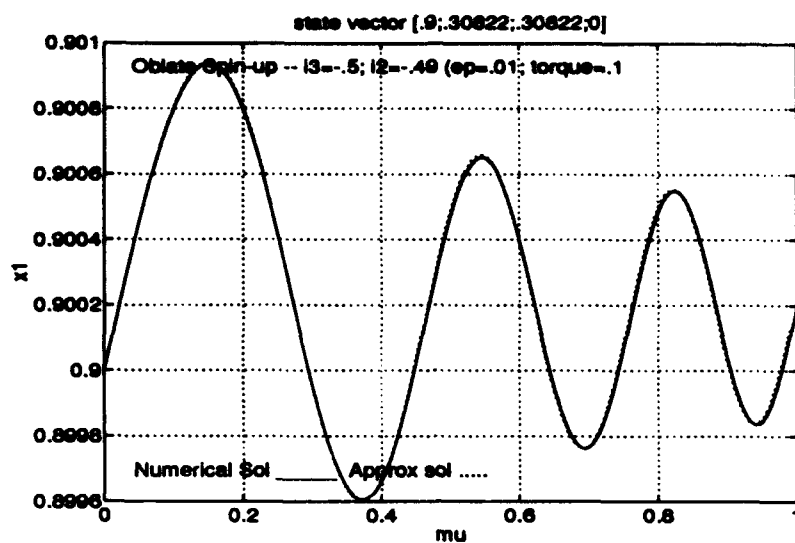
Figure 3.2.   Straightforward expansion method approximate solution of the x_1 component of angular momentum of an oblate gyrostat with initial conditions $x_1 = 0.9, x_2 = x_3 = 0.30822$ and $\varepsilon = 0.01$; $g = 0.1$.
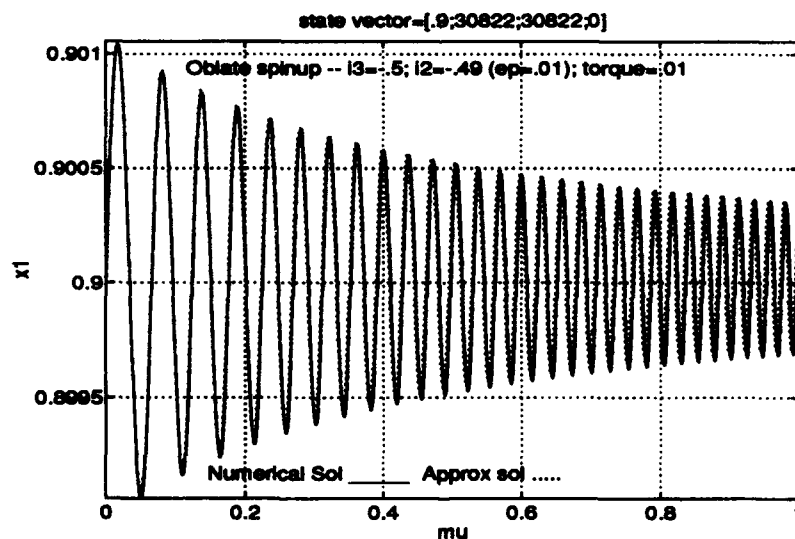
Figure 3.3.   Straightforward expansion method approximate solution of the x_1 component of angular momentum of an oblate gyrostat with initial conditions $x_1 = 0.9, x_2 = x_3 = 0.30822$ and $\varepsilon = 0.01$; $g = 0.01$.

3-10

state vector [.9;.30822;.30822;0]
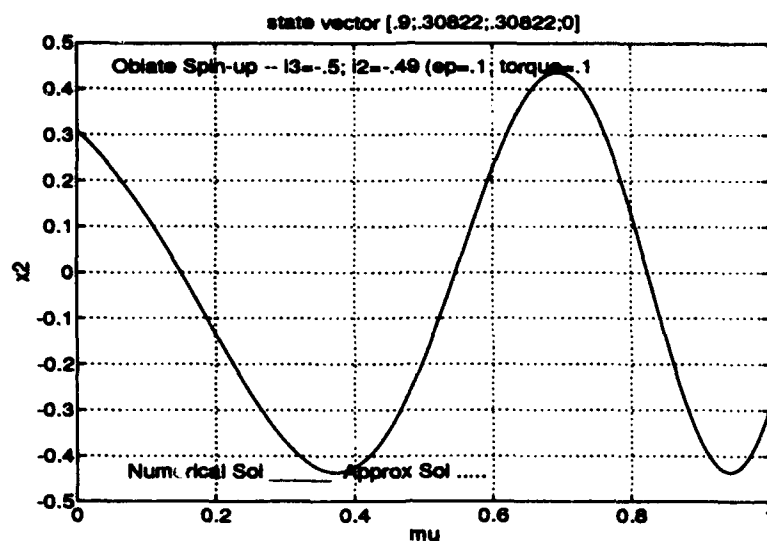
Figure 3.4. Straightforward expansion method approximate solution of the x₂ component of angular momentum of an oblate gyrostat with initial conditions $x_1 = 0.9, x_2 = x_3 = 0.30822$ and $\varepsilon = 0.01$; $g = 0.1$.

state vector=[.9;30822;30822;0]
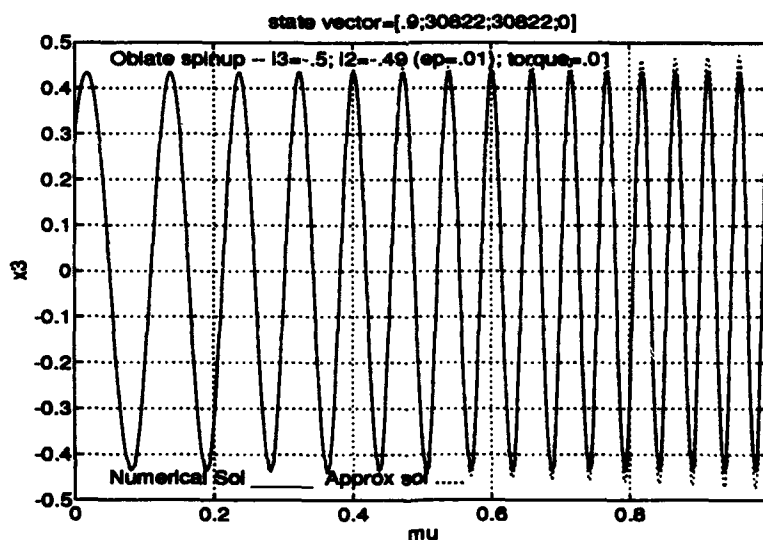
Figure 3.5. Straightforward expansion method approximate solution of the x₂ component of angular momentum of an oblate gyrostat with initial conditions $x_1 = 0.9, x_2 = x_3 = 0.30822$ and $\varepsilon = 0.01$; $g = 0.01$.

3-11
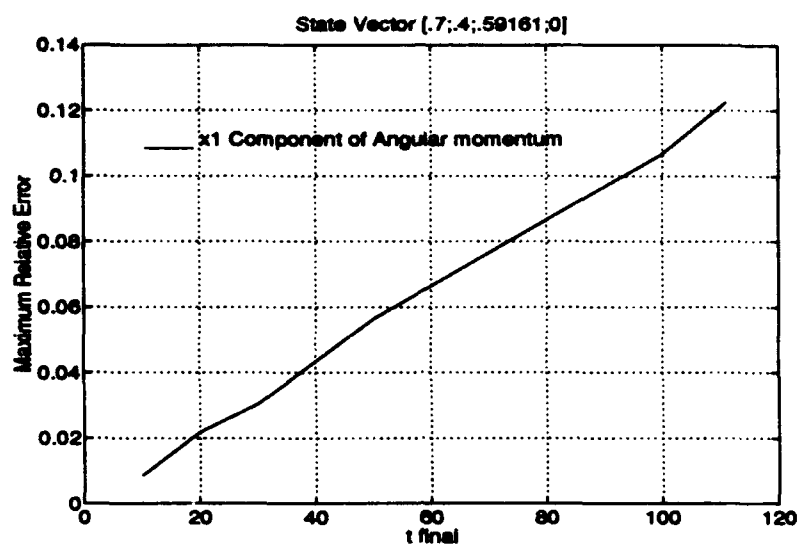
Figure 3.6. Maximum error detected in the x_1 component of angular momentum as a function of t_{final} (or g) for an oblate gyrostat using the straightforward expansion method.
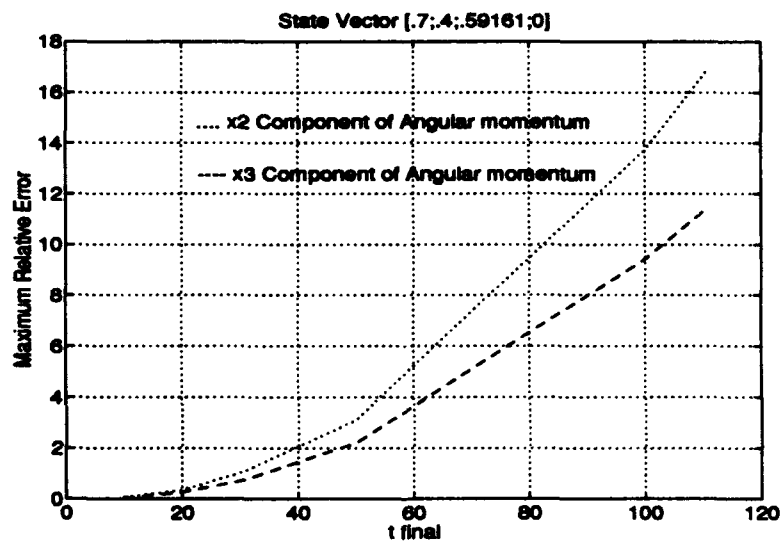
Figure 3.7. Maximum error detected in the x_2, x_3 component of angular momentum as a function of t_{final} (or g) for an oblate gyrostat using the straightforward expansion method.

3.2 Conclusions

The analysis thus far has demonstrated that the straightforward expansion method provides reasonable results for the small class of oblate gyrostats that have a near axisymmetric configuration with a very large torque value. However, the secular terms and the length of the equations in the solution both contribute to its general failure. The approach did point out the areas with which the solution needs to address itself. The equations of motion, when numerically integrated, will produce solutions which have time varying frequency and amplitude. The method of multiple scales is ideally suited to handle these problems and is the subject of the next chapter.

IV. The Method of Multiple Scales

As seen in Chapter 3 and specifically Figure 3.7, the straightforward expansion method only produces acceptable results for times (or equivalently torque values) that are very small (large) compared to $1/\varepsilon$. This is an inherent problem with series expansions or perturbation solutions of nonlinear differential equations. The problem arises due to the fact that $\mathcal{O}(\varepsilon)$ and higher terms produced by the straightforward expansion method are proportional to the independent variable, t. These terms, commonly referred to as *secular* terms, destroy the fundamental assumption of a perturbation solution. Specifically, in a series expansion, each successive power of the small parameter, ε, has decreasing importance in the series solution. By being proportional to the independent variable, these terms rapidly become large in relation to the $\mathcal{O}(1)$ term (11:24-25). This result is also known as a *nonuniform expansion*.

The Method of Multiple Scales was developed to overcome this deficiency. Eq. 3.32 contains the $\mathcal{O}(\varepsilon)$ term for the x_2 component of angular momentum in the straightforward expansion solution. The functional dependence of x_2 on t and ε can also be written as

$$x_2(t; \varepsilon) = \hat{x}_2(t, \varepsilon t, \varepsilon^2 t, \cdots; \varepsilon) \tag{4.1}$$

Or

$$x_2(t; \varepsilon) = \hat{x}_2(t_0, t_1, t_2, \cdots; \varepsilon) \tag{4.2}$$

where the t_n are defined as

$$t_0 = t, \quad t_1 = \varepsilon t, \quad t_2 = \varepsilon^2 t \tag{4.3}$$

Note that the t_n are different time scales. If $\varepsilon = \frac{1}{60}$, then variations on t_0 could be observed on the second hand of a watch. Variations on t_1 could be observed on the minute hand. Further, variations on t_2 could be observed on the hour hand and so on (12:122-123). As a result, the functional dependence of x_2 on a single independent

variable, t, changes to dependence on $t_0, t_1, t_2, \cdots$. To incorporate this dependence in the solution we use the differential operator

$$\frac{d}{dt} = \frac{\partial}{\partial t_0} + \epsilon \frac{\partial}{\partial t_1} + \epsilon^2 \frac{\partial}{\partial t_2} + \cdots \tag{4.4}$$

The assumed series solution for x_i is now

$$x_i = x_{i0}(t_0, t_1, t_2, ...) + \epsilon x_{i1}(t_0, t_1, t_2, ...) + \epsilon^2 x_{i2}(t_0, t_1, t_2, ...) + \mathcal{O}(\epsilon^3); \quad i = 1, 2, 3 \tag{4.5}$$

If these relations are substituted into a differential equation and powers of ϵ collected, they result in a series of partial differential equations as functions of the time scales t_n. Solutions to these PDE's involve the determination of functions which cause *secular* terms to vanish (2:120-123).

We begin the multiple scales solution approach with the four first order differential equations that describe the system.

$$\dot{x}_1 = (i_2 - i_3) x_2 x_3 \tag{4.6}$$

$$\dot{x}_2 = (i_3 x_1 - \mu) x_3 \tag{4.7}$$

$$\dot{x}_3 = -(i_2 x_1 - \mu) x_2 \tag{4.8}$$

$$\dot{\mu} = g \tag{4.9}$$

This system is subject to the following initial conditions

$$\mathbf{x}(0) = \begin{bmatrix} x_1(0) \\ x_2(0) \\ x_3(0) \\ \mu(0) \end{bmatrix} \tag{4.10}$$

Note that x_i refers to the total component of angular momentum while x_{ij} refers to the terms which make up the solution for x_i. The small parameter about which we

want to perturb the system is the difference in the transverse inertias

$$i_2 - i_3 = \alpha \, \epsilon \tag{4.11}$$

where α is $\mathcal{O}(1)$. We only use two time scales and seek bounded solutions of the form

$$x_i(t_0, t_1; \epsilon) = x_{i0}(t_0, t_1) + \epsilon x_{i1}(t_0, t_1) + \epsilon^2 x_{i2}(t_0, t_1) + \mathcal{O}(\epsilon^3); \quad i = 1, 2, 3 \tag{4.12}$$

The fast time "t_0" is defined as t while the slow time "t_1" is defined as ϵ t. In order to incorporate the different time scales, the following differential operator is used.

$$\frac{d}{dt} = \frac{\partial}{\partial t_0} + \epsilon \, \frac{\partial}{\partial t_1} \tag{4.13}$$

In order to insure that angular momentum is conserved, we impose the constraint

$$\|\mathbf{x}\|^2 = 1, \forall \, t \geq 0 \tag{4.14}$$

Expanding this relation using Eq. 4.12 we see

$$1 = \|\mathbf{x}(t_0, t_1; \epsilon)\|^2 = \mathbf{x} \cdot \mathbf{x} = \|\mathbf{x}_0\|^2 + 2\epsilon \mathbf{x}_0 \cdot \mathbf{x}_1 + \epsilon^2 \left[\|\mathbf{x}_1\|^2 + 2\mathbf{x}_0 \cdot \mathbf{x}_2 \right] + \cdots \tag{4.15}$$

This imposes an orthogonality condition on the $\mathcal{O}(\epsilon)$ terms. Plugging Eqs. 4.11, 4.12 and 4.13 into Eqs. 4.6 through 4.8 and collecting terms of $\mathcal{O}(\epsilon)$ yields the following systems of equations.

$$\mathcal{O}(1): \quad \frac{\partial x_{10}}{\partial t_0} = 0 \tag{4.16}$$

$$\frac{\partial x_{20}}{\partial t_0} = (i_3 x_{10} - \mu) x_{30} \tag{4.17}$$

$$\frac{\partial x_{30}}{\partial t_0} = -(i_3 x_{10} - \mu) x_{20} \tag{4.18}$$

Subject to

$$x_{i0}(0,0) = x_i(0), \ i = 1,2,3$$

$$\|\mathbf{x}_0\|^2 = 1, \forall \ t > 0$$

$$\mathcal{O}(\varepsilon): \quad \frac{\partial x_{11}}{\partial t_0} = \alpha \ x_{20}x_{30} - \frac{\partial x_{10}}{\partial t_1} \tag{4.20}$$

$$\frac{\partial x_{21}}{\partial t_0} = (i_3 x_{10} - \mu)x_{31} + i_3 x_{11}x_{30} - \frac{\partial x_{20}}{\partial t_1} \tag{4.21}$$

$$\frac{\partial x_{31}}{\partial t_0} = -(i_3 x_{10} - \mu)x_{21} - i_3 x_{11}x_{20} - \alpha \ x_{10}x_{20} - \frac{\partial x_{30}}{\partial t_1} \tag{4.22}$$

Subject to

$$x_{i1}(0,0) = 0, \ i = 1,2,3$$

$$\mathbf{x}_0 \cdot \mathbf{x}_1 = 0, \ \forall \ t > 0$$

Starting with the $\mathcal{O}(1)$ system of equations, the x_{10} term has the solution

$$x_{10}(t_0, t_1) = A_1(t_1) \tag{4.23}$$

where $A_1(t_1)$ is the "constant" of integration. The term "constant" is used to indicate that although the term has time dependance in t_1, it is constant with respect to t_0. In order to determine the dependence of t_1 on x_{10}, we must solve the next higher order of the system of equations, $\mathcal{O}(\varepsilon)$. The x_{20} and x_{30} terms are coupled partial differential equations. Note that μ is only a function of the fast time t_0. This can be seen by noting that μ reflects the energy that is being put into the system. It is the result of a simple ordinary differential equation and, as a result, has no dependence

on the slow time. Making use of Eq. 4.23, the system of equations can be written as

$$\frac{\partial x_{20}}{\partial t_0} = [i_3 A_1(t_1) - \mu(t_0)] x_{30}(t_0, t_1) \tag{4.24}$$

$$\frac{\partial x_{30}}{\partial t_0} = -[i_3 A_1(t_1) - \mu(t_0)] x_{20}(t_0, t_1) \tag{4.25}$$

This system can be represented as

$$\frac{\partial}{\partial t_0} \mathbf{X}_0 = B(t_0, t_1) \mathbf{X}_0(t_0, t_1) \tag{4.26}$$

$$\mathbf{X}_j = \begin{bmatrix} x_{2j} \\ x_{3j} \end{bmatrix} \tag{4.27}$$

and the B matrix is

$$B = \begin{bmatrix} 0 & [i_3 A(t_1) - \mu(t_0)] \\ -[i_3 A(t_1) - \mu(t_0)] & 0 \end{bmatrix} \tag{4.28}$$

This matrix is very similar to the matrix developed in Chapter 3 using the straight-forward expansion method. It still satisfies the property of commutativity and so we make use of the following relation (7:600)

$$\text{If } B(t_1)B(t_2) = B(t_2)B(t_1); \quad \text{then } \Phi(t, \tau) = \exp \int_\tau^t B(\sigma) d\sigma \tag{4.29}$$

and the system of equations has the solution

$$\mathbf{X} = \Phi(t, 0) \mathbf{X}_0(0, t_1) \tag{4.30}$$

The matrix $\Phi(t, 0)$ is termed the state transition matrix and $\mathbf{X}_0$ are the constants (with respect to t_0) of integration of the system. The integration of the B matrix is easily done

$$\int_0^{t_0} (g\sigma + \mu_0 - i_3 A(t_1)) d\sigma = \frac{g t_0^2}{2} + (\mu_0 - i_3 A(t_1)) t_0 \tag{4.31}$$

To simplify the equations we make the following definitions.

$$k = \mu_0 - i_3 A_1(t_1) \tag{4.32}$$

$$f(t_0) = \frac{g t_0^2}{2} + k t_0 \tag{4.33}$$

As a result, the state transition matrix is again

$$\Phi(t, 0) = \exp \begin{bmatrix} 0 & -f(t_0) \\ f(t_0) & 0 \end{bmatrix} = \begin{bmatrix} \cos f(t_0) & -\sin f(t_0) \\ \sin f(t_0) & \cos f(t_0) \end{bmatrix} \tag{4.34}$$

Finally, the solution to the set of coupled PDE's (Eqs. 4.17 and 4.18) is

$$x_{20}(t_0, t_1) = A_2(t_1) \cos f(t_0) - A_3(t_1) \sin f(t_0) \tag{4.35}$$

$$x_{30}(t_0, t_1) = A_2(t_1) \sin f(t_0) + A_3(t_1) \cos f(t_0) \tag{4.36}$$

We now proceed to solve the $\mathcal{O}(\varepsilon)$ system of equations to find the t_1 dependence in x_{i0}. The $\mathcal{O}(\varepsilon)$ equations are listed here again for convenience.

$$\frac{\partial x_{11}}{\partial t_0} = \alpha \, x_{20} x_{30} - \frac{\partial x_{10}}{\partial t_1} \tag{4.37}$$

$$\frac{\partial x_{21}}{\partial t_0} = (i_3 x_{10} - \mu) x_{31} + i_3 x_{11} x_{30} - \frac{\partial x_{20}}{\partial t_1} \tag{4.38}$$

$$\frac{\partial x_{31}}{\partial t_0} = -(i_3 x_{10} - \mu) x_{21} - i_3 x_{11} x_{20} - \alpha \, x_{10} x_{20} - \frac{\partial x_{30}}{\partial t_1} \tag{4.39}$$

Noting Eq. 4.23, the x_{11} term can be written

$$\frac{\partial x_{11}}{\partial t_0} = -A_1'(t_1) + \alpha \, \times$$
$$[A_2(t_1) \cos f(t_0) - A_3(t_1) \sin f(t_0)] \times$$
$$[A_2(t_1) \sin f(t_0) + A_3(t_1) \cos f(t_0)] \tag{4.40}$$

It is now implied that the constants of integration A_i, $i = 1, 2, 3$ are functions of the slow time t_1. Further, the $'$ now represents the derivative with respect to the slow time (ie $()' = \partial()/\partial t_1$). Integrating this equation yields

$$x_{11}(t_0, t_1) = \int_0^t \left\{ -A' + \alpha \ x_{20}x_{30} \right\} dt_0 = -A_1' t_0 \mid_0^t + \left(S \left[\frac{\sqrt{2/\pi}(k + gt_0)}{\sqrt{g}} \right] b_1 \right.$$

$$\left. + C \left[\frac{\sqrt{2/\pi}(k + gt_0)}{\sqrt{g}} \right] b_2 \right) \Bigg|_0^t + A_{11}(t_1)$$

$$(4.41)$$

$$b_1 = \alpha \sqrt{\frac{\pi}{8g}} \left(A_2^2 \cos \frac{k^2}{g} - A_3^2 \cos \frac{k^2}{g} + 2A_2 A_3 \sin \frac{k^2}{g} \right)$$

$$b_2 = \alpha \sqrt{\frac{\pi}{8g}} \left(-A_2^2 \sin \frac{k^2}{g} + A_3^2 \sin \frac{k^2}{g} + 2A_2 A_3 \cos \frac{k^2}{g} \right)$$

The Fresnel Sine (S) and Fresnel Cosine (C) functions are as defined in Chapter 3. As can be seen, A_1' is the only secular term in the solution. In order for x_{11} to be bounded as $t \to \infty$, we must have $A_1'(t_1) = 0$. Further, application of initial conditions for the $\mathcal{O}(1)$ system results in

$$A_1(t_1) = \text{constant} = x_1(0) \qquad (4.42)$$

We now "redefine" Eqs. 4.23 and 4.32.

$$x_{10}(t_0, t_1) = x_1(0) \qquad (4.43)$$

$$k = \mu_0 - i_3 x_{10} \qquad (4.44)$$

The dependence of the new "constant" of integration, $A_{11}(t_1)$, cannot be determined unless we go to the $\mathcal{O}(\varepsilon^2)$ system of equations. Finally,

$$
\begin{aligned}
x_{11}(t_0, t_1) \;=\; & S\left[\frac{\sqrt{2/\pi}(k + gt)}{\sqrt{g}}\right] b_1 + C\left[\frac{\sqrt{2/\pi}(k + gt)}{\sqrt{g}}\right] b_2 \\
& - C\left[k\frac{\sqrt{2/\pi}}{\sqrt{g}}\right] b_2 - S\left[k\frac{\sqrt{2/\pi}}{\sqrt{g}}\right] b_1 + A_{11}(t_1) \qquad (4.45)
\end{aligned}
$$

The dependence of x_{11} on the fast time is shown in the Fresnel Sine/Cosine terms while its slow time dependence appears in the constants of integration contained in b_1 and b_2.

We now have a set of coupled PDE's in the $\mathcal{O}(\varepsilon)$ system of equations which must be solved. The equations are repeated here

$$
\begin{aligned}
\frac{\partial x_{21}}{\partial t_0} &= (i_3 x_{10} - \mu)x_{31} + i_3 x_{11} x_{30} - \frac{\partial x_{20}}{\partial t_1} \\
\frac{\partial x_{31}}{\partial t_0} &= -(i_3 x_{10} - \mu)x_{21} - i_3 x_{11} x_{20} - \alpha\, x_{10} x_{20} - \frac{\partial x_{30}}{\partial t_1}
\end{aligned}
$$

where

$$
\begin{aligned}
\frac{\partial x_{20}}{\partial t_1} &= A_2'(t_1)\cos f(t_0) - A_3'(t_1)\sin f(t_0) \\
\frac{\partial x_{30}}{\partial t_1} &= A_2'(t_1)\sin f(t_0) + A_3'(t_1)\cos f(t_0)
\end{aligned}
$$

This system of equations can be written as

$$
\frac{\partial}{\partial t_0}\mathbf{X}_1 = B(t_0)\mathbf{X}_1(t_0, t_1) + \mathbf{u}(t_0, t_1) \qquad (4.46)
$$

$$
\mathbf{X}_j = \begin{bmatrix} x_{2j} \\ x_{3j} \end{bmatrix} \qquad (4.47)
$$

4-8

Notice that at this point, the B matrix is only a function of the fast time.

$$B(t_0) = \begin{bmatrix} 0 & [i_3 x_1(0) - \mu(t_0)] \\ -[i_3 x_1(0) - \mu(t_0)] & 0 \end{bmatrix} \tag{4.48}$$

and

$$\mathbf{u}(t_0, t_1) = \begin{bmatrix} i_3 x_{11} x_{30} - A_2' \cos{(f(t_0))} + A_3' \sin{(f(t_0))} \\ -i_3 x_{11} x_{20} - \alpha\ x_{10} x_{20} - A_2' \sin{(f(t_0))} - A_3' \cos{(f(t_0))} \end{bmatrix} \tag{4.49}$$

This system has a solution of the form

$$\mathbf{X}(t_0, t_1) = \Phi(t, 0) \mathbf{X}(0, 0) + \Phi(t, 0) \int_0^t \Phi^{-1}(\tau) \mathbf{u}(\tau) d\tau + \begin{bmatrix} A_{21}(t_1) \\ A_{31}(t_1) \end{bmatrix} \tag{4.50}$$

The initial conditions for this system will be implemented after we complete the derivation of the $\mathcal{O}(\varepsilon)$ terms. As a result, we are only interested in the particular solution. A_{21} and A_{31} are the constants of integration resulting from the integration of the system of PDE's. Because the B matrix is only dependent on t_0, the state transition matrix is exactly the same as that in the $\mathcal{O}(1)$ system of equations (Eq. 4.34). Multiplication of the inverse of the state transition matrix Φ^{-1} and the forcing function matrix $\mathbf{u}$ yields the following

$$\Phi^{-1}\mathbf{u}(t_0, t_1) = \begin{bmatrix} -A_2' + A_3 i_3 x_{11} - \frac{1}{2}\sin{(2f(t_0))}x_{10}\alpha\ A_2 + \frac{1}{2}A_3\alpha\ x_{10} - \\ \frac{1}{2}\cos{(2f(t_0))}A_3\alpha\ x_{10} \\ -A_3' - A_2 i_3 x_{11} + \frac{1}{2}\sin{(2f(t_0))}x_{10}\alpha\ A_3 - \frac{1}{2}A_2\alpha\ x_{10} - \\ \frac{1}{2}\cos{(2f(t_0))}A_2\alpha\ x_{10} \end{bmatrix} \tag{4.51}$$

In order to achieve a uniform expansion, we require that the coefficients of the secular terms must go to zero. The first, second and fourth terms in each row of the matrix, when integrated, will produce secular terms. The secular terms form the following

system of PDE's

$$-A_2' = -(\tfrac{1}{2}\alpha \; x_{10} + i_3 x_{11})A_3 \tag{4.52}$$

$$-A_3' = (\tfrac{1}{2}\alpha \; x_{10} + i_3 x_{11})A_2 \tag{4.53}$$

This system allows us to determine the dependence of A_2 and A_3 on the slow time, t_1, however, the system is extremely complex. First, x_{11} (Eq. 4.45) contains b_1 and b_2 which are functions of A_2 and A_3. This makes the system of equations nonlinear. Second, x_{11} also contains the $A_{11}(t_1)$ term which is unknown at this time and can only be determined by solving the $\mathcal{O}(\varepsilon^2)$ system of equations. While the prospect of deriving an approximate solution at this point appears grim, reasonable results can still be obtained. Note that the system of equations for A_2 and A_3 could easily be solved if the x_{11} term were a constant. In order to make this approximation, we must ignore all time dependence in x_{11} so that it can be decoupled from the x_{21} and x_{31} system of equations. This approximation requires that the variables A_2 and A_3 given in b_1 and b_2 be given the values of the initial conditions $x_2(0)$ and $x_3(0)$ respectively. Further, since the time dependence in x_{11} is ignored, the A_{11} term is also dropped. Figure 4.1 depicts x_{11} as a function of time for an oblate gyrostat with a 1 percent difference in transverse inertias and an initial state $[0.7, 0.4, 0.59161, 0]$. The two curves represent the gyrostat with two different non-dimensional torque values of 0.01 and 0.1. As can be seen, the x_{11} function oscillates and asymptotically approaches a constant value as $t \to \infty$. By making use of the fact that both the Fresnel Sine and Fresnel Cosine approach $\tfrac{1}{2}$ as $t \to \infty$, this value can be determined as

$$x_{11approx} = \frac{1}{2}(c_1 + c_2) - S\left[k\frac{\sqrt{2/\pi}}{\sqrt{g}}\right]c_1 - C\left[k\frac{\sqrt{2/\pi}}{\sqrt{g}}\right]c_2 \tag{4.54}$$

where now

$$c_1 = b_1(0) = \alpha\sqrt{\frac{\pi}{8g}}\left(x_2(0)^2\cos\frac{k^2}{g} - x_3(0)^2\cos\frac{k^2}{g} + 2x_2(0)x_3(0)\sin\frac{k^2}{g}\right)$$

State Vector [.7;.4;.59161;0]
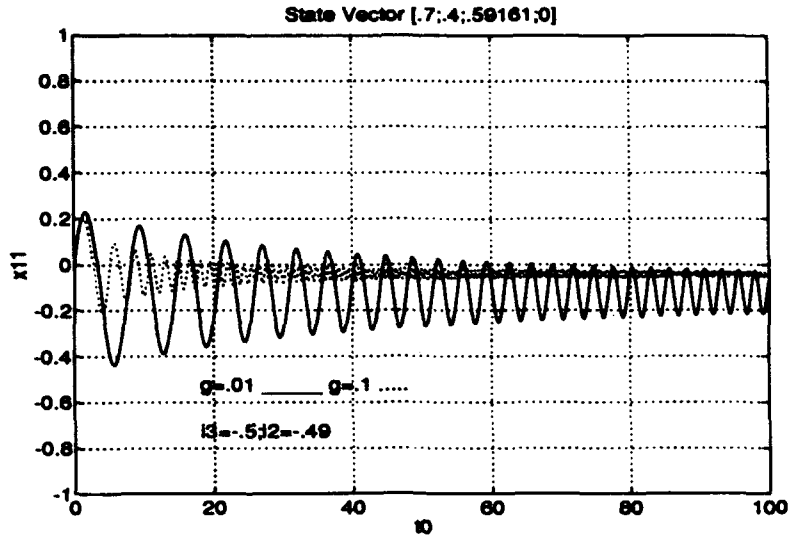
Figure 4.1. x_{11} Variation for an oblate gyrostat with initial conditions $x_1 = 0.7, x_2 = 0.4$, $x_3 = 0.59161$ and $\varepsilon = 0.01$; $g = 0.01$.

$$c_2 \;=\; b_2(0) = \alpha\sqrt{\frac{\pi}{8g}}\left(-x_2(0)^2 \sin\frac{k^2}{g} + x_3(0)^2 \sin\frac{k^2}{g} + 2x_2(0)x_3(0)\cos\frac{k^2}{g}\right)$$

Using this approximation for x_{11} produces some excellent results. Returning to the coupled set of PDE's given by Eqs. 4.52 and 4.53, we have now reduced them to a constant coefficient coupled set of PDE's based on the approximation of no slow time dependence in x_1. This system of equations now yields the following result.

$$A_2(t_1) \;=\; \;\;A_2 \cos\left(Lt_1\right) + A_3 \sin\left(Lt_1\right) \tag{4.55}$$

$$A_3(t_1) \;=\; \;-A_2 \sin\left(Lt_1\right) + A_3 \cos\left(Lt_1\right) \tag{4.56}$$

where

$$L = \left(\frac{1}{2}\alpha\; x_{10} + i_3 x_{11approx}\right) \tag{4.57}$$

4-11

These solutions for A_2 and A_3 as functions of t_1 must now be applied to the $\mathcal{O}(1)$ system of equations. Therefore Eqs. 4.35 and 4.36 now become

$$
\begin{aligned}
x_{20}(t_0) &= [A_2 \cos\left(L\epsilon\ t_0\right) + A_3 \sin\left(L\epsilon\ t_0\right)] \cos f(t_0) \\
&\quad - [-A_2 \sin\left(L\epsilon\ t_0\right) + A_3 \cos\left(L\epsilon\ t_0\right)] \sin f(t_0) \\
x_{30}(t_0) &= [A_2 \cos\left(L\epsilon\ t_0\right) + A_3 \sin\left(L\epsilon\ t_0\right)] \sin f(t_0) \\
&\quad + [-A_2 \sin\left(L\epsilon\ t_0\right) + A_3 \cos\left(L\epsilon\ t_0\right)] \cos f(t_0)
\end{aligned}
$$

Further, with these solutions in hand, the secular terms of the $\Phi^{-1}\mathbf{u}(t_0, t_1)$ matrix (Eq. 4.51) may now be ignored. The integration from 0 to t followed by the multiplication of the state transition matrix results in

$$
\begin{aligned}
x_{21} = \frac{1}{\sqrt{g}}\alpha\ \sqrt{\frac{\pi}{8}}x_{10} \Bigg\{ &A_3 \cos\left(\frac{k^2}{g} + kt + \frac{gt^2}{2}\right) C\left[k\frac{\sqrt{2/\pi}}{\sqrt{g}}\right] \\
&- A_3 \cos\left(\frac{k^2}{g} + kt + \frac{gt^2}{2}\right) C\left[\frac{\sqrt{2/\pi}(k+gt)}{\sqrt{g}}\right] \\
&+ A_2 \cos\left(\frac{k^2}{g} + kt + \frac{gt^2}{2}\right) S\left[k\frac{\sqrt{2/\pi}}{\sqrt{g}}\right] \\
&- A_2 \cos\left(\frac{k^2}{g} + kt + \frac{gt^2}{2}\right) S\left[\frac{\sqrt{2/\pi}(k+gt)}{\sqrt{g}}\right] \\
&- A_2 C\left[k\frac{\sqrt{2/\pi}}{\sqrt{g}}\right] \sin\left(\frac{k^2}{g} + kt + \frac{gt^2}{2}\right) \\
&+ A_2 C\left[\frac{\sqrt{2/\pi}(k+gt)}{\sqrt{g}}\right] \sin\left(\frac{k^2}{g} + kt + \frac{gt^2}{2}\right) \\
&+ A_3 S\left[k\frac{\sqrt{2/\pi}}{\sqrt{g}}\right] \sin\left(\frac{k^2}{g} + kt + \frac{gt^2}{2}\right) \\
&- A_3 S\left[\frac{\sqrt{2/\pi}(k+gt)}{\sqrt{g}}\right] \sin\left(\frac{k^2}{g} + kt + \frac{gt^2}{2}\right) \Bigg\} + A_{21}(t_1)
\end{aligned} \tag{4.58}
$$

and

$$
\begin{aligned}
x_{31} = \ &\frac{1}{\sqrt{g}}\alpha\sqrt{\frac{\pi}{8}}x_{10}\left\{A_2\cos\left(\frac{k^2}{g}+kt+\frac{gt^2}{2}\right)C\left[\frac{k\sqrt{2/\pi}}{\sqrt{g}}\right]\right.\\
&- A_2\cos\left(\frac{k^2}{g}+kt+\frac{gt^2}{2}\right)C\left[\frac{\sqrt{2/\pi}(k+gt)}{\sqrt{g}}\right]\\
&- A_3\cos\left(\frac{k^2}{g}+kt+\frac{gt^2}{2}\right)S\left[\frac{k\sqrt{2/\pi}}{\sqrt{g}}\right]\\
&+ A_3\cos\left(\frac{k^2}{g}+kt+\frac{gt^2}{2}\right)S\left[\frac{\sqrt{2/\pi}(k+gt)}{\sqrt{g}}\right]\\
&+ A_3C\left[\frac{k\sqrt{2/\pi}}{\sqrt{g}}\right]\sin\left(\frac{k^2}{g}+kt+\frac{gt^2}{2}\right)\\
&- A_3C\left[\frac{\sqrt{2/\pi}(k+gt)}{\sqrt{g}}\right]\sin\left(\frac{k^2}{g}+kt+\frac{gt^2}{2}\right)\\
&+ A_2S\left[\frac{k\sqrt{2/\pi}}{\sqrt{g}}\right]\sin\left(\frac{k^2}{g}+kt+\frac{gt^2}{2}\right)\\
&\left.- A_2S\left[\frac{\sqrt{2/\pi}(k+gt)}{\sqrt{g}}\right]\sin\left(\frac{k^2}{g}+kt+\frac{gt^2}{2}\right)\right\} + A_{31}(t_1)
\end{aligned}
\tag{4.59}
$$

The total solution can now be formed.

$$
x_1 = x_{10} + \epsilon\, x_{11} + \mathcal{O}(\epsilon^2)
\tag{4.60}
$$

In expanded form this is

$$
\begin{aligned}
x_1 = \ &x_1(0) + \epsilon\left\{S\left[\frac{\sqrt{2/\pi}(k+gt)}{\sqrt{g}}\right]c_1 + C\left[\frac{\sqrt{2/\pi}(k+gt)}{\sqrt{g}}\right]c_2\right.\\
&\left.- C\left[\frac{\sqrt{2/\pi}}{\sqrt{g}}\right]c_2 - S\left[\frac{\sqrt{2/\pi}}{\sqrt{g}}\right]c_1\right\} + \mathcal{O}(\epsilon^2)
\end{aligned}
\tag{4.61}
$$

The x_2 approximate solution is as follows.

$$x_2 = x_{20} + \varepsilon\, x_{21} + \mathcal{O}(\varepsilon^2) \tag{4.62}$$

In a slightly expanded form this is

$$
\begin{aligned}
x_2 &= \left[A_2 \cos\left(\left(\tfrac{1}{2}\alpha\, x_1 + i_3 x_{11approx}\right)\varepsilon\, t \right) + A_3 \sin\left(\tfrac{1}{2}\alpha\, x_1 + i_3 x_{11approx}\right)\varepsilon\, t \right) \right] \times \\
&\quad \cos\left(\frac{gt^2}{2} + kt \right) \\
&\quad + \left[A_2 \sin\left(\left(\tfrac{1}{2}\alpha\, x_1 + i_3 x_{11approx}\right)\varepsilon\, t \right) - A_3 \sin\left(\left(\tfrac{1}{2}\alpha\, x_1 + i_3 x_{11approx}\right)\varepsilon\, t \right) \right] \times \\
&\quad \sin\left(\frac{gt^2}{2} + kt \right) + \varepsilon\, x_{21} + \mathcal{O}(\varepsilon^2) \tag{4.63}
\end{aligned}
$$

The x_3 approximate solution is as follows.

$$x_3 = x_{30} + \varepsilon\, x_{31} + \mathcal{O}(\varepsilon^2) \tag{4.64}$$

$$
\begin{aligned}
x_3 &= \left[A_2 \cos\left(\left(\tfrac{1}{2}\alpha\, x_1 + i_3 x_{11approx}\right)\varepsilon\, t \right) + A_3 \sin\left(\tfrac{1}{2}\alpha\, x_1 + i_3 x_{11approx}\right)\varepsilon\, t \right) \right] \times \\
&\quad \sin\left(\frac{gt^2}{2} + kt \right) \\
&\quad + \left[-A_2 \sin\left(\left(\tfrac{1}{2}\alpha\, x_1 + i_3 x_{11approx}\right)\varepsilon\, t \right) + A_3 \sin\left(\left(\tfrac{1}{2}\alpha\, x_1 + i_3 x_{11approx}\right)\varepsilon\, t \right) \right] \times \\
&\quad \cos\left(\frac{gt^2}{2} + kt \right) + \varepsilon\, x_{31} + \mathcal{O}(\varepsilon^2) \tag{4.65}
\end{aligned}
$$

The solutions used for x_{21} and x_{31} are not exact in that we have not solved for $A_{21}(t_1)$ and $A_{31}(t_1)$. This would involve solving the $\mathcal{O}(\varepsilon^2)$ system of equations which requires solving the following integrals analytically or approximately.

$$\int_0^t S(\sigma) \cos \sigma\, d\sigma$$

$$\int_0^t C(\sigma) \sin \sigma\, d\sigma$$

Being unable to accomplish this, we assume this error to be small and proceed.

To determine A_2 and A_3, we apply the initial conditions to x_2 and x_3.

$$x_2(0,0) = x_2(0) = A_2 \tag{4.66}$$

$$x_3(0,0) = x_3(0) = A_3 \tag{4.67}$$

Earlier we noted that for the $\mathcal{O}(1)$ system, the norm of the components of angular momentum must equal one to satisfy the conservation of angular momentum. The equations developed for x_{10}, x_{20}, and x_{30} do satisfy this condition. Since we have found x_{10} to be a constant, however, we note that the sum of squares of the transverse angular momentum components must also be constant for $t > 0$. This is essentially the same result that was found by Sen and Bainum (13). There have been no limitations on geometry to this point and so this result is valid for near axisymmetric oblate or prolate configurations.

4.1 Method of Multiple Scales Results

We will investigate the validity of this approximate solution for the three types of spinup problems described in Chapter 2. Recalling the discussion in section 2.4, we note that there should not be any complications associated with instantaneous separatrix crossings for an oblate gyrostat. As seen in Figure 2.3, the instantaneous separatrices associated with unstable equilibria migrate to the south pole of the momentum sphere as μ increases. An oblate trajectory, however, would begin and stay in the northern hemisphere throughout spinup.

Dual-spin gyrostat dynamics become interesting when the initial condition starts in the southern hemisphere of the momentum sphere. A perfectly modelled system would be able to accommodate the non-linearity associated with migration of the instantaneous separatrices in the southern hemisphere. Recall, however, that by choosing the difference in transverse inertias to be the small parameter, the system

of equations that describe the spinup are transformed from a non-linear system to a sequence of linear systems. As a result, the approximate solution does not contain any of the separatrices associated with the non-linear system. Since both prolate spinup and transverse spinup have trajectories that interact with and are influenced by instantaneous separatrices, we expect to see some degradation in the approximate solution for these spinup problems.

4.1.1 Oblate Gyrostats. Figures 4.2 through 4.7 compare the approximate solution versus the solution obtained by a 4th order Runge-Kutta numerical integration scheme. The gyrostat modelled is oblate with a 1 percent difference in transverse inertias and an initial state $[0.7; 0.4; 0.59161; 0]$. The non-dimensional torque value is $g = 0.01$. Again, μ is the time scale for the beginning of spinup to the end of spinup. Because the scale of the plots is large, the relative error between each graph is also presented. The relative error is given by the following equation.

$$\text{Percent Relative Error} = \frac{|x_{i,\text{numerical}} - x_{i,\text{approximate}}| \times 100}{x_i(0)}; i = 1, 2, 3 \quad (4.68)$$

The assumption of no slow time dependence in the x_1 component of angular momentum allowed the derivation of an analytic solution for the terms of the approximate solution. Thus, the result for the x_1 component is identical to that developed in the straightforward expansion method. Recalling the results from Chapter 3, even though this solution does go in and out of phase with the numerical solution, the error is less than one percent due to the small magnitude of the phase error compared to the initial value in the x_1 component. Further, we can now see that the phase error is caused by ignoring the slow time dependence in this component of angular momentum. Figures 4.4 through 4.7 depict the x_2 and x_3 components of angular momentum. Qualitative results are excellent. Although there are two curves in Figures 4.4 and 4.6, only one is visible. Notice, however, the large error at $\mu \simeq 0.05$ in
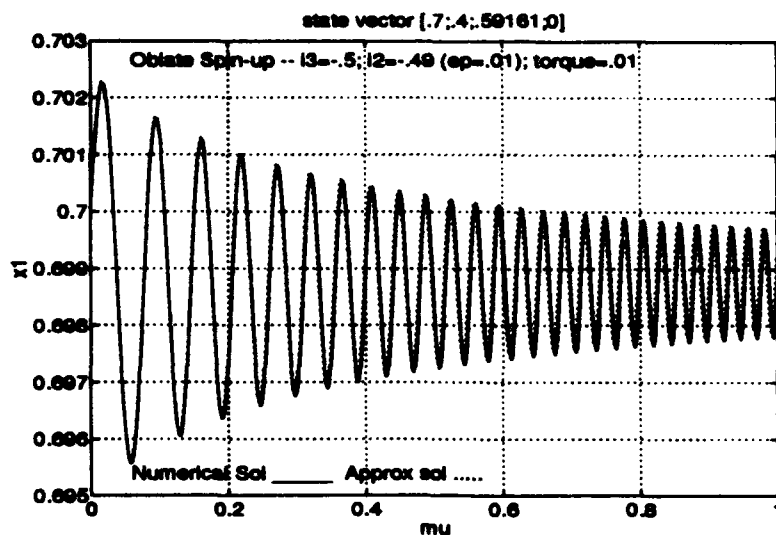
Figure 4.2. Numerical vs approximate solution of the x_1 component of angular momentum of an oblate gyrostat with initial conditions $x_1 = 0.7$, $x_2 = 0.4$, $x_3 = 0.59161$ and $\varepsilon = g = 0.01$.
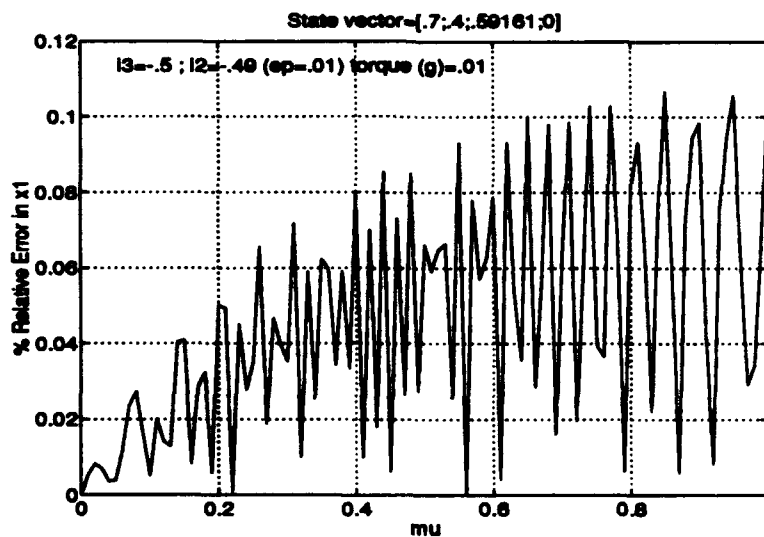
Figure 4.3. Percent relative error of the x_1 component of angular momentum of an oblate gyrostat with initial conditions $x_1 = 0.7$, $x_2 = 0.4$, $x_3 = 0.59161$ and $\varepsilon = g = 0.01$.

4-17
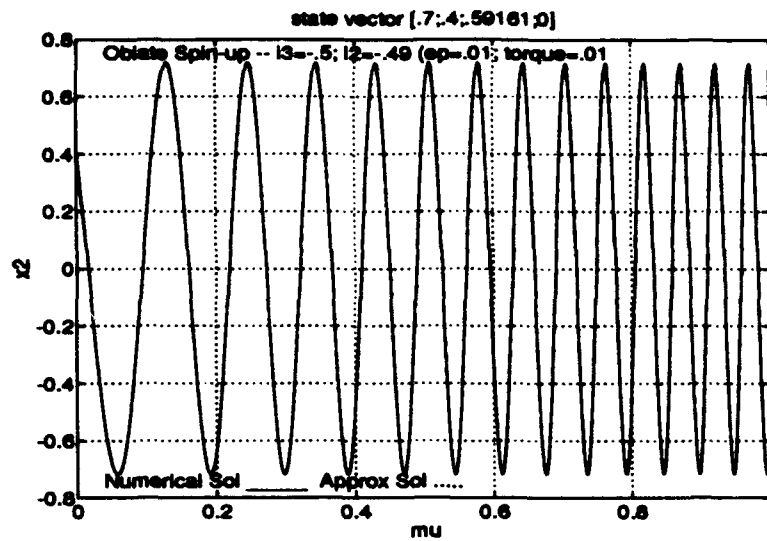
Figure 4.4. Numerical vs approximate solution of the x_2 component of angular momentum of an oblate gyrostat with initial conditions $x_1 = 0.7$, $x_2 = 0.4$, $x_3 = 0.59161$ and $\epsilon = g = 0.01$.
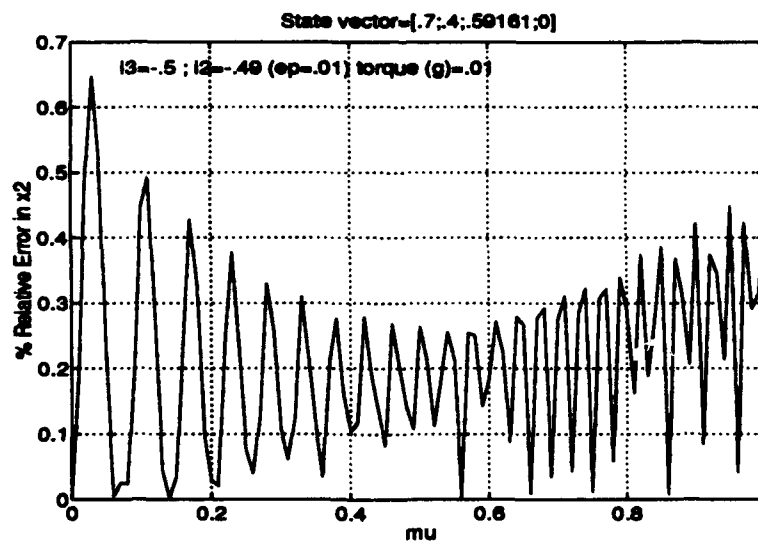
Figure 4.5. Percent relative error of the x_2 component of angular momentum of an oblate gyrostat with initial conditions $x_1 = 0.7$, $x_2 = 0.4$, $x_3 = 0.59161$ and $\epsilon = g = 0.01$.

4-18
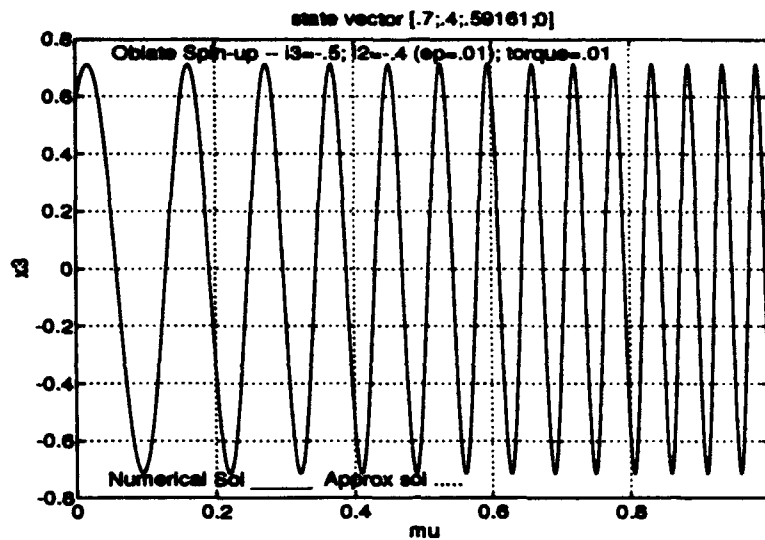
Figure 4.6. Numerical vs approximate solution of the x_3 component of angular momentum of an oblate gyrostat with initial conditions $x_1 = 0.7$, $x_2 = 0.4$, $x_3 = 0.59161$ and $\varepsilon = g = 0.01$.
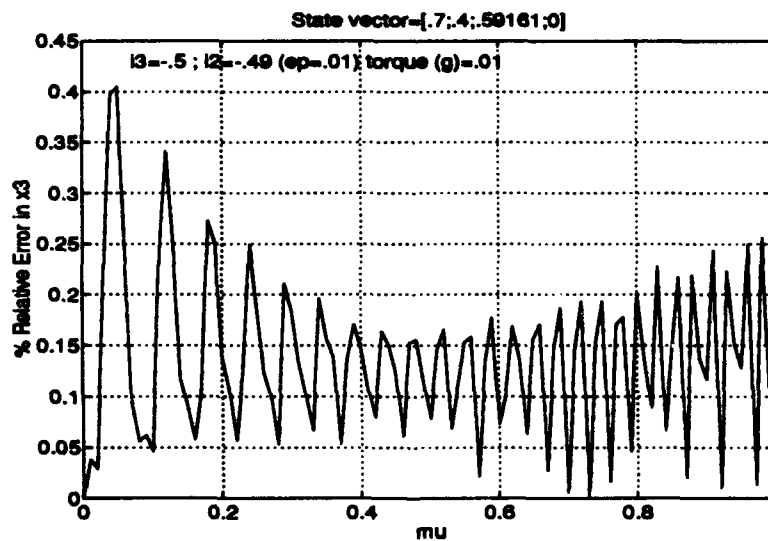
Figure 4.7. Percent relative error of the x_3 component of angular momentum of an oblate gyrostat with initial conditions $x_1 = 0.7$, $x_2 = 0.4$, $x_3 = 0.59161$ and $\varepsilon = g = 0.01$.

4-19

Figures 4.5 and 4.7 during the early portion of the spinup. This "spike" is caused by the assumption of a constant value for the x_{11} function in the approximate solution. Further, the error induced by the assumption manifests itself as phase error. To show this, observe Figure 4.8 which depicts the amplitude error associated with the spinup of this gyrostat. We see that the amplitude error is very small in the early portion of the spinup maneuver. Recalling the derivation of the approximate solution, the approximation made for x_{11} impacted the solution for the slow time variation of the transverse components of angular momentum. The solution to Eqs. 4.52 and 4.53 are themselves sines and cosines and are the means by which the approximate solution captures the slowly varying frequency in the transverse components of the system. The amount of initial phase error is related to how far the gyrostat starts from the oblate equilibrium point. Figure 4.9 depicts the x_{11} function for two different oblate trajectories. One trajectory begins very close to the oblate equilibrium point while the other begins very far away. As seen, the approximation of the x_{11} function very early in the spinup is not as accurate as at the end of the spinup. The approximation gets worse as the initial conditions get further away from the equilibrium point. The same phenomena occurs for different values of g (see Figure 4.1). A smaller non-dimensional torque value results in a larger initial approximation error. Since this error is incorporated as phase error in the x_2 and x_3 components of the approximate solution, we can expect higher initial phase error in the approximate solution for oblate gyrostats that begin spinup further away from the oblate equilibrium point and/or are torqued by smaller values of g.

These results are for one particular gyrostat which begins spinup at one initial condition. In order to determine the *envelope* of the solution for an oblate gyrostat, we look at three different variables in the equations; initial conditions, torque (g) values and differences in transverse inertias (ϵ).

4.1.1.1 Initial Conditions. Figure 4.10 depicts the maximum error detected throughout spin up for a gyrostat with $\epsilon = g = 0.01$ starting at various

Figure 4.8. Amplitude error for the x_2 component of angular momentum of an oblate gyrostat with initial conditions $x_1 = 0.7$, $x_2 = 0.4$, $x_3 = 0.59161$ and $\varepsilon = g = 0.01$.
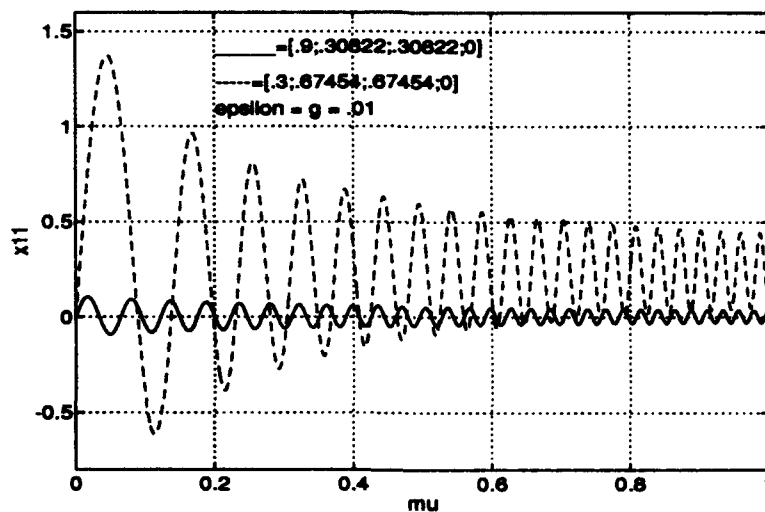

Figure 4.9. x_{11} For two different initial conditions.
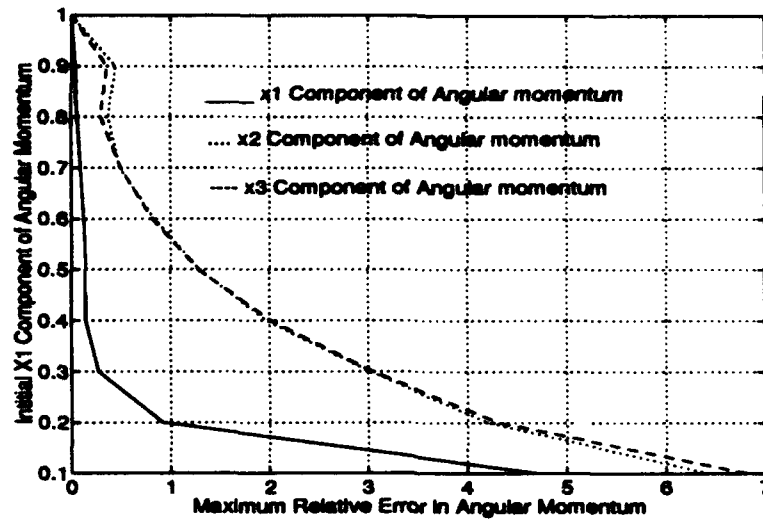
Figure 4.10. Maximum error detected as a function of initial conditions for an oblate gyrostat.

initial conditions (note that the maximum error may have occurred at different times for each component). The y axis is the x_1 initial condition with $x_2 = x_3 = \sqrt{(1 - x_1^2)/2}$ being the transverse initial conditions. Figure 4.10 shows less than 1 percent error in all three axes for gyrostats that start spinup from a point half way down the north (oblate) half of the momentum sphere. As the initial condition progresses further away from the oblate equilibrium point, however, the approximate solution rapidly begins to diverge. This is caused by the large phase error induced early in the spinup maneuver by assuming a constant value for the x_{11} function. Since the primary interest in the spinup maneuver is the angular momentum at the end of spinup, Figure 4.11 depicts the maximum error detected during the last 10 percent of the spinup maneuver. As seen, with the initial phase error absent, the approximate solution is valid to within one percent for the vast majority of initial conditions.
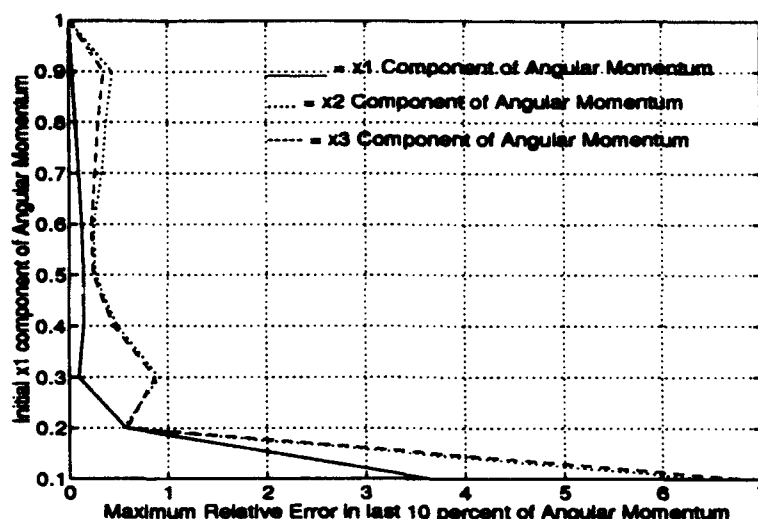
Figure 4.11. Maximum error detected in the last 10 percent of spinup as a function of initial conditions for an oblate gyrostat.

4.1.1.2 Torque Values.   The torque value is directly related to the validity of the solution through Eq. 2.25. Because the approximate solution has only incorporated two time scales, the solution is only valid to $t = \mathcal{O}(\varepsilon^{-1})$. The reason is that for t much greater then $\mathcal{O}(\varepsilon^{-1})$, the t_1 variable ceases to be an $\mathcal{O}(1)$ quantity, and as a result, the solution breaks down (11:228-230). This fact limits the torque values to those which are larger than the asymmetry in the gyrostat. The unfortunate result is that this solution is unable to model accurately the spinup of gyrostats with relatively large asymmetry and small spinup torque. This is not to say, however, that we cannot get good qualitative results. Figures 4.12 and 4.13 illustrate this point. Here we model the same gyrostat as in Figures 4.2 through 4.7, but reduce the torque value to $g = 0.001$. As can be seen, there is excellent qualitative accuracy, but a closeup reveals a slight phase error this far into spinup (see Figure 4.14). Figure 4.15 illustrates the idea graphically.

A second quality associated with the range of validity is the error of the approximate solution. In general, multiple scales solutions carried out to $\mathcal{O}(\varepsilon)$ have an

Figure 4.12. Numerical vs approximate solution of the x_2 component of angular momentum of an oblate gyrostat with initial conditions $x_1 = 0.7$, $x_2 = 0.4$, $x_3 = 0.59161$ and $\varepsilon = 0.01; g = 0.001$.

error of $\mathcal{O}(1)$ when $t = \mathcal{O}(\varepsilon^{-2})$. This is because the constants of integration which develop in the $\mathcal{O}(1)$ terms are solved for to $\mathcal{O}(\varepsilon)$ (cf Eqs. 4.55 and 4.56). These constants of integration are of $\mathcal{O}(1)$ when $t = \mathcal{O}(\varepsilon^{-2})$ which fixes the overall error of the solution. Such an orderly generalization cannot be applied to the approximate solution developed in this thesis. The approximation made for the x_{11} function will cause varying degrees of error as spinup time increases. Further, we employ an approximation for the Fresnel Sine/Cosine functions which have their own order of error.

4.1.1.3 Difference in Transverse Inertias.

Perturbation solutions assume that the *small parameter*, ε, is "small." While an exact definition of "small" cannot be made, the validity of the solution can be demonstrated for different "small" values. Figure 4.16 plots the maximum error detected throughout spinup for an oblate gyrostat with different values of ε. This figure shows that we can expect results with less than 2.4 percent error for an oblate gyrostat that has a 5 percent difference
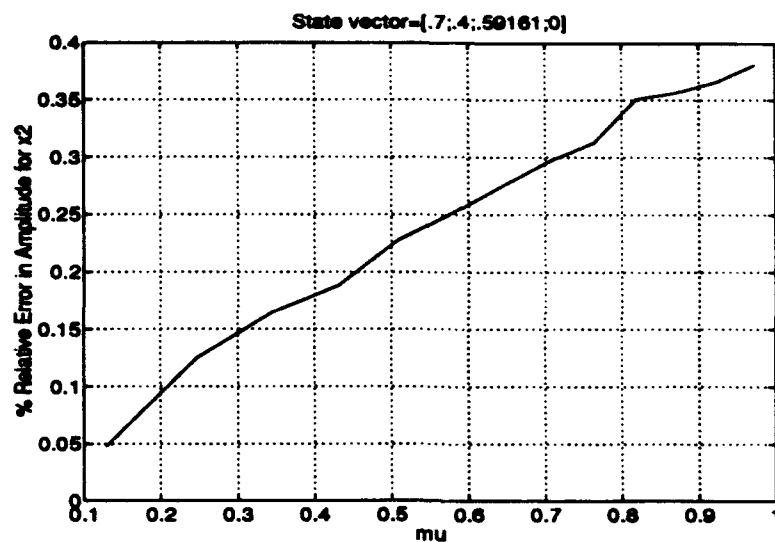
4-24

Figure 4.13. Numerical vs approximate solution of the x_3 component of angular momentum of an oblate gyrostat with initial conditions $x_1 = 0.7$, $x_2 = 0.4$, $x_3 = 0.59161$ and $\varepsilon = 0.01; g = 0.001$.
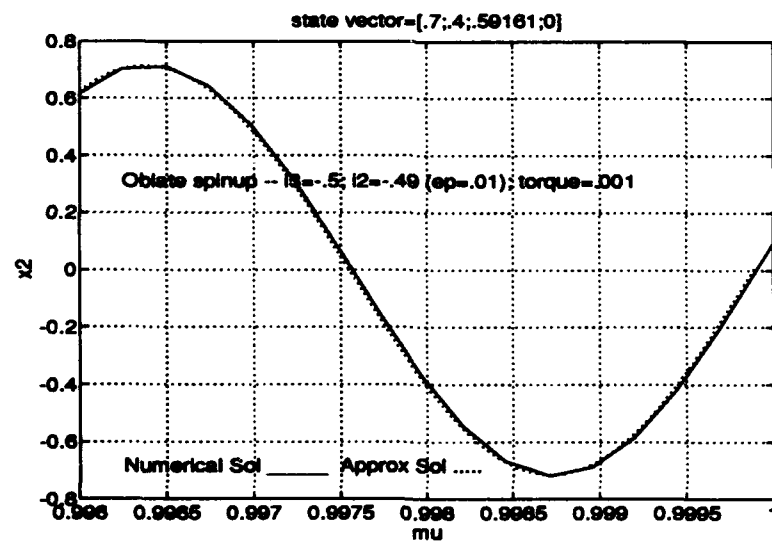

Figure 4.14. Phase error that develops for an oblate gyrostat with $g \ll \varepsilon$.

4-25
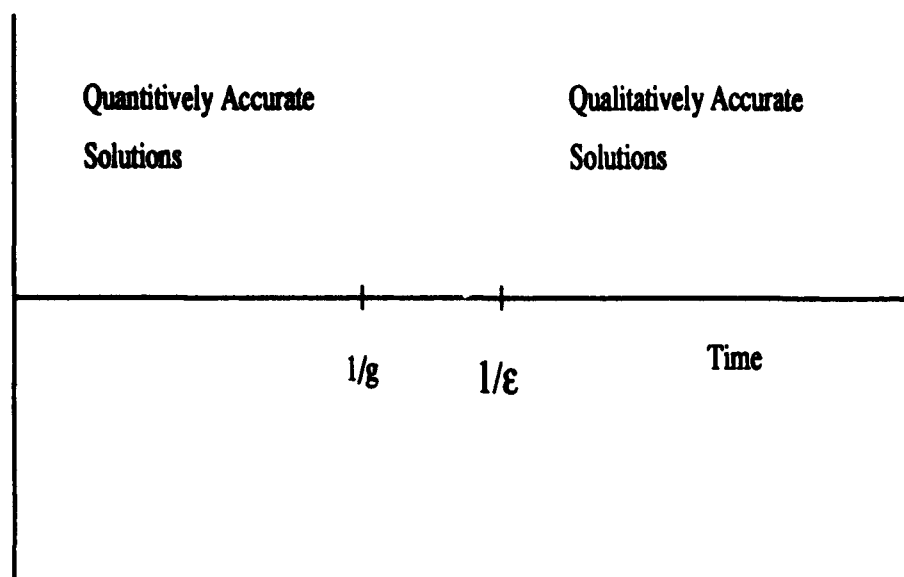
Figure 4.15. Validity of solutions with $g \ll \varepsilon$.

in transverse inertias and approximately 1 percent error for a gyrostat that has a 2 percent difference in transverse inertias. The data in this figure must be viewed carefully, however, since this gyrostat has started with an initial condition fairly close to the oblate equilibrium point. We know the error values will increase as the initial conditions move further from the oblate equilibrium point. In contrast, recall that the maximum error associated with oblate gyrostats starting spinup further away from the oblate equilibrium point is caused by the phase error induced early in the spinup maneuver. The error is considerably less when the comparisons are confined to the last 10 percent of the spinup maneuver.

4.1.1.4 Cone Angle Approximations. As discussed in Chapter 2, the cone (or nutation) angle is the angle formed by the total angular momentum vector and the symmetry axis of the gyrostat. The equation for this angle is given by Eq. 2.23. Throughout the analysis for oblate gyrostats, the maximum error associated with the x_1 component of angular momentum has been less then one
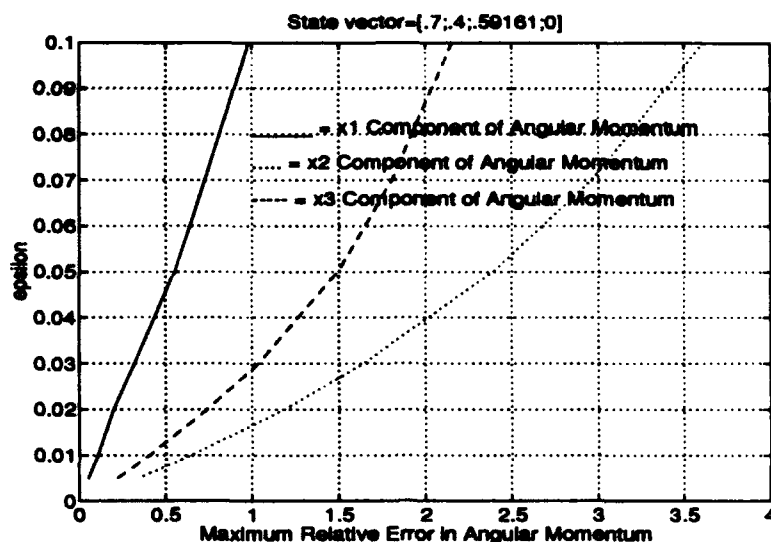
Figure 4.16. Maximum error detected as a function of ε for an oblate gyrostat with initial conditions $x_1 = 0.7, x_2 = 0.4$, $x_3 = 0.59161$; $g = \varepsilon$.

percent. From Figure 4.10, this maximum error occurred for an oblate gyrostat with a one percent difference in transverse inertias but starting just north of the equator of the momentum sphere. From Figure 4.16, this maximum error occurred for an oblate gyrostat starting fairly close to the oblate equilibrium point but with a ten percent difference in transverse inertias. The essential result, however, is that Eq. 4.61 is a reasonable approximation for near axisymmetric oblate gyrostats which begin the spinup maneuver with initial conditions in the northern half of the momentum sphere. Further, this equation can be used to determine the cone angle at any time during the spinup maneuver.

4.1.2 Prolate Gyrostats. As mentioned earlier, our selection of the difference in transverse inertias allows us to solve linear systems of equations for the terms of the approximate solution. Because the systems of equations are linear, our approximate solution does not incorporate any of the separatrices associated with the original nonlinear governing equations. The result is that a phase error will develop

4-27

as the instantaneous separatrices begin to migrate toward the prolate equilibrium point.

To see this, recall that in a $g = 0$ system, the separatrix separates different kinds of motion. In Figure 4.17, we present a cartoon of this concept in the x_2, x_3 plane. It is clear that the phase of the trajectory inside the separatrix is different than that on the outside. As μ increases, the prolate equilibrium point will go through two bifurcations as discussed in Chapter 2, and the phase of the trajectories on either side of the separatrix will change. The net result is that the instantaneous separatrices in the nonlinear system influence the phase of the trajectories on either side of the separatrix. Since the approximate solution does not contain any separatrices to influence the trajectories, we expect a phase error to develop. We also expect the magnitude of the phase error to be larger when the separatrix is near the equator of the momentum sphere since the trajectory paths are longer.

Unfortunately, the phase error induced by the instantaneous separatrices is not the only phase error in the approximate solution. Just as for an oblate gyrostat, the x_{11} approximation induces an additional phase error. The combination of these errors greatly hinders the usefulness of this approximate solution for prolate spinup.

Figures 4.18 through 4.20 illustrate the spinup of a prolate gyrostat. We can see that the approximate solution begins to get out of phase near $\mu = 0.1$. Unfortunately, because the approximate solution begins with a relatively large error, which is compounded by an additional phase error from its inability to model the instantaneous separatrices, the remainder of the solution is flawed. Notice that the gyrostat begins spinup fairly close to the prolate equilibrium point (P_μ). Because the x_{11} approximation gets worse as the initial conditions move further from P_μ, we do not expect any results better than those shown.

As discussed in Section 2.4, the last bifurcation associated with the instantaneous separatrices occurs at μ equal to the larger of $|i_2|$ or $|i_3|$. After this point, the momentum sphere contains only two equilibrium points, both of which are centers.
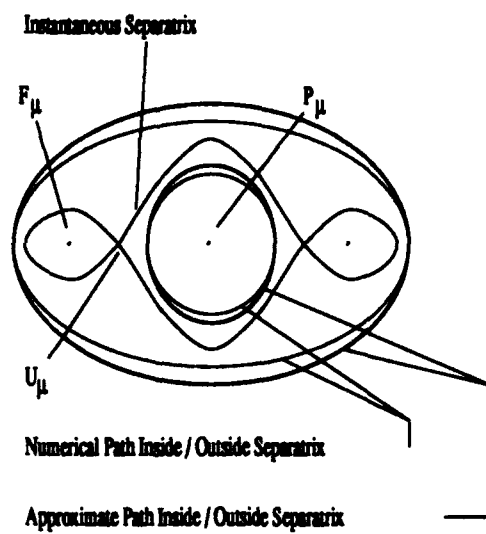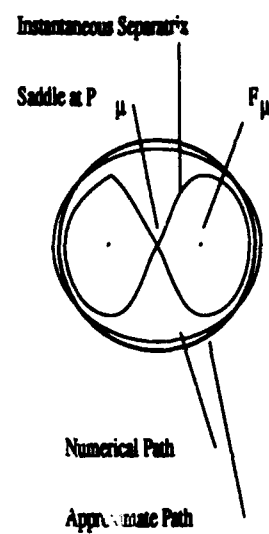
Figure 4.17. Cartoon of different trajectory paths in a $g = 0$ nonlinear system.
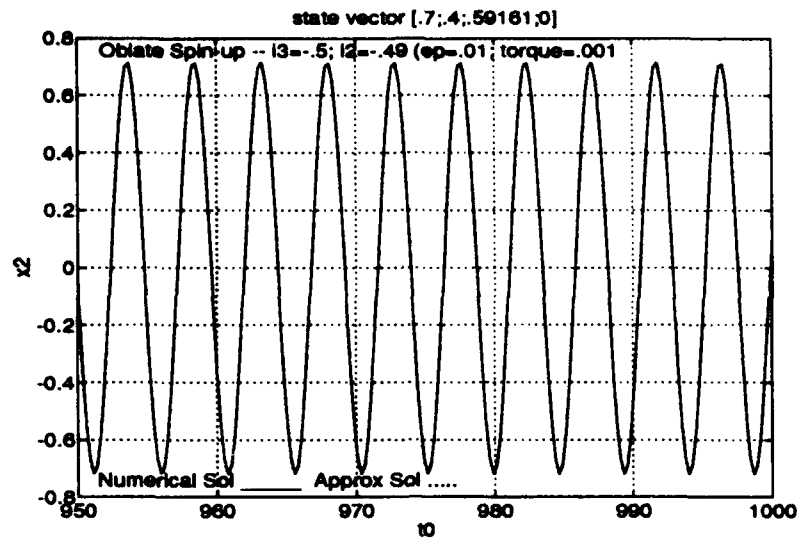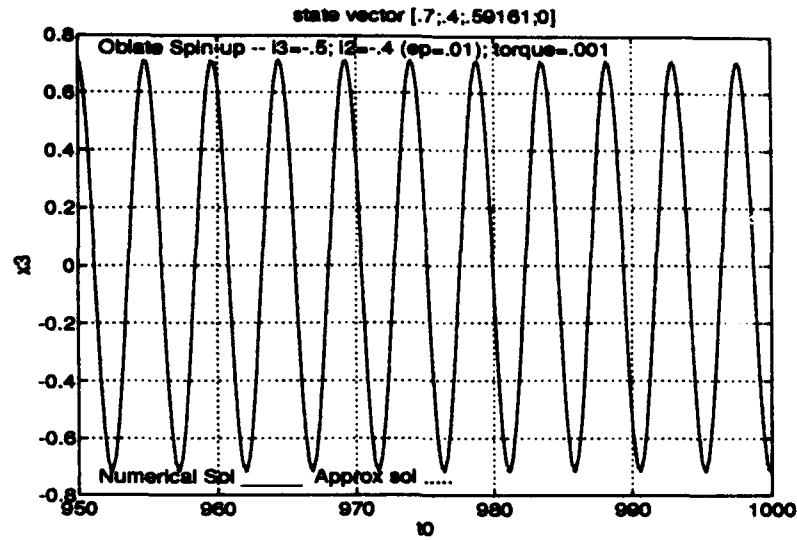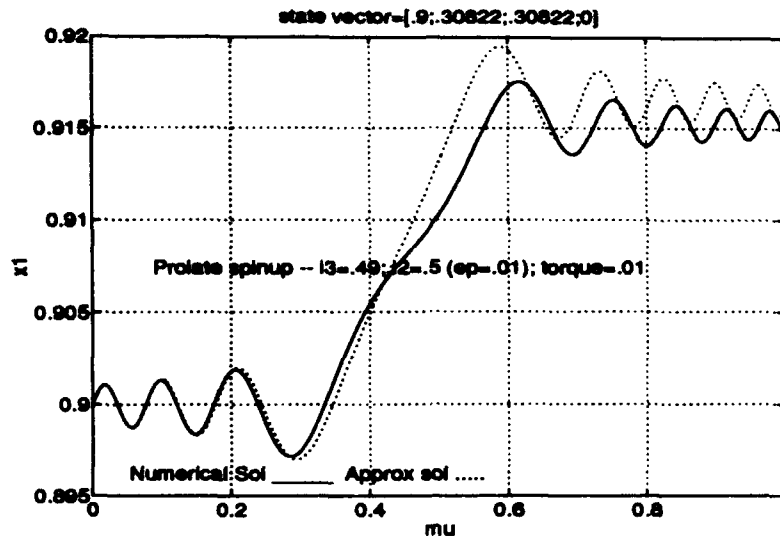
Figure 4.18. Numerical vs approximate solution of the x_1 component of angular momentum of a prolate gyrostat with initial conditions $x_1 = 0.9$, $x_2 = 0.30822$, $x_3 = 0.30822$ and $\varepsilon = g = 0.01$.
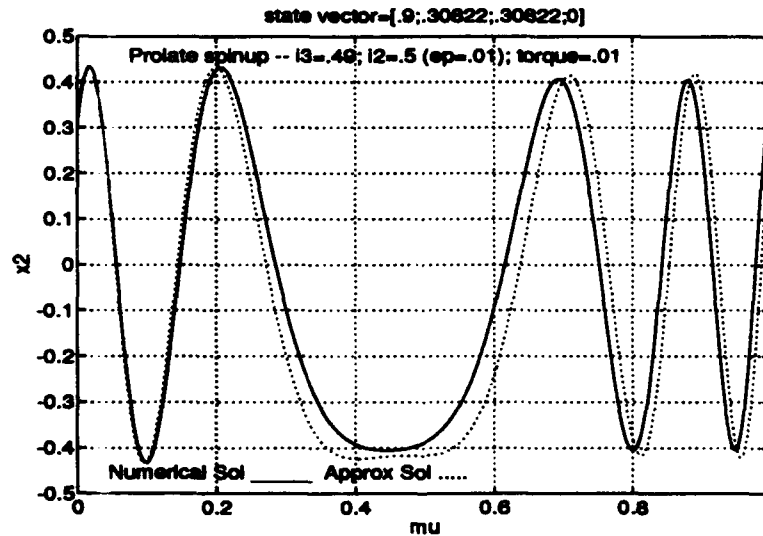

Figure 4.19. Numerical vs approximate solution of the x_2 component of angular momentum of a prolate gyrostat with initial conditions $x_1 = 0.9$, $x_2 = 0.30822$, $x_3 = 0.30822$ and $\varepsilon = g = 0.01$.

4-30

Because there are no more instantaneous separatrices to influence the trajectories, the approximate solution should well approximate the system again after the last bifurcation occurs. Figures 4.21 through 4.23 illustrate this idea. These graphs represent the error between the two solutions. We used the numerical results at $\mu = 0.505$ as the initial conditions for the last portion of the spinup. These graphs also clearly show the early phase error associated with the x_{11} approximation and the instantaneous separatrices. The small error seen during the last portion of the spinup is on the same order as that seen during oblate spinup. Recognize that if we use the numerical results anywhere from when the solution starts to get out of phase to $\mu =$ the larger of $|i_2|$ or $|i_3|$ as initial conditions, the approximate solution will not be as accurate. The reason is that even though the approximate solution is starting from a correct initial condition, it does not have the correct frequency information until the effects of the instantaneous separatrices are eliminated.

4.1.3 Transverse Spinup. Transverse spinup should experience the same problems associated with prolate spinup except the errors will be more pronounced. Recall that in this case, the trajectory starts near a stable flat spin equilibrium point. Further, unless the torque value is extremely small, the trajectory will have too much energy and cross an instantaneous separatrix almost immediately. This will result in a large phase error between the approximate and numerical solutions. The error is the composite of the x_{11} approximation, which is the worst at small μ, and the magnitude of the phase error which is largest near the equator. Figures 4.24 through 4.26 compare the approximate and numerical solutions for a prolate gyrostat starting at the exact transverse equilibrium point. Figures 4.27 through 4.29 show the same gyrostat starting spinup just offset from the equilibrium point. In each case, the instantaneous separatrix crossing occurs almost immediately. This is evidenced by the fact that the x_2 and x_3 components immediately begin to oscillate between -1 and 1.
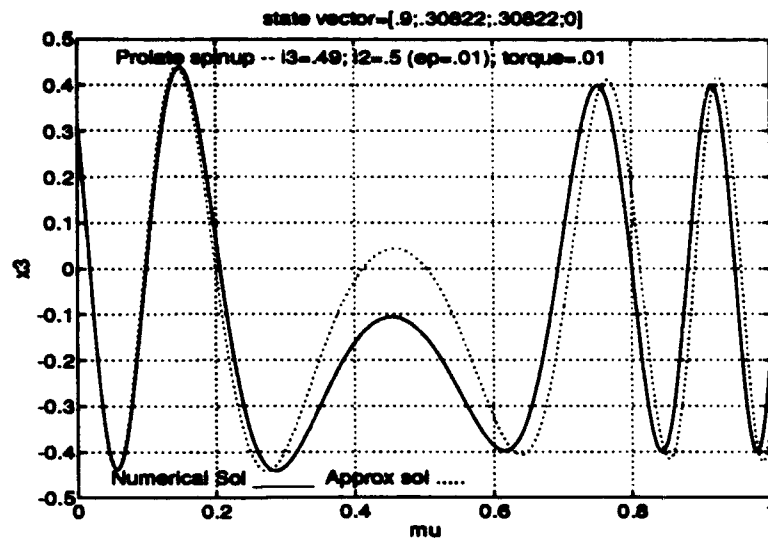
Figure 4.20. Numerical vs approximate solution of the x_3 component of angular momentum of a prolate gyrostat with initial conditions $x_1 = 0.9$, $x_2 = 0.30822$, $x_3 = 0.30822$ and $\varepsilon = q = 0.01$.
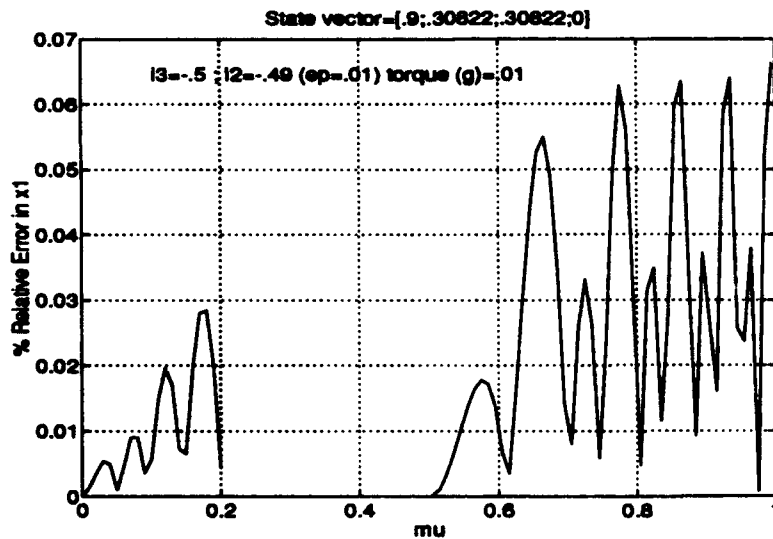
Figure 4.21. Percent relative error in the x_1 component of angular momentum of a prolate gyrostat. Initial conditions are matched at $\mu = 0$ and $\mu = 0.505$.

State vector=[.9;.30822;.30822;0]

I3=.49 ; I2=.5 (ep=.01) torque (g)=.01
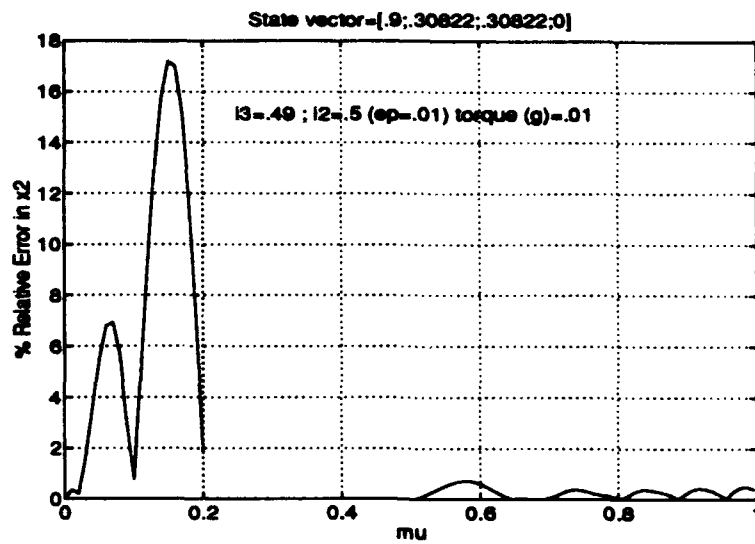
Figure 4.22. Percent relative error in the x_2 component of angular momentum of a prolate gyrostat. Initial conditions are matched at $\mu = 0$ and $\mu = 0.505$.

State vector=[.9;.30822;.30822;0]

I3=.49 ; I2=.5 (ep=.01) torque (g)=.01
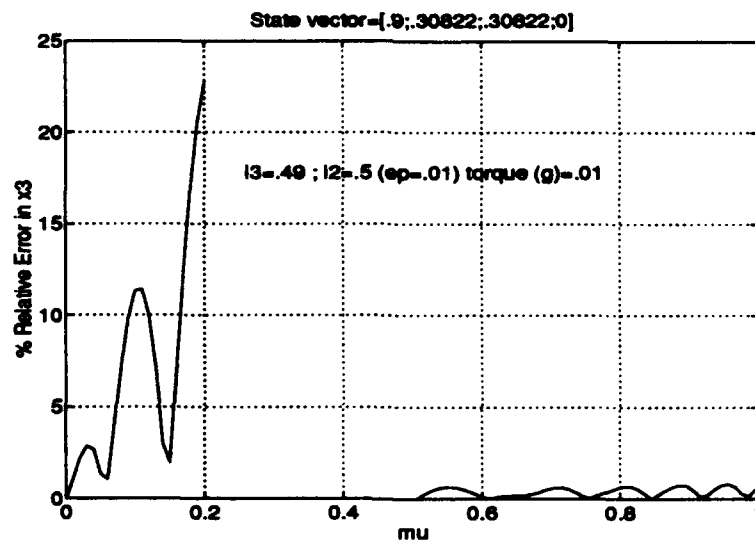
Figure 4.23. Percent relative error in the x_3 component of angular momentum of a prolate gyrostat. Initial conditions are matched at $\mu = 0$ and $\mu = 0.505$.

state vector=[0;0;1;0]

Transverse spinup -- I3=.49; I2=.5 (ep=.01); torque=.01

Numerical Sol _____ Approx sol .....
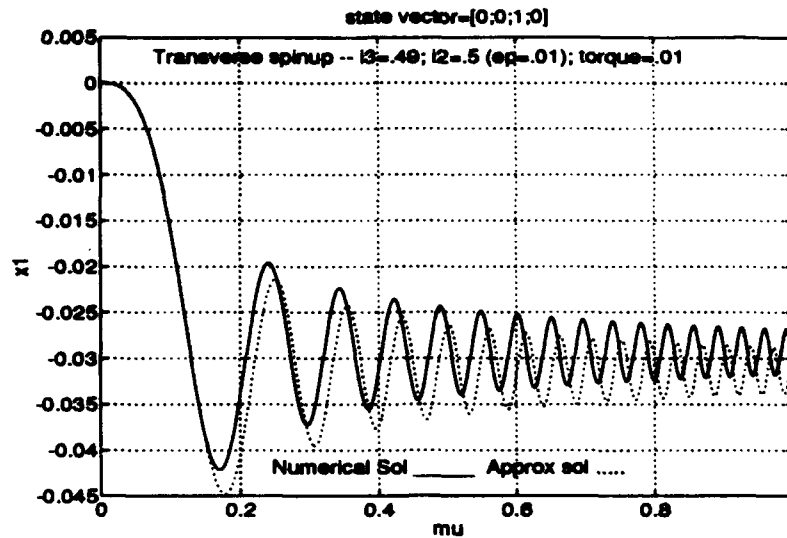
Figure 4.24. Numerical vs approximate solution of the x_1 component of angular momentum of a prolate gyrostat during transverse spinup.

Recall that our solution is only valid for $g > \epsilon$. In order to make use of this approximate solution, we would need to model extremely near axisymmetric gyrostats ($\epsilon = 0.00001$) with extremely small torque values. This is not very practical since, in the limit, it approaches the exact solution for $\epsilon = g = 0$ (i.e. axisymmetric and no spinup).

4.2 Summary

The approximate solution developed in this chapter essentially employs the method of multiple scales. The solutions are not complete in that we are unable to solve the $\mathcal{O}(\epsilon^2)$ system of equations to determine the constants of integration in the $\mathcal{O}(\epsilon)$ system. Further, in order to derive an analytical expression for the $\mathcal{O}(1)$ system, we ignore the slow time dependence in the x_1 component of angular momentum. While this approximation leads to large phase errors in x_1, the magnitude of the error is small compared to the magnitude of the overall component of angular momentum. The result is an overall small error in the x_1 component. The benefit

4-34
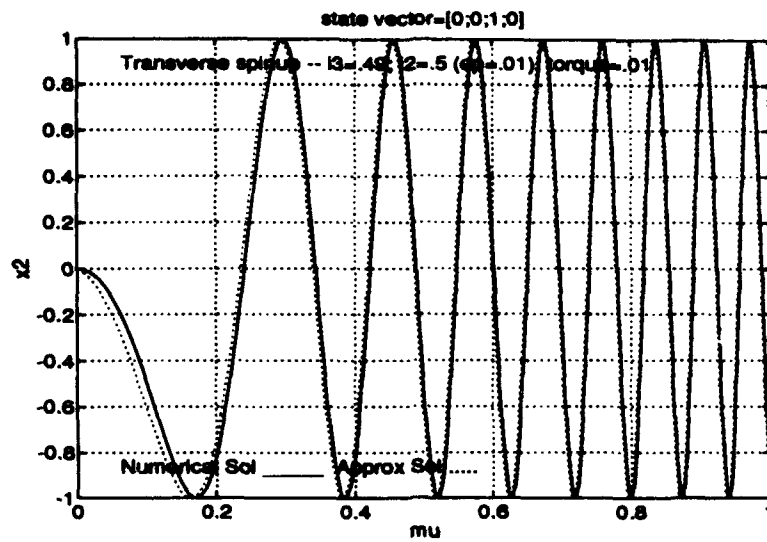
Figure 4.25. Numerical vs approximate solution of the x_2 component of angular momentum of a prolate gyrostat during transverse spinup.
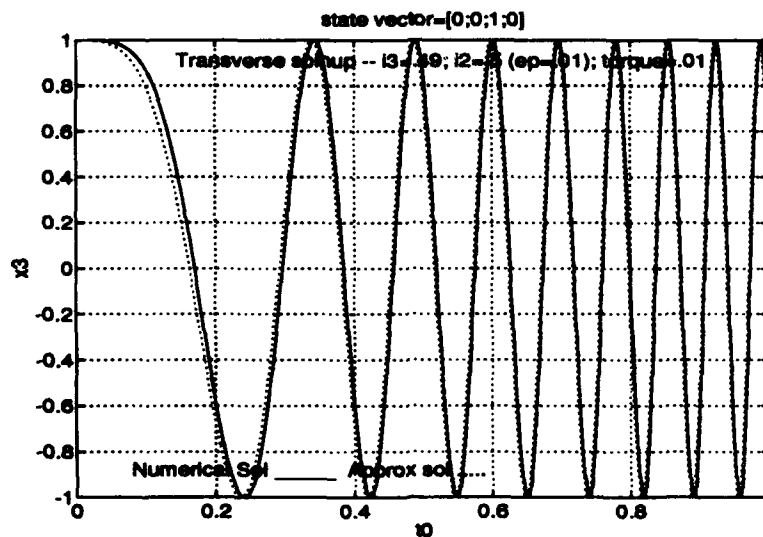
Figure 4.26. Numerical vs approximate solution of the x_3 component of angular momentum of a prolate gyrostat during transverse spinup.
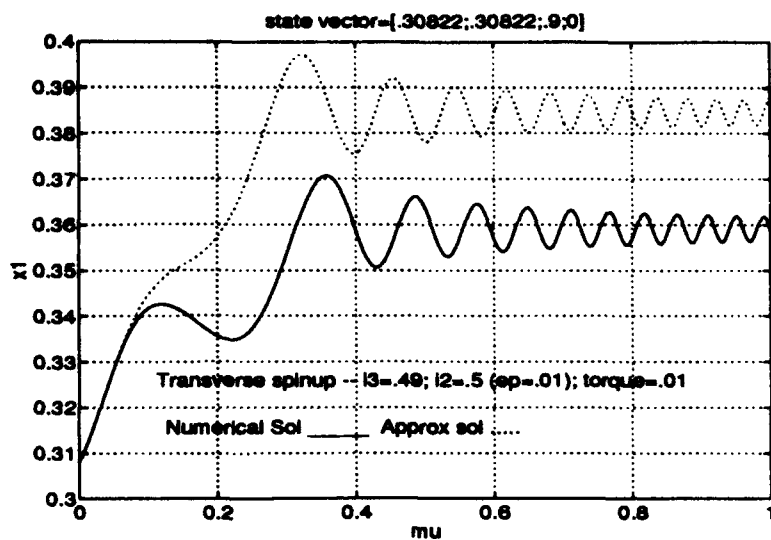
Figure 4.27. Numerical vs approximate solution of the x_1 component of angular momentum of a prolate gyrostat during transverse spinup.
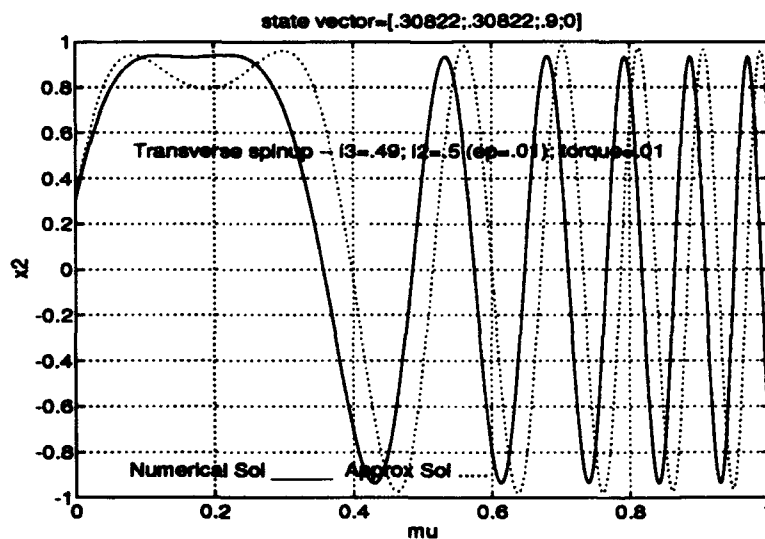
Figure 4.28. Numerical vs approximate solution of the x_2 component of angular momentum of a prolate gyrostat during transverse spinup.

4-36
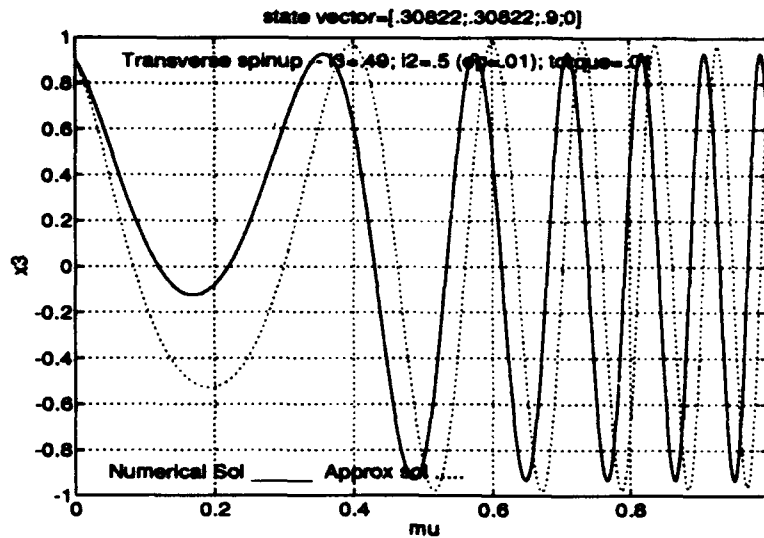
Figure 4.29. Numerical vs approximate solution of the x_3 component of angular momentum of a prolate gyrostat during transverse spinup.

of the approximation is that it allows the analytical development of the transverse components of angular momentum.

We compared the approximate solution to the three spinup problems discussed in Chapter 2. For oblate spinup, the approximate solution provides excellent results. For oblate gyrostats that begin spinup close to the oblate equilibrium point, the error in all three components of angular momentum are very small. The reason is that the influence of the instantaneous separatrices are initially small and remain small as the spinup maneuver continues. As the initial conditions for the gyrostat get close to the equator of the momentum sphere, the influence of the instantaneous separatrices are initially felt and result in a large initial phase error. However, as the spinup maneuver progresses, the instantaneous separatrices migrate further away from the trajectory and the error values decrease. Additionally, we discussed the validity of the approximate solution in terms of time and/or torque value. Because we only use two time scales, the approximate solution is only valid to $t = \mathcal{O}(\varepsilon^{-1})$. This implies that the torque must be greater than the ε value to achieve quantitatively

4-37

accurate solutions. However, qualitatively accurate solutions are available out to $t = \mathcal{O}(\varepsilon^{-2})$. Finally, we determined that oblate gyrostats with a one percent difference in transverse inertias are well approximated.

For prolate spinup, the approximate solution is hindered by phase errors arising from the x_{11} approximation and its inability to account for instantaneous separatrices. This results in an "instantaneous separatrix window" in which the approximate solution is not able to compensate for the frequency change as much as the nonlinear system. The "window" closes after the last bifurcation occurs at the south pole of the momentum sphere. Numerical results for the components of angular momentum at any time after the last bifurcation are valid initial conditions to approximate the remainder of the spinup.

The approximate solution is not well suited to model transverse spinup. The torque values required for accurate use of the approximate solution are so small, that the solution is rendered impractical.

V. Cylindrical Coordinates

The approximate solution derived in Chapter 4 provides excellent results for oblate gyrostats with initial conditions that start in the upper half of the momentum sphere. The approximate solution begins to breakdown, however, due to the phase error introduced by assuming a constant value of the x_{11} function. This is most clearly demonstrated in Figure 4.10. The maximum error that begins to develop in the transverse components of angular momentum is due to this approximation. We have noted that this error occurs early in the spinup maneuver where the x_{11} approximation is least valid. The idea of this chapter is to derive an approximate solution that does not suffer this deficiency.

A different approximate solution was developed by Lt Col William P. Baker, Associate Professor of Mathematics, Air Force Institute of Technology and is included here for evaluation and completeness. Lt Col Baker observed that the transverse angular momentum components are characterized by constant amplitude but varying frequency. His idea was to transform the system of equations to cylindrical coordinates and then use the method of multiple scales to derive another approximate solution.

To develop the solution we proceed as follows. Eqs. 2.18 through 2.20 with the substitution of $\alpha \varepsilon = i_2 - i_3$ reduce to

$$\dot{x}_1 = \alpha \varepsilon x_2 x_3 \tag{5.1}$$

$$\dot{x}_2 = (i_3 x_1 - \mu) x_3 \tag{5.2}$$

$$\dot{x}_3 = -(i_3 x_1 - \mu) x_2 - \alpha \varepsilon x_1 x_2 \tag{5.3}$$

$$\dot{\mu} = g \tag{5.4}$$

Let

$$x_1 = x_1 \qquad (5.5)$$

$$x_2 = \rho \cos \phi \qquad (5.6)$$

$$x_3 = \rho \sin \phi \qquad (5.7)$$

where ρ is the amplitude and ϕ is the phase angle of the system. The system is subject to the following initial conditions

$$x_1(0) = x_1(0)$$

$$\rho(0) = \sqrt{x_2^2(0) + x_3^2(0)}$$

$$\phi(0) = \tan^{-1}\left(\frac{x_3(0)}{x_2(0)}\right)$$

To get the system of equations into a form from which we can employ a multiple scales approach, we start with

$$\rho^2 = x_2^2 + x_3^2$$

$$\phi = \tan^{-1}(x_3/x_2)$$

The time derivative of these expressions are

$$\rho\dot{\rho} = x_2\dot{x}_2 + x_3\dot{x}_3 \qquad (5.8)$$

$$= -\alpha\varepsilon x_1 x_2 x_3 = -\alpha\varepsilon x_1 \rho^2 \cos\phi \sin\phi \qquad (5.9)$$

$$\dot{\phi} = \frac{1}{1 + (x_3/x_2)^2} \cdot \frac{\dot{x}_3 x_2 - \dot{x}_2 x_3}{x_2^2} \qquad (5.10)$$

One further manipulation is

$$\rho^2\dot{\phi} = \dot{x}_3 x_2 - \dot{x}_2 x_3 = -(i_3 x_1 - \mu)\rho^2 - \alpha\varepsilon x_1 \rho^2 \cos^2\phi \qquad (5.11)$$

Substituting Eqs. 5.6 and 5.7 into Eq. 5.1 and using Eq. 5.9 and 5.11 results in the following system of equations.

$$\dot{x}_1 = \alpha\epsilon\rho^2\cos\phi\sin\phi = \frac{\alpha\epsilon}{2}\rho^2\sin 2\phi$$

$$\dot{\rho} = -\alpha\epsilon x_1\rho\cos\phi\sin\phi = -\frac{\alpha\epsilon}{2}x_1\rho\sin 2\phi$$

$$\dot{\phi} = -(i_3 x_1 - \mu) - \frac{\alpha\epsilon}{2}x_1 - \frac{\alpha\epsilon}{2}x_1\cos 2\phi$$

We simplify these equations further by letting

$$\psi = 2\phi \tag{5.12}$$

$$\delta = \frac{\alpha\epsilon}{2} \tag{5.13}$$

and obtain the following system of equations.

$$\dot{x}_1 = \delta\rho^2\sin\psi \tag{5.14}$$

$$\dot{\rho} = -\delta x_1\rho\sin\psi \tag{5.15}$$

$$\dot{\psi} = -2(i_3 x_1 - \mu) - 2\delta x_1 - 2\delta x_1\cos\psi \tag{5.16}$$

We seek solutions of the form

$$x_1(t_0, t_1; \delta) = x_{10}(t_0, t_1) + \delta x_{11}(t_0, t_1) + \delta^2 x_{12}(t_0, t_1) + \mathcal{O}(\delta^3) \tag{5.17}$$

$$\rho(t_0, t_1; \delta) = \rho_0(t_0, t_1) + \delta\rho_1(t_0, t_1) + \delta^2\rho_2(t_0, t_1) + \mathcal{O}(\delta^3) \tag{5.18}$$

$$\psi(t_0; \delta) = \psi_0(t_0) + \delta\psi_1(t_0) + \delta^2\psi_2(t_0) + \mathcal{O}(\delta^3) \tag{5.19}$$

Again the fast time "t_0" is defined as t while the slow time "t_1" is defined as δt. Note that we make the initial assumption of no slow time dependence in the phase angle. This assumption will be discussed in the final form of the approximate solution. We

employ the following differential operator to incorporate the different time scales.

$$\frac{d}{dt} = \frac{\partial}{\partial t_0} + \delta \frac{\partial}{\partial t_1} \tag{5.20}$$

Further, we still must conserve angular momentum and so we impose the constraint

$$\|\mathbf{x}\|^2 = 1, \forall\, t \geq 0 \tag{5.21}$$

This results in the same orthogonality condition on all $\mathcal{O}(\varepsilon)$ terms as seen in the cartesian solution. Substituting Eqs. 5.17 through 5.20 into Eqs. 5.14 through 5.16 and collecting $\mathcal{O}(1)$ terms yields

$$\frac{\partial x_{10}}{\partial t_0} = 0 \tag{5.22}$$

$$\frac{\partial \rho_0}{\partial t_0} = 0 \tag{5.23}$$

$$\frac{\partial \psi_0}{\partial t_0} = -2(i_3 x_{10} - \mu) \tag{5.24}$$

This system is subject to the following initial conditions.

$$
\begin{aligned}
x_{10}(0,0) &= x_1(0) \\
\rho_0(0,0) &= \rho(0) \\
\psi_0(0) &= 2\phi(0) \\
\|\mathbf{x}_0\|^2 &= 1, \forall\, t > 0
\end{aligned}
$$

Note that the constraint refers to the total component of angular momentum. The solution to the $\mathcal{O}(1)$ system with the application of initial conditions is

$$
\begin{aligned}
x_{10}(t_0, t_1) &= A_0(t_1) \implies x_{10}(0,0) = A_0(0) = x_1(0) \\
\rho_0(t_0, t_1) &= \rho_0(t_1) \implies \rho_0(0,0) = \rho_0(0) = \rho(0)
\end{aligned}
$$

$$\psi_0(t_0) \;=\; \int_0^{t_0} \left[2g\sigma + 2\mu_0 - 2i_3 x_{10}\right] d\sigma$$

$$= \; gt_0^2 + 2\left(\mu_0 - i_3 x_{10}\right)t_0 + \theta_0 \qquad (5.25)$$

where θ_0 is defined so that the initial conditions are satisfied.

$$\theta_0 = 2\tan^{-1}\left(x_3(0)/x_2(0)\right) \qquad (5.26)$$

To simplify the equations, we make the following definitions.

$$k \;=\; \mu_0 - i_3 x_1(0) \qquad (5.27)$$

$$f(t_0) \;=\; gt_0^2 + 2kt_0 + \theta_0 \implies \psi_0(t_0) = f(t_0) \qquad (5.28)$$

The $\mathcal{O}(\delta)$ system of equations is

$$\frac{\partial x_{11}}{\partial t_0} \;=\; \rho_0^2 \sin\psi_0 - \frac{\partial x_{10}}{\partial t_1} \qquad (5.29)$$

$$\frac{\partial \rho_1}{\partial t_0} \;=\; -x_{10}\rho_0 \sin\psi_0 - \frac{\partial \rho_0}{\partial t_1} \qquad (5.30)$$

$$\frac{\partial \psi_1}{\partial t_0} \;=\; -2i_3 x_{11} - 2x_{10} - 2x_{10}\cos\psi_0 \qquad (5.31)$$

subject to the following initial conditions

$$x_{11}(0,0) \;=\; 0$$

$$\rho_1(0,0) \;=\; 0$$

$$\psi_1(0) \;=\; 0$$

$$\mathbf{x}_0 \cdot \mathbf{x}_1 \;=\; 0, \; \forall\, t > 0$$

We solve Eq. 5.29 to find the slow time dependence of A_0.

$$x_{11} \;=\; \int_0^{t_0} \left[\rho_0(t_1)^2 \sin\left(g\sigma^2 + 2k\sigma + \theta_0\right) - A_0'(t_1)\right] d\sigma \qquad (5.32)$$

$$
\begin{aligned}
= \quad & \rho_0(t_1)^2 \left[\frac{\sqrt{\pi}}{2g} \left\{ \cos\left(k^2/g - \theta_0\right) S\left(\frac{\sqrt{2}}{g\pi}(k + gt_0)\right) \right. \right. \\
& - \quad C\left(\frac{\sqrt{2}}{g\pi}(k + gt_0)\right) \sin\left(k^2/g - \theta_0\right) \\
& - \quad \cos\left(k^2/g - \theta_0\right) S\left(\frac{\sqrt{2}}{g\pi}(k)\right) \\
& + \quad \left. \left. C\left(\frac{\sqrt{2}}{g\pi}(k)\right) \sin\left(k^2/g - \theta_0\right) \right\} \right] - A_0{}'(t_1)t_0 + A_1(t_1) \quad \text{(5.33)}
\end{aligned}
$$

The "constant" of integration for this equation is $A_1(t_1)$. Again, the term "constant" indicates that the term is constant with respect to t_0. The complete form of the solution is as given, however, to simplify the remainder of the analysis we use the following definitions.

$$
\begin{aligned}
C_o(f) \quad = \quad & \int_0^{t_o} \cos f \, d\sigma \\
= \quad & \frac{\sqrt{\pi}}{2g} \left\{ \cos\left(k^2/g - \theta_0\right) C\left(\frac{\sqrt{2}}{g\pi}(k + gt_0)\right) \right. \\
& + \quad S\left(\frac{\sqrt{2}}{g\pi}(k + gt_0)\right) \sin\left(k^2/g - \theta_0\right) \\
& - \quad \cos\left(k^2/g - \theta_0\right) C\left(\frac{\sqrt{2}}{g\pi}(k)\right) \\
& - \quad \left. S\left(\frac{\sqrt{2}}{g\pi}(k)\right) \sin\left(k^2/g - \theta_0\right) \right\} \quad \text{(5.34)}
\end{aligned}
$$

$$\text{(5.35)}$$

$$
\begin{aligned}
S_o(f) \quad = \quad & \int_0^{t_o} \sin f \, dt \\
= \quad & \frac{\sqrt{\pi}}{2g} \left\{ \cos\left(k^2/g - \theta_0\right) S\left(\frac{\sqrt{2}}{g\pi}(k + gt_0)\right) \right. \\
& - \quad C\left(\frac{\sqrt{2}}{g\pi}(k + gt_0)\right) \sin\left(k^2/g - \theta_0\right) \\
& - \quad \cos\left(k^2/g - \theta_0\right) S\left(\frac{\sqrt{2}}{g\pi}(k)\right) \\
& + \quad \left. C\left(\frac{\sqrt{2}}{g\pi}(k)\right) \sin\left(k^2/g - \theta_0\right) \right\} \quad \text{(5.36)}
\end{aligned}
$$

where

$$f(\sigma) = g\sigma^2 + 2k\sigma + \theta_0 \qquad (5.37)$$

The Fresnel Sine and Fresnel Cosine functions are as defined in Chapter 3, and their integrals are developed in detail in Appendix B. Each term in the x_{11} solution is bounded with the exception of $A_0'(t_1)$. In order to have a completely bounded solution, $A_0'(t_1)$ must equal zero and by application of the initial condition

$$A_0(t_1) = \text{constant} = x_1(0) \qquad (5.38)$$

The resulting solution for x_{11} is

$$x_{11}(t_0, t_1) = \rho_0^2(t_1)S_o(f) + A_1(t_1) \qquad (5.39)$$

We now solve Eq. 5.30.

$$\rho_1 = \int_0^{t_0} \left[-x_1(0)\rho_0(t_1)\sin\left(g\sigma^2 + 2k\sigma + \theta_0\right) - \rho_0\prime(t_1) \right] d\sigma \qquad (5.40)$$

This equation is very similar to Eq. 5.32. Again, in order to have bounded solutions, we must have $\rho_0'(t_1) = 0$ and by application of the initial condition

$$\rho_0(t_1) = \text{constant} = \rho(0) \qquad (5.41)$$

As a result

$$\rho_1(t_0, t_1) = -x_1(0)\rho^2(0)S_o(f) + \rho_1(t_1) \qquad (5.42)$$

Turning our attention to Eq. 5.31, we write it in terms of the Eqs. 5.39 and 5.25 which have been derived.

$$\frac{\partial \psi_1}{\partial t_0} = -2i_3\rho^2(0)S_o(f) - 2i_3A_1(t_1) - 2x_1(0) - 2x_1(0)\cos f \qquad (5.43)$$

We employ the following relation (see Appendix B).

$$\int_0^t S_o\left(f(\sigma)\right) d\sigma$$
$$= t S_o\left(f(t)\right) + \frac{1}{2g}\left(\cos f - \cos\theta_0\right) + \frac{k}{g} S_o\left(f(t)\right)$$

Thus, the solution is

$$
\begin{aligned}
\psi_1(t_0) &= -2i_3\rho^2(0)\left[t_0 S_o(f) + \frac{1}{2g}\left(\cos f - \cos\theta_0\right) + \frac{k}{g} S_o(f)\right] \\
&\quad - 2t_0\left[i_3 A_1(t_1) + x_1(0)\right] - 2x_1(0)C_o(f) + \beta
\end{aligned} \tag{5.44}
$$

The constant of integration is β and by application of the initial condition we see that $\beta = 0$. With the $\mathcal{O}(\delta)$ system of equations solved, we must determine the nature of the constants of integrations $A_1(t_1)$ and $\rho_1(t_1)$. Note that from the orthogonality condition specified on the $\mathcal{O}(\delta)$ system, we require that

$$\mathbf{x}_0 \cdot \mathbf{x}_1 = 0, \ \forall \, t > 0$$

Performing this product results in

$$x_1(0)A_1(t_1) + \rho(0)\rho_1(t_1) = 0 \tag{5.45}$$

Therefore, if $A_1(t_1) = 0$, we must require $\rho_1(t_1) = 0$. In order to determine $A_1(t_1)$, we proceed to the $\mathcal{O}(\delta^2)$ system of equations.

$$\frac{\partial x_{12}}{\partial t_0} = 2\rho_0\rho_1 \sin\psi_0 + \rho_0^2\psi_1 \cos\psi_0 - \frac{\partial x_{11}}{\partial t_1} \tag{5.46}$$

$$\frac{\partial \rho_2}{\partial t_0} = -(x_{10}\rho_1 + x_{11}\rho_0)\sin\psi_0 - \rho_0 x_{10}\psi_1 \cos\psi_0 - \frac{\partial \rho_1}{\partial t_1} \tag{5.47}$$

$$\frac{\partial \psi_2}{\partial t_0} = -2i_3 x_{12} - 2x_{10} - 2x_{10}\cos\psi_0 - 2x_{10}\psi_1 \cos\psi_0 - 2x_{10}\sin\psi_0 \tag{5.48}$$

This system is subject to the following initial conditions.

$$x_{12}(0,0) = 0$$

$$\rho_2(0,0) = 0$$

$$\psi_2(0) = 0$$

$$\|x_1\|^2 + 2x_0 \cdot x_2 = 0, \ \forall \ t > 0$$

Expressing Eq. 5.46 in terms of known functions

$$
\begin{aligned}
\frac{\partial x_{12}}{\partial t_0} =\ & -2\rho^2(0)x_1(0)S_o(f)\sin f + 2\rho(0)\rho_1(t_1)\sin f \\
& - 2i_3\rho^4(0)\left[t_0 S_o(f) + \frac{1}{2g}(\cos f - \cos\theta_0) + \frac{k}{g}S_o(f)\right]\cos f \\
& - 2\rho^2(0)\left[i_3 A_1(t_1) + x_1(0)\right]t_0 \cos f \\
& - 2x_1(0)\rho^2(0)C_o(f)\cos f - A_1{}'(t_1)
\end{aligned}
\tag{5.49}
$$

The solution to Eq. 5.46 is

$$
\begin{aligned}
x_{12}(t_0, t_1) =\ & -\rho^2(0)x_1(0)\left[S_o(f)\right]^2 + 2\rho(0)\rho_1(t_1)S_o(f) \\
& - \frac{2\rho^2(0)}{2g}\left(i_3 A_1(t_1) + x_1(0)\right)\left[\sin f - \sin\theta_0\right] \\
& + \frac{2k\rho^2(0)}{g}\left(i_3 A_1(t_1) + x_1(0)\right)C_o(f) \\
& - x_1(0)\rho^2(0)\left[C_o(f)\right]^2 + \frac{2i_3\rho^2(0)}{2g}\cos\theta_0 C_o(f) \\
& - \frac{2i_3\rho^4(0)}{2g}\left[\frac{t_0}{2} + \frac{1}{2}C_o(2f)\right] \\
& - \frac{2i_3\rho^4(0)}{2g}\left[S_o(f)\sin f - \frac{t_0}{2}\right. \\
& + \left.\frac{1}{2}C_o(2f)\right] + t_0 A_1{}'(t_1) + A_2(t_1)
\end{aligned}
\tag{5.50}
$$

Every term in the solution is bounded except $A_1'(t_1)$. Therefore we require that it be equal to zero and by application of initial conditions we find that $A_1(t_1) = 0$.

Further, by Eq. 5.45 we find that $\rho_1(t_1)$ must also equal zero. However, we show the same process that we applied to Eq. 5.47 to verify this.

$$
\begin{aligned}
\frac{\partial \rho_2}{\partial t_0} =\ & -\rho_0(\rho_0^2 - x_1{}^2)S_o(f) - x_1\rho_1 \sin f \\
& + 2i_3\rho_0^3 x_1\left[t_0 S_o(f) + \frac{1}{2g}(\cos f - \cos\theta_0) + \frac{k}{g}S_o(f)\right]\cos f \\
& + 2x_1{}^2\rho_0 t_0 \cos f + 2x_1{}^2\rho_0 C_o(f)\cos f - \rho_1{}'(t_1)
\end{aligned}
\tag{5.51}
$$

Using the same relations that solved Eq. 5.46 we have the solution

$$
\begin{aligned}
\rho_2(t_0, t_1) =\ & \frac{1}{2}\rho(0)\left[\rho^2(0) - x_1{}^2(0)\right][S_o(f)]^2 - x_1(0)\rho_1(t_1)S_o(f) \\
& + 2i_3\rho^3(0)x_1(0)\left[\frac{1}{2g}S_o(f)\sin f + \frac{1}{2g}C_o(2f)\right. \\
& \left. - \frac{1}{2g}\cos\theta_0 C_o(f)\right] + \frac{2x_1{}^2\rho(0)}{2g}[\sin f - \sin\theta_0] \\
& - \frac{2x_1{}^2(0)\rho(0)k}{g}C_o(f) + \frac{2x_1{}^2(0)\rho(0)}{2}[C_o(f)]^2 \\
& - t_0\rho_1{}'(t_1) + \rho_2(t_1)
\end{aligned}
\tag{5.52}
$$

This solution is the same as that for the x_{12} solution in that all terms are bounded except $\rho_1'(t_1)$. Therefore $\rho_1(t_1) = 0$ and by application of initial conditions, we find that $\rho_1(t_1) = 0$ as required. With the constants of integration determined, we now return to Eqs. 5.39 and 5.42 and note their final solution.

$$
x_{11}(t_0, t_1) = -\rho_0^2(0)S_o(f)
\tag{5.53}
$$

$$
\rho_1(t_0, t_1) = -x_1(0)\rho_0(0)S_o(f)
\tag{5.54}
$$

To summarize, the approximate solution to $\mathcal{O}(\varepsilon)$ using cylindrical coordinates is as follows.

$$
x_1(t) = x_1 - \frac{\alpha\varepsilon}{2}\rho_0^2(0)S_o(f) + \mathcal{O}(\varepsilon^2)
\tag{5.55}
$$

$$\rho(t) = \rho_0(0) - \frac{\alpha\epsilon}{2}x_1(0)\rho(0)S_o(f) + \mathcal{O}(\epsilon^2) \tag{5.56}$$

$$\phi(t) = \frac{\psi(t)}{2} = \frac{1}{2}\left\{f - \alpha\epsilon\left\{i_3\rho^2(0)\left[tS_o(f) + \frac{1}{2g}(\cos f - \cos\theta_0)\right.\right.\right.$$

$$\left.\left.\left. + \frac{k}{g}S_o(f)\right] + tx_1(0) - x_1(0)C_o(f)\right\}\right\} + \mathcal{O}(\epsilon^2) \tag{5.57}$$

Finally

$$x_2(t) = \rho(t)\cos\phi(t) \tag{5.58}$$

$$x_3(t) = \rho(t)\sin\phi(t) \tag{5.59}$$

Recognize that to $\mathcal{O}(1)$, we have satisfied the conservation of angular momentum requirement. In the beginning of the analysis, we made the assumption of no slow time dependence in the phase angle. Careful analysis of Eqs. 5.55 through 5.57 reveal some interesting results. Although the equations for x_1 and ρ were derived with the assumption of *some slow time dependence*, it never shows up in the final form of the solution. However, slow time dependence is implicitly found in the equation for ϕ (Eq. 5.57) even though it was not assumed to be there initially. As a result, by using cylindrical coordinates, the approximate solution is essentially a series expansion of the system of equations using a single time scale.

5.1 A Comparison Between the Cartesian and Cylindrical Approximate Solutions

5.1.1 Oblate Gyrostats.

Figures 5.1 through 5.3 present the relative error associated with each component of angular momentum for both the cartesian and cylindrical solutions. The model is a near axisymmetric ($\epsilon = 0.01$) oblate gyrostat with initial state [0.7; 0.4.; 0.59161; 0]. As seen, the solutions for the x_1 component are identical. This is expected since the underlying assumptions between the solutions are the same. Specifically, the initial conditions for x_2 and x_3 are used in both forms. Further, both solutions use the assumption of no slow time dependence. The

transverse components show a dramatic difference in the early portion of the spinup maneuver. The cylindrical solution does not exhibit the "spike" that the cartesian solution displays. In order to examine this finding in more detail, we compare the two solutions using the same oblate gyrostat starting at a point further from the oblate equilibrium point (Figures 5.4 and 5.5). Here we observe the same behavior early in the spinup, but also notice that the cartesian solution displays less error than the cylindrical solution towards the end of the spinup maneuver. To explain this behavior, recall the development of each solution. In the cartesian solution, the "spike" is the result of phase error caused by the approximation of a constant value for the x_{11} function. The cylindrical solutions makes no such approximation and so there should not be any significant phase error associated with this region of the spinup. Towards the end of the spinup maneuver, the lower error of the cartesian solution is the result of the x_{11} approximation. This illustrates an interesting result between the two solutions. As noted in Chapter 4, the x_{11} approximation impacts the transverse components in that it captures the slowly varying frequency of the system. The cartesian solution is based on a fast and a slow time scale. The slow time scale captures the phase or frequency of the system. By assuming the constant value for the x_{11} function was $x_{11approx}(t = \infty)$, the frequency adjustment of the system is incorporated in the transverse components for $t \rightarrow \infty$. As seen, this phase correction is not as accurate in the early portion of the spinup, but increases in accuracy as time increases. The cylindrical solution implicitly incorporates slow time dependence but it does not benefit from the $t \rightarrow \infty$ phase correction that the cartesian solution has. As a result, the cylindrical solution has a larger error in the latter portion of the spinup maneuver.

To illustrate this point in a different light, observe Figure 5.6. Here we compare the maximum error detected between cartesian and cylindrical solutions in the last ten percent of spinup for a near axisymmetric ($\varepsilon = 0.01$) oblate gyrostat starting at incremental points on the momentum sphere. The initial x_1 component is the y axis
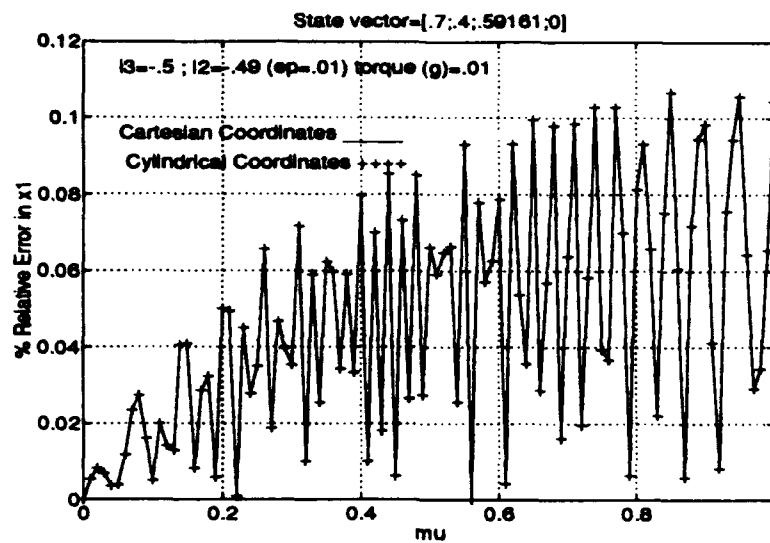
Figure 5.1.   Comparison between cartesian and cylindrical equations for percent relative error of the x_1 component of angular momentum of an oblate gyrostat with initial conditions $x_1 = 0.7, x_2 = 0.4, x_3 = 0.59161$ and $\varepsilon = g = 0.01$.
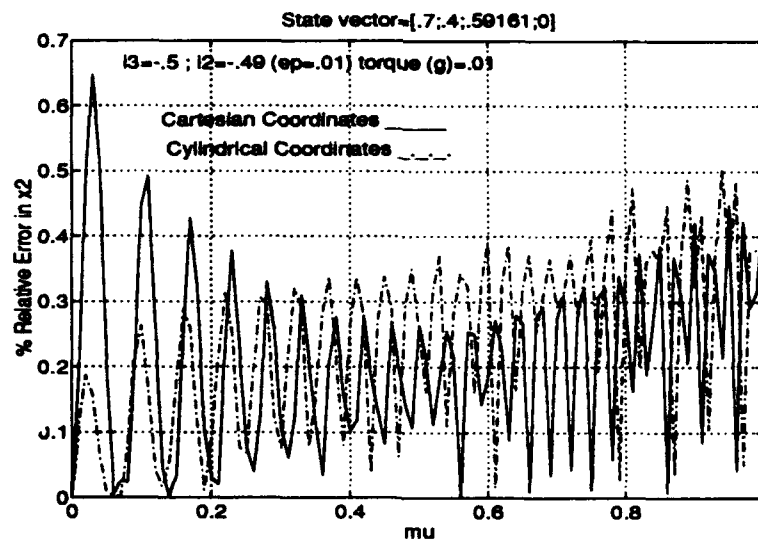
Figure 5.2.   Comparison between cartesian and cylindrical equations for percent relative error of the x_2 component of angular momentum of an oblate gyrostat with initial conditions $x_1 = 0.7, x_2 = 0.4, x_3 = 0.59161$ and $\varepsilon = g = 0.01$.
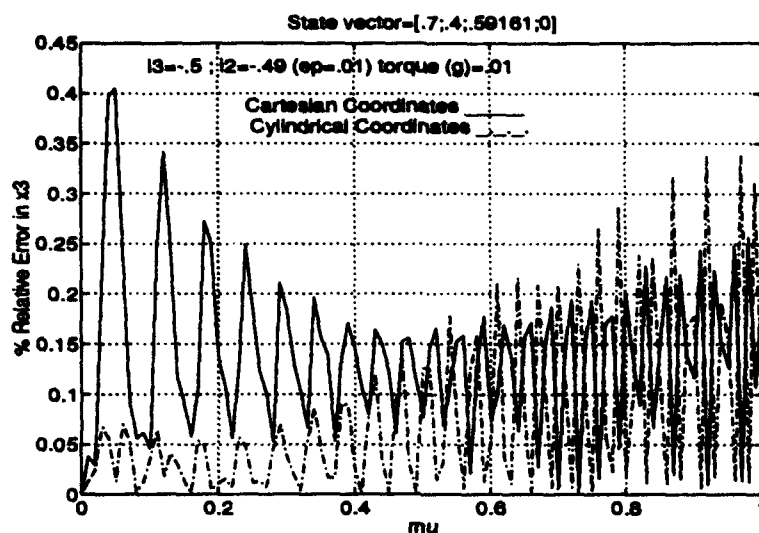
Figure 5.3. Comparison between cartesian and cylindrical equations for percent relative error of the x_3 component of angular momentum of an oblate gyrostat with initial conditions $x_1 = 0.7, x_2 = 0.4, x_3 = 0.59161$ and $\varepsilon = g = 0.01$.

Figure 5.4. Comparison between cartesian and cylindrical equations for percent relative error of the x_2 component of angular momentum of an oblate gyrostat with initial conditions $x_1 = 0.4, x_2 = 0.64807, x_3 = 0.64807$ and $\varepsilon = g = 0.01$.

State vector=[.4;.64807;.64807;0]

I3=.49 ; I2=.5 (ep=.01) torque (g)=.01

Cartesian Coordinates .....

Cylindrical Coordinates -.-.-.

Figure 5.5. Comparison between cartesian and cylindrical equations for percent relative error of the x_3 component of angular momentum of an oblate gyrostat with initial conditions $x_1 = 0.4, x_2 = 0.64807, x_3 = 0.64807$ and $\epsilon = g = 0.01$.

while the initial x_2 and x_3 components are $x_2 = x_3 = \sqrt{(1 - x_1^2)/2}$. The increased accuracy of the $t \to \infty$ phase approximation in the cartesian solution is clearly seen.

5.1.2 *Prolate Gyrostats.*

Observation of the early portion of spinup in Figures 5.4 through 5.5 leads us to believe that the cylindrical solution is better equipped to approximate prolate spinup than the cartesian solution. Because the cylindrical solution is not hampered by a relatively large phase error in the early portion of the spinup maneuver, we expect better performance in the region near the instantaneous separatrices.

Figures 5.7 through 5.9 compare the numerical, cylindrical and cartesian solutions for spinup of a prolate gyrostat. Here we see the large influence of the error made by the x_{11} approximation in the cartesian solution. In essence, the cartesian solution starts out with the wrong information and the solutions keeps getting worse.
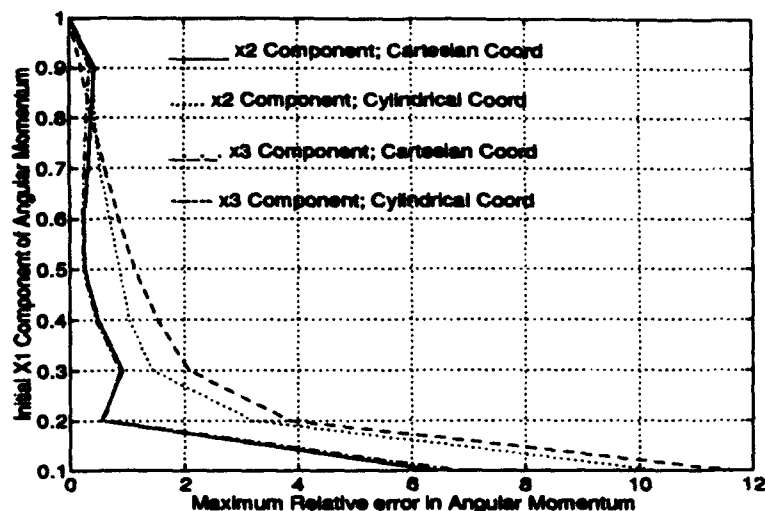
Figure 5.6. Comparison between cartesian and cylindrical equations of maximum error detected in the last ten percent of spin up as a function of initial conditions for an oblate gyrostat.

The cylindrical solution, however, approximates the numerical results very closely in the early portion of the spinup. There is still the small phase error that occurs at the point were the instantaneous separatrix crossing really does occur. Remember that both solutions are derived from linear systems that approximate the nonlinear governing equations. The total absence of a separatrix in either approximate solution is the cause of the phase error that develops when the approximate solutions attempt to model the governing nonlinear equations. Figures 5.10 through 5.12 illustrate the phase error in the cylindrical solution induced by inaccurate modelling of an instantaneous separatrix crossing. While excellent qualitative results are evident in Figures 5.7 through 5.9, the phase error at the instantaneous separatrix crossing propagates the error in the solution through out the remainder of the spinup.

5.1.3 Transverse Spinup.   Figures 5.13 through 5.15 compare both multiple scales solutions with numerical results for the transverse spinup of a prolate gyrostat. The initial conditions are slightly offset from the stable flat spin equilibrium point.

Figure 5.7. Numerical vs cylindrical and cartesian coordinate approximate solution of the x_1 component of angular momentum of a prolate gyrostat with initial conditions $x_1 = 0.4$, $x_2 = 0.64807$, $x_3 = 0.64807$ and $\epsilon = g = 0.01$
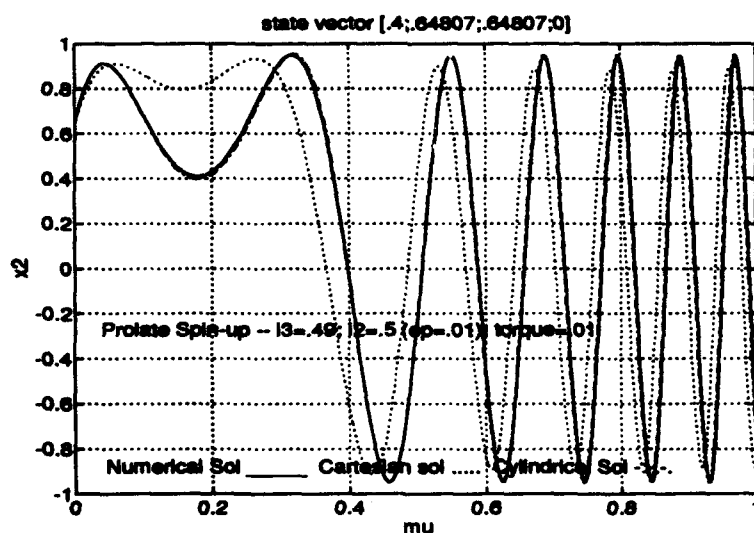

Figure 5.8. Numerical vs cylindrical and cartesian coordinate approximate solution of the x_2 component of angular momentum of a prolate gyrostat with initial conditions $x_1 = 0.4$, $x_2 = 0.64807$, $x_3 = 0.64807$ and $\epsilon = g = 0.01$
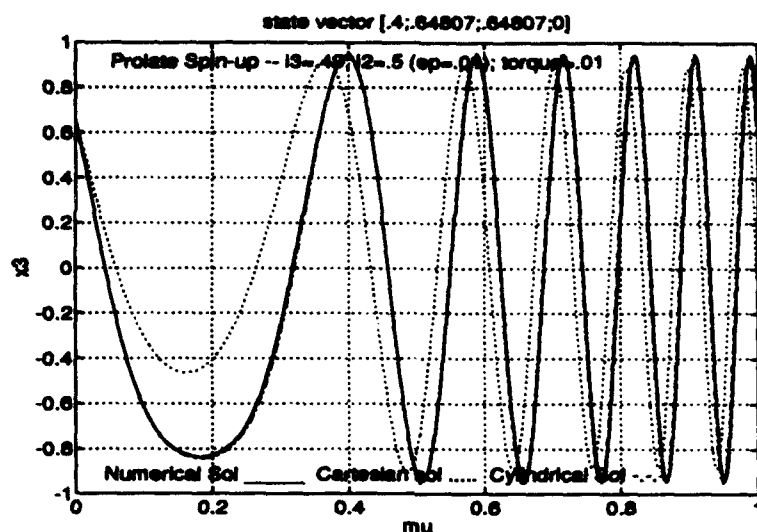
Figure 5.9. Numerical vs cylindrical and cartesian coordinate approximate solution of the x_3 component of angular momentum of a prolate gyrostat with initial conditions $x_1 = 0.4$, $x_2 = 0.64807$, $x_3 = 0.64807$ and $\varepsilon = g = 0.01$
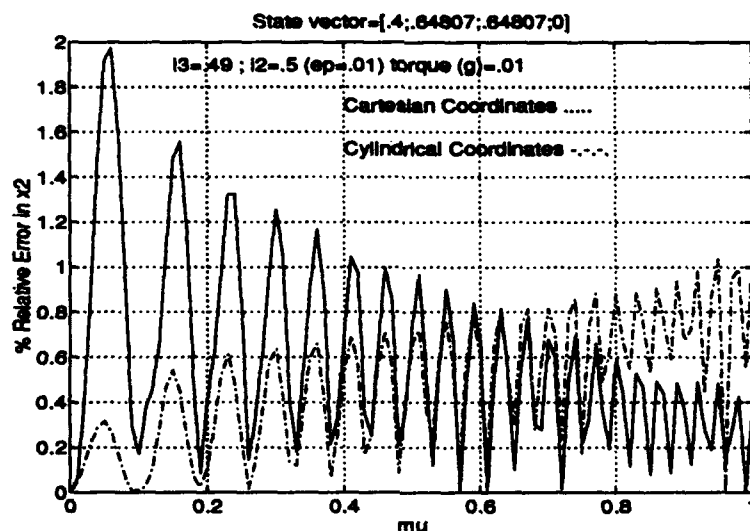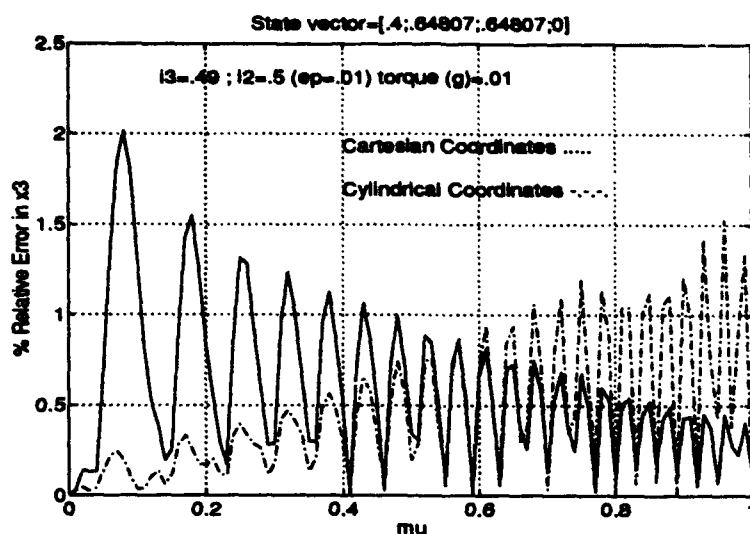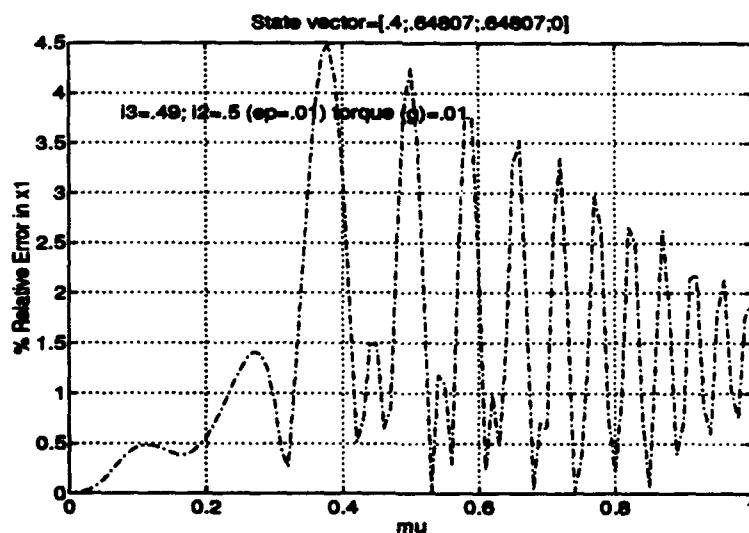

Figure 5.10. Percent relative error of the x_1 component of angular momentum of a prolate gyrostat using cylindrical coordinates with initial conditions $x_1 = 0.7$, $x_2 = 0.4$, $x_3 = 0.59161$ and $\varepsilon = g = 0.01$
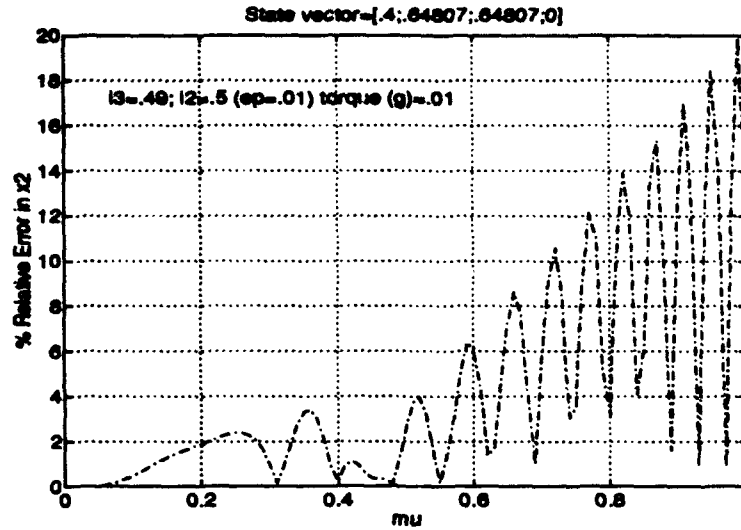
Figure 5.11. Percent relative error of the x_2 component of angular momentum of
a prolate gyrostat using cylindrical coordinates with initial conditions
$x_1 = 0.7$, $x_2 = 0.4$, $x_3 = 0.59161$ and $\epsilon = g = 0.01$
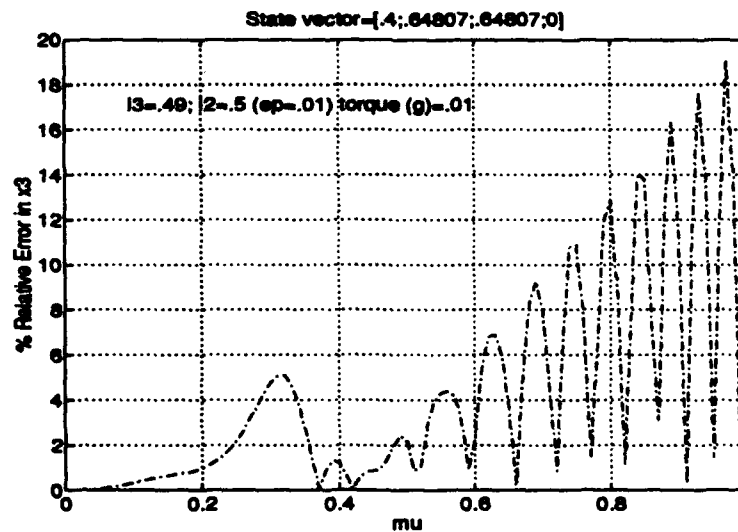
Figure 5.12. Percent relative error of the x_3 component of angular momentum of
a prolate gyrostat using cylindrical coordinates with initial conditions
$x_1 = 0.7$, $x_2 = 0.4$, $x_3 = 0.59161$ and $\epsilon = g = 0.01$
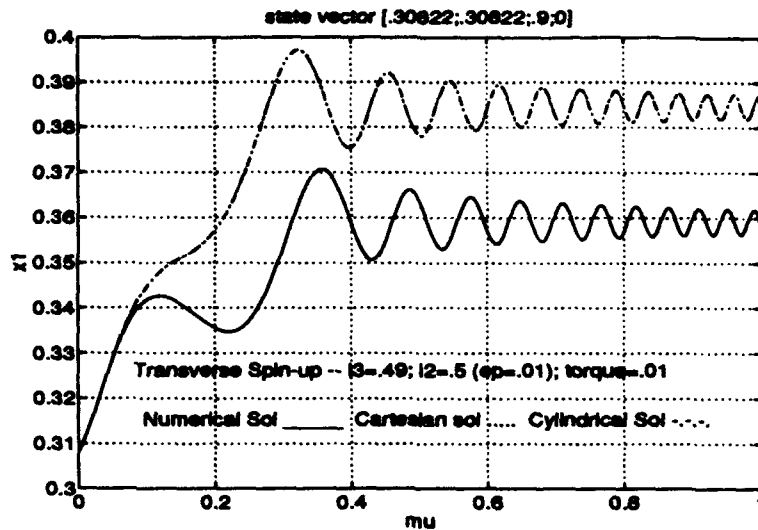
Figure 5.13. Numerical vs cylindrical and cartesian coordinate approximate solution of the x_1 component of angular momentum of a prolate gyrostat during transverse spinup.

The significant increase in accuracy during the early portion of the spinup for the cylindrical solution is evident. The reason for the improved accuracy is the same as seen during prolate spinup. The cylindrical solution is not hampered by a larger error early in the spinup. However, the essential result is the same as in the cartesian solution. Extremely small torque values (which implies extremely small ϵ values) are required to keep the trajectory near the stable flat spin equilibrium point.

5.2 Summary

The cylindrical coordinate multiple scales solution developed by Lt Col Baker provides excellent results. When used to model oblate gyrostats, the approximate solution is much more accurate in the early portion of the spinup maneuver. This is due to the fact that the cylindrical solution is not dependent on the x_{11} approximation that the cartesian solution has. An interesting result, however, is that this same

5-20
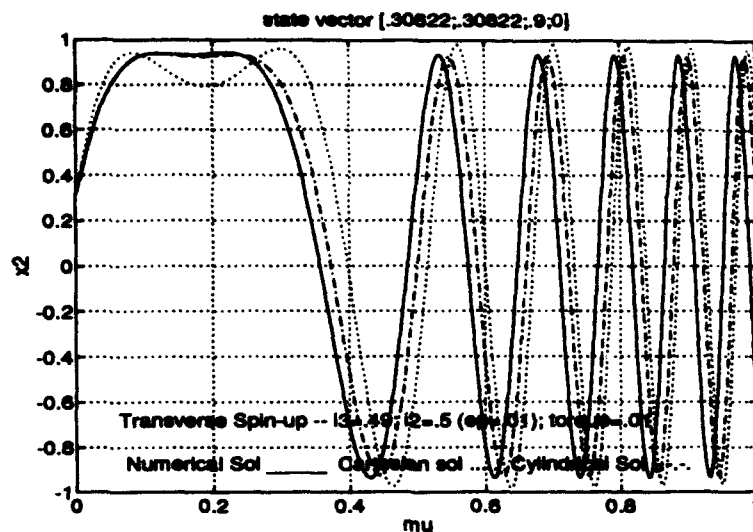
Figure 5.14. Numerical vs cylindrical and cartesian coordinate approximate solution of the x_2 component of angular momentum of a prolate gyrostat during transverse spinup.
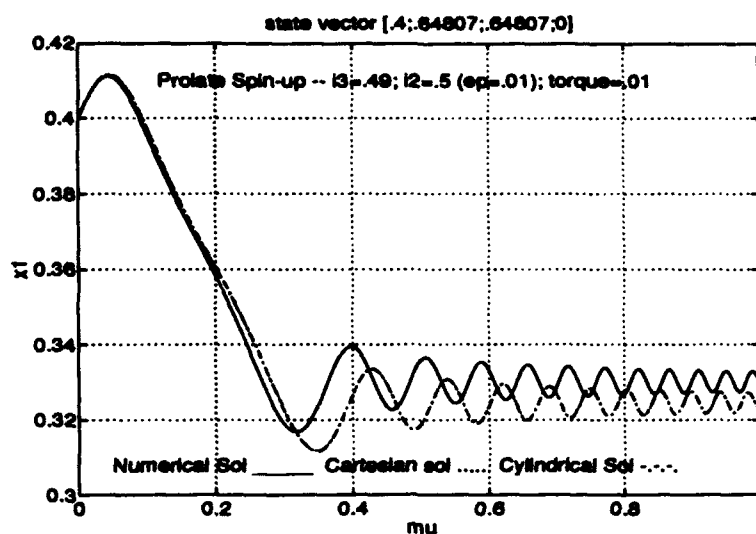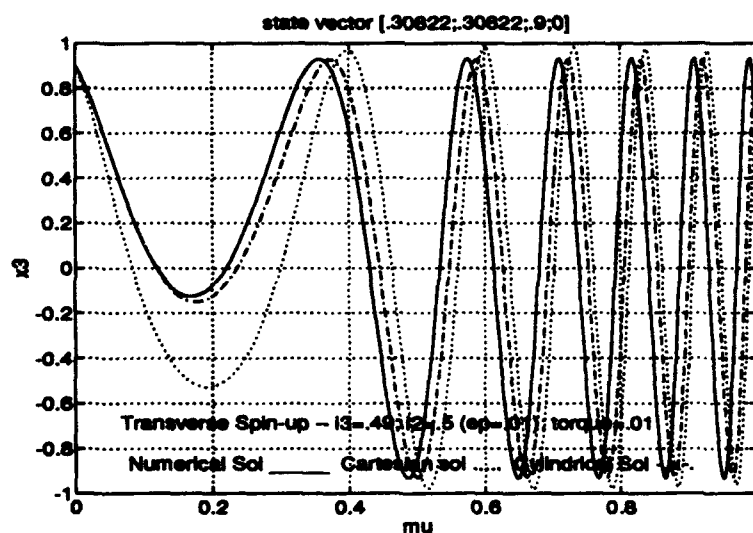

Figure 5.15. Numerical vs cylindrical and cartesian coordinate approximate solution of the x_3 component of angular momentum of a prolate gyrostat during transverse spinup.

x_{11} approximation provides better results for oblate gyrostats in the latter portion of the spinup maneuver.

The cylindrical solution does have superior performance when modelling prolate gyrostats. While the solution is still not able to model an instantaneous separatrix crossing accurately, it does provide excellent qualitative information for the spinup maneuver. Further, we expect that spinup which begins closer to the prolate equilibrium point results in more accurate approximations.

Finally, both the cartesian and cylindrical solutions prove to be inadequate when modelling transverse spinup. The extremely small torque values required render the solution impractical.

VI. Conclusions and Recommendations

6.1 Conclusions

Two approximate solutions for the spinup of a near axisymmetric gyrostat using the method of multiple scales were derived. The difference in transverse inertias was chosen as the small parameter. This selection had the fortunate property of transforming the system of equations that described the spinup from a nonlinear system to a series of linear systems. The first solution, derived from cartesian coordinates, incorporated the use of two different time scales to capture the slowly varying frequency of the system. To derive the solutions, an approximation had to be made for the $\mathcal{O}(\varepsilon)$ term of the x_1 component of angular momentum. This approximation induced a large phase error in the transverse components during the first ten percent of spinup but had the effect of reducing phase error in the last ten percent of spinup. The solution was compared to the results of numerical integration for oblate and prolate configurations. Further, the solution was compared for the flat spin recovery of a prolate gyrostat. Excellent results were obtained for oblate configurations. When we confined our error analysis to the last ten percent of the spinup maneuver, we found less then one percent error in all three components of angular momentum. This result applied to gyrostats with a one percent difference in transverse inertias and initial conditions in the northern half of the momentum sphere.

The results for prolate configurations were hampered by the extremely non-linear nature of prolate spinup trajectories. Because the approximate solution was developed from a series of linear systems, the approximation breaks down in regions where the trajectory is really influenced by the instantaneous separatrices associated with prolate spinup. It was found, however, that if the solution of the numerical integration at a point in time after the last bifurcation on the momentum sphere were used, reasonable results could still be obtained for the remainder of spinup.

6-1

Finally, the transverse spinup of a prolate gyrostat was shown to be completely inadequate. The trajectory for the spinup began near a stable flat spin center and almost immediately crossed an instantaneous separatrix due to an excessively large torque value. Reducing the torque value to an acceptably small value would require a truly axisymmetric gyrostat.

A second multiple scales solution was derived by Lt Col William P. Baker, Associate Professor of Mathematics, United States Air Force Institute of Technology. Lt Col Baker surmised that by transforming the governing equations to cylindrical coordinates, a solution could be derived that did not have such a large phase error early in the spinup maneuver. In its final form, the cylindrical solution did not have an explicit slow time dependence, but did have the slow time dependence show up implicitly in the phase equation. A comparison between the cartesian and cylindrical solutions for oblate gyrostats produced two interesting findings. In the early portion of the spinup, the cylindrical solution proved far superior to the cartesian solution. The reason was that the cylindrical solution was not hampered by any approximations in its derivation. However, in the final portion of the spinup, the cartesian solutions phase correction at $t = \infty$ proved more accurate than the cylindrical solution.

The cylindrical solution was much better at modelling prolate spinup than the cartesian solution. By not having the initial phase error induced by the x_{11} approximation, the cylindrical solution was better at modelling the trajectory as the instantaneous separatrices approached. However, the solution was still not able to accurately model the instantaneous separatrix crossing.

6.2 Recommendations

There are three areas in which further study is warranted.

1). The approximate solutions developed in this thesis were only derived to approximately $\mathcal{O}(\varepsilon)$. The term "approximately" is used because we ignored some of

the constants of integration in both the cartesian and cylindrical solutions. Additionally, the $\mathcal{O}(\epsilon)$ expansion limits the amount of torque that might be applied to the system. If more accurate, or much smaller torque values are desired, the system of equations must be extended to $\mathcal{O}(\epsilon^2)$. This will require either an analytic or approximate solution to the following integrals.

$$\int S_o(\sigma) \cos \sigma d\sigma$$
$$\int C_o(\sigma) \sin \sigma d\sigma$$

2). For prolate configurations, the actual trajectories lie in regions of the momentum sphere influenced by instantaneous separatrices. If the initial conditions start fairly close to the prolate equilibrium point, the trajectory encounters smaller phase error at the separatrix crossing. A matched asymptotic expansion might be able to correct the approximate solution in this region.

3). The approximate solution derived in this thesis is for a near axisymmetric gyrostat. Analysis of the solutions indicated that reasonable results could be achieved for a gyrostat with a two percent difference in transverse inertias. In order to expand the range of asymmetry further, an alternate technique will have to be used on the nonlinear system of equations.

Appendix A. Straightforward Expansion Method Solution Terms

The following terms are to be used in Eqs. 3.32 and 3.33 for the approximate solution using the straightforward expansion method. Overbracketed terms are secular.

$$
\begin{aligned}
a1 \;=\;& \frac{1}{\sqrt{g}}\alpha\,\sqrt{\frac{\pi}{8}}x_{10}x_2\cos\left(\frac{k^2}{g}\right)\cos\left(f\right) \\[2mm]
&-\;\frac{1}{g^{3/2}}\alpha\,i_3k\sqrt{\frac{\pi}{8}}x_2^2 x_3\cos\left(\frac{k^2}{g}\right)\cos\left(f\right) \\[2mm]
&-\;\frac{1}{\sqrt{g}}\alpha\,i_3\sqrt{\frac{\pi}{8}}x_2^2 x_3\cos\left(\frac{k^2}{g}\right)\cos\left(f\right) \\[2mm]
&+\;\frac{1}{g^{3/2}}\alpha\,i_3k\sqrt{\frac{\pi}{8}}x_3^3\cos\left(\frac{k^2}{g}\right)\cos\left(f\right) \\[2mm]
&+\;\overbrace{\frac{1}{\sqrt{g}}\alpha\,i_3\sqrt{\frac{\pi}{8}}t x_3^3\cos\left(\frac{k^2}{g}\right)\cos\left(f\right)} \\[2mm]
&+\;\frac{1}{\sqrt{g}}\alpha\,\sqrt{\frac{\pi}{8}}x_{10}x_3\cos\left(f\right)\sin\left(\frac{k^2}{g}\right) \\[2mm]
&-\;\frac{2}{g^{3/2}}\alpha\,i_3k\sqrt{\frac{\pi}{8}}x_2 x_3^2\cos\left(f\right)\sin\left(\frac{k^2}{g}\right) \\[2mm]
&-\;\overbrace{\frac{2}{\sqrt{g}}\alpha\,i_3\sqrt{\frac{\pi}{8}}t x_2 x_3^2\cos\left(f\right)\sin\left(\frac{k^2}{g}\right)} \\[2mm]
&-\;\frac{1}{g^{3/2}}\alpha\,i_3k\sqrt{\frac{\pi}{8}}x_2^3\cos\left(\frac{k^2}{g}\right)\sin\left(f\right) \\[2mm]
&-\;\overbrace{\frac{1}{\sqrt{g}}\alpha\,i_3\sqrt{\frac{\pi}{8}}t x_2^3\cos\left(\frac{k^2}{g}\right)\sin\left(f\right)} \\[2mm]
&+\;\frac{1}{\sqrt{g}}\alpha\,\sqrt{\frac{\pi}{8}}x_{10}x_3\cos\left(\frac{k^2}{g}\right)\sin\left(f\right) \\[2mm]
&+\;\frac{1}{g^{3/2}}\alpha\,i_3k\sqrt{\frac{\pi}{8}}x_2 x_3^2\cos\left(\frac{k^2}{g}\right)\sin\left(f\right) \\[2mm]
&+\;\overbrace{\frac{1}{\sqrt{g}}\alpha\,i_3\sqrt{\frac{\pi}{8}}t x_2 x_3^2\cos\left(\frac{k^2}{g}\right)\sin\left(f\right)}
\end{aligned}
$$

$$- \frac{1}{\sqrt{g}}\alpha \sqrt{\frac{\pi}{8}}x_{10}x_2 \sin\left(\frac{k^2}{g}\right)\sin(f)$$

$$- \frac{2}{g^{3/2}}\alpha \, i_3 k\sqrt{\frac{\pi}{8}}x_2^2 x_3 \sin\left(\frac{k^2}{g}\right)\sin(f)$$

$$- \overline{\frac{2}{\sqrt{g}}\alpha \, i_3\sqrt{\frac{\pi}{8}}t x_2^2 x_3 \sin\left(\frac{k^2}{g}\right)\sin(f)} \qquad\qquad \text{(A.1)}$$

$$
\begin{aligned}
a2 \;=\; & \frac{1}{\sqrt{g}}\alpha \sqrt{\frac{\pi}{8}}x_{10}x_3 \cos\left(\frac{k^2}{g}\right)\cos(f) \\[1mm]
& - \frac{2}{g^{3/2}}\alpha \, i_3 k\sqrt{\frac{\pi}{8}}x_2 x_3^2 \cos\left(\frac{k^2}{g}\right)\cos(f) \\[1mm]
& - \overline{\frac{2}{\sqrt{g}}\alpha \, i_3\sqrt{\frac{\pi}{8}}t x_2 x_3^2 \cos\left(\frac{k^2}{g}\right)\cos(f)} \\[1mm]
& - \frac{1}{\sqrt{g}}\alpha \sqrt{\frac{\pi}{8}}x_{10}x_2 \cos(f)\sin\left(\frac{k^2}{g}\right) \\[1mm]
& + \frac{1}{g^{3/2}}\alpha \, i_3 k\sqrt{\frac{\pi}{8}}x_2^2 x_3 \cos(f)\sin\left(\frac{k^2}{g}\right) \\[1mm]
& + \overline{\frac{1}{\sqrt{g}}\alpha \, i_3\sqrt{\frac{\pi}{8}}t x_2^2 x_3 \cos(f)\sin\left(\frac{k^2}{g}\right)} \\[1mm]
& - \frac{1}{g^{3/2}}\alpha \, i_3 k\sqrt{\frac{\pi}{8}}x_3^3 \cos(f)\sin\left(\frac{k^2}{g}\right) \\[1mm]
& - \overline{\frac{1}{\sqrt{g}}\alpha \, i_3\sqrt{\frac{\pi}{8}}t x_3^3 \cos(f)\sin\left(\frac{k^2}{g}\right)} \\[1mm]
& - \frac{1}{\sqrt{g}}\alpha \sqrt{\frac{\pi}{8}}x_{10}x_2 \cos\left(\frac{k^2}{g}\right)\sin(f) \\[1mm]
& - \frac{2}{g^{3/2}}\alpha \, i_3 k\sqrt{\frac{\pi}{8}}x_2^2 x_3 \cos\left(\frac{k^2}{g}\right)\sin(f) \\[1mm]
& - \overline{\frac{2}{\sqrt{g}}\alpha \, i_3\sqrt{\frac{\pi}{8}}t x_2^2 x_3 \cos\left(\frac{k^2}{g}\right)\sin(f)} \\[1mm]
& + \frac{1}{g^{3/2}}\alpha \, i_3 k\sqrt{\frac{\pi}{8}}x_2^3 \sin\left(\frac{k^2}{g}\right)\sin(f)
\end{aligned}
$$

$$+ \; \frac{1}{\sqrt{g}}\alpha\; i_3\sqrt{\frac{\pi}{8}}tx_2^3\sin\left(\frac{k^2}{g}\right)\sin\left(f\right)$$

$$- \; \frac{1}{\sqrt{g}}\alpha\; \sqrt{\frac{\pi}{8}}x_{10}x_3\sin\left(\frac{k^2}{g}\right)\sin\left(f\right)$$

$$- \; \frac{1}{g^{3/2}}\alpha\; i_3k\sqrt{\frac{\pi}{8}}x_2x_3^2\sin\left(\frac{k^2}{g}\right)\sin\left(f\right)$$

$$- \; \frac{1}{\sqrt{g}}\alpha\; i_3\sqrt{\frac{\pi}{8}}tx_2x_3^2\sin\left(\frac{k^2}{g}\right)\sin\left(f\right) \qquad (A.2)$$

$$
\begin{aligned}
a3 \;=\; & -\frac{1}{\sqrt{g}}\alpha\;\sqrt{\frac{\pi}{8}}x_{10}x_2\cos\left(\frac{k^2}{g}\right)\cos\left(f\right) \\
& +\frac{1}{g^{3/2}}\alpha\; i_3k\sqrt{\frac{\pi}{8}}x_2^2x_3\cos\left(\frac{k^2}{g}\right)\cos\left(f\right) \\
& -\frac{1}{g^{3/2}}\alpha\; i_3k\sqrt{\frac{\pi}{8}}x_3^3\cos\left(\frac{k^2}{g}\right)\cos\left(f\right) \\
& -\frac{1}{\sqrt{g}}\alpha\;\sqrt{\frac{\pi}{8}}x_{10}x_3\cos\left(f\right)\sin\left(\frac{k^2}{g}\right) \\
& +\frac{2}{g^{3/2}}\alpha\; i_3k\sqrt{\frac{\pi}{8}}x_2x_3^2\cos\left(f\right)\sin\left(\frac{k^2}{g}\right) \\
& +\frac{1}{\sqrt{g}}\alpha\; i_3\sqrt{\frac{\pi}{8}}tx_3\cos\left(f\right)\times \\
& \quad \left[x_2^2\cos\left(\frac{k^2}{g}\right)-x_3^2\cos\left(\frac{k^2}{g}\right)+2x_2x_3\sin\left(\frac{k^2}{g}\right)\right] \\
& +\frac{1}{g^{3/2}}\alpha\; i_3k\sqrt{\frac{\pi}{8}}x_2^3\cos\left(\frac{k^2}{g}\right)\sin\left(f\right) \\
& -\frac{1}{\sqrt{g}}\alpha\;\sqrt{\frac{\pi}{8}}x_{10}x_3\cos\left(\frac{k^2}{g}\right)\sin\left(f\right) \\
& -\frac{1}{g^{3/2}}\alpha\; i_3k\sqrt{\frac{\pi}{8}}x_2x_3^2\cos\left(\frac{k^2}{g}\right)\sin\left(f\right) \\
& +\frac{1}{\sqrt{g}}\alpha\;\sqrt{\frac{\pi}{8}}x_{10}x_2\sin\left(\frac{k^2}{g}\right)\sin\left(f\right) \\
& +\frac{2}{g^{3/2}}\alpha\; i_3k\sqrt{\frac{\pi}{8}}x_2^2x_3\sin\left(\frac{k^2}{g}\right)\sin\left(f\right)
\end{aligned}
$$

$$- \overbrace{\frac{1}{\sqrt{g}}\alpha\, i_3\sqrt{\frac{\pi}{8}}tx_2} \times$$

$$\left[-\left(x_2^2\cos\left(\frac{k^2}{g}\right)\right) + x_3^2\cos\left(\frac{k^2}{g}\right) - 2x_2x_3\sin\left(\frac{k^2}{g}\right)\right]\sin(f) \qquad \text{(A.3)}$$

$$
\begin{aligned}
a4 \;=\;& -\frac{1}{\sqrt{g}}\alpha\,\sqrt{\frac{\pi}{8}}x_{10}x_3\cos\left(\frac{k^2}{g}\right)\cos(f)\\[4pt]
&+ \frac{2}{g^{3/2}}\alpha\, i_3k\sqrt{\frac{\pi}{8}}x_2x_3^2\cos\left(\frac{k^2}{g}\right)\cos(f)\\[4pt]
&+ \frac{1}{\sqrt{g}}\alpha\,\sqrt{\frac{\pi}{8}}x_{10}x_2\cos(f)\sin\left(\frac{k^2}{g}\right)\\[4pt]
&- \frac{1}{g^{3/2}}\alpha\, i_3k\sqrt{\frac{\pi}{8}}x_2^2x_3\cos(f)\sin\left(\frac{k^2}{g}\right)\\[4pt]
&+ \frac{1}{g^{3/2}}\alpha\, i_3k\sqrt{\frac{\pi}{8}}x_3^3\cos(f)\sin\left(\frac{k^2}{g}\right)\\[4pt]
&+ \overbrace{\frac{1}{\sqrt{g}}\alpha\, i_3\sqrt{\frac{\pi}{8}}tx_3\cos(f)} \times\\[4pt]
&\quad \left[2x_2x_3\cos\left(\frac{k^2}{g}\right) - x_2^2\sin\left(\frac{k^2}{g}\right) + x_3^2\sin\left(\frac{k^2}{g}\right)\right]\\[4pt]
&+ \frac{1}{\sqrt{g}}\alpha\,\sqrt{\frac{\pi}{8}}x_{10}x_2\cos\left(\frac{k^2}{g}\right)\sin(f)\\[4pt]
&+ \frac{2}{g^{3/2}}\alpha\, i_3k\sqrt{\frac{\pi}{8}}x_2^2x_3\cos\left(\frac{k^2}{g}\right)\sin(f)\\[4pt]
&- \frac{1}{g^{3/2}}\alpha\, i_3k\sqrt{\frac{\pi}{8}}x_2^3\sin\left(\frac{k^2}{g}\right)\sin(f)\\[4pt]
&+ \frac{1}{\sqrt{g}}\alpha\,\sqrt{\frac{\pi}{8}}x_{10}x_3\sin\left(\frac{k^2}{g}\right)\sin(f)\\[4pt]
&+ \frac{1}{g^{3/2}}\alpha\, i_3k\sqrt{\frac{\pi}{8}}x_2x_3^2\sin\left(\frac{k^2}{g}\right)\sin(f)\\[4pt]
&- \overbrace{\frac{1}{\sqrt{g}}\alpha\, i_3\sqrt{\frac{\pi}{8}}tx_2} \times\\[4pt]
&\quad \left[-2x_2x_3\cos\left(\frac{k^2}{g}\right) + x_2^2\sin\left(\frac{k^2}{g}\right) - x_3^2\sin\left(\frac{k^2}{g}\right)\right]\sin(f) \qquad \text{(A.4)}
\end{aligned}
$$

$$
\begin{aligned}
b1 \;=\; & \frac{1}{g^{3/2}}\alpha\; i_3 k\sqrt{\frac{\pi}{8}}\, x_2^3 \cos\!\left(\frac{k^2}{g}\right)\cos\left(f\right) \\[4pt]
+\; & \frac{1}{\sqrt{g}}\alpha\; i3\sqrt{\frac{\pi}{8}}\, t x_2^3 \cos\!\left(\frac{k^2}{g}\right)\cos\left(f\right) \\[4pt]
-\; & \frac{1}{\sqrt{g}}\alpha\; \sqrt{\frac{\pi}{8}}\, x_{10} x_3 \cos\!\left(\frac{k^2}{g}\right)\cos\left(f\right) \\[4pt]
-\; & \frac{1}{g^{3/2}}\alpha\; i_3 k\sqrt{\frac{\pi}{8}}\, x_2 x_3^2 \cos\!\left(\frac{k^2}{g}\right)\cos\left(f\right) \\[4pt]
-\; & \frac{1}{\sqrt{g}}\alpha\; i3\sqrt{\frac{\pi}{8}}\, t x_2 x_3^2 \cos\!\left(\frac{k^2}{g}\right)\cos\left(f\right) \\[4pt]
+\; & \frac{1}{\sqrt{g}}\alpha\; \sqrt{\frac{\pi}{8}}\, x_{10} x_2 \cos\left(f\right)\sin\!\left(\frac{k^2}{g}\right) \\[4pt]
+\; & \frac{2}{g^{3/2}}\alpha\; i_3 k\sqrt{\frac{\pi}{8}}\, x_2^2 x_3 \cos\left(f\right)\sin\!\left(\frac{k^2}{g}\right) \\[4pt]
+\; & \frac{2}{\sqrt{g}}\alpha\; i3\sqrt{\frac{\pi}{8}}\, t x_2^2 x_3 \cos\left(f\right)\sin\!\left(\frac{k^2}{g}\right) \\[4pt]
+\; & \frac{1}{\sqrt{g}}\alpha\; \sqrt{\frac{\pi}{8}}\, x_{10} x_2 \cos\!\left(\frac{k^2}{g}\right)\sin\left(f\right) \\[4pt]
-\; & \frac{1}{g^{3/2}}\alpha\; i_3 k\sqrt{\frac{\pi}{8}}\, x_2^2 x_3 \cos\!\left(\frac{k^2}{g}\right)\sin\left(f\right) \\[4pt]
-\; & \frac{1}{\sqrt{g}}\alpha\; i3\sqrt{\frac{\pi}{8}}\, t x_2^2 x_3 \cos\!\left(\frac{k^2}{g}\right)\sin\left(f\right) \\[4pt]
+\; & \frac{1}{g^{3/2}}\alpha\; i_3 k\sqrt{\frac{\pi}{8}}\, x_3^3 \cos\!\left(\frac{k^2}{g}\right)\sin\left(f\right) \\[4pt]
+\; & \frac{1}{\sqrt{g}}\alpha\; i3\sqrt{\frac{\pi}{8}}\, t x_3^3 \cos\!\left(\frac{k^2}{g}\right)\sin\left(f\right) \\[4pt]
+\; & \frac{1}{\sqrt{g}}\alpha\; \sqrt{\frac{\pi}{8}}\, x_{10} x_3 \sin\!\left(\frac{k^2}{g}\right)\sin\left(f\right) \\[4pt]
-\; & \frac{2}{g^{3/2}}\alpha\; i_3 k\sqrt{\frac{\pi}{8}}\, x_2 x_3^2 \sin\!\left(\frac{k^2}{g}\right)\sin\left(f\right) \\[4pt]
-\; & \frac{2}{\sqrt{g}}\alpha\; i3\sqrt{\frac{\pi}{8}}\, t x_2 x_3^2 \sin\!\left(\frac{k^2}{g}\right)\sin\left(f\right)
\end{aligned}
\tag{A.5}
$$

$$
\begin{aligned}
b2 \;=\;& \frac{1}{\sqrt{g}}\alpha\,\sqrt{\frac{\pi}{8}}x_{10}x_2\cos\left(\frac{k^2}{g}\right)\cos\left(f\right) \\[2mm]
&+\;\frac{2}{g^{3/2}}\alpha\,i_3 k\sqrt{\frac{\pi}{8}}x_2^2 x_3\cos\left(\frac{k^2}{g}\right)\cos\left(f\right) \\[2mm]
&+\;\overbrace{\frac{2}{\sqrt{g}}\alpha\,i3\sqrt{\frac{\pi}{8}}t x_2^2 x_3\cos\left(\frac{k^2}{g}\right)\cos\left(f\right)} \\[2mm]
&-\;\frac{1}{g^{3/2}}\alpha\,i_3 k\sqrt{\frac{\pi}{8}}x_2^3\cos\left(f\right)\sin\left(\frac{k^2}{g}\right) \\[2mm]
&-\;\overbrace{\frac{1}{\sqrt{g}}\alpha\,i3\sqrt{\frac{\pi}{8}}t x_2^3\cos\left(f\right)\sin\left(\frac{k^2}{g}\right)} \\[2mm]
&+\;\frac{1}{\sqrt{g}}\alpha\,\sqrt{\frac{\pi}{8}}x_{10}x_3\cos\left(f\right)\sin\left(\frac{k^2}{g}\right) \\[2mm]
&+\;\frac{1}{g^{3/2}}\alpha\,i_3 k\sqrt{\frac{\pi}{8}}x_2 x_3^2\cos\left(f\right)\sin\left(\frac{k^2}{g}\right) \\[2mm]
&+\;\overbrace{\frac{1}{\sqrt{g}}\alpha\,i3\sqrt{\frac{\pi}{8}}t x_2 x_3^2\cos\left(f\right)\sin\left(\frac{k^2}{g}\right)} \\[2mm]
&+\;\frac{1}{\sqrt{g}}\alpha\,\sqrt{\frac{\pi}{8}}x_{10}x_3\cos\left(\frac{k^2}{g}\right)\sin\left(f\right) \\[2mm]
&-\;\frac{2}{g^{3/2}}\alpha\,i_3 k\sqrt{\frac{\pi}{8}}x_2 x_3^2\cos\left(\frac{k^2}{g}\right)\sin\left(f\right) \\[2mm]
&-\;\overbrace{\frac{2}{\sqrt{g}}\alpha\,i3\sqrt{\frac{\pi}{8}}t x_2 x_3^2\cos\left(\frac{k^2}{g}\right)\sin\left(f\right)} \\[2mm]
&-\;\frac{1}{\sqrt{g}}\alpha\,\sqrt{\frac{\pi}{8}}x_{10}x_2\sin\left(\frac{k^2}{g}\right)\sin\left(f\right) \\[2mm]
&+\;\frac{1}{g^{3/2}}\alpha\,i_3 k\sqrt{\frac{\pi}{8}}x_2^2 x_3\sin\left(\frac{k^2}{g}\right)\sin\left(f\right) \\[2mm]
&+\;\overbrace{\frac{1}{\sqrt{g}}\alpha\,i3\sqrt{\frac{\pi}{8}}t x_2^2 x_3\sin\left(\frac{k^2}{g}\right)\sin\left(f\right)} \\[2mm]
&-\;\frac{1}{g^{3/2}}\alpha\,i_3 k\sqrt{\frac{\pi}{8}}x_3^3\sin\left(\frac{k^2}{g}\right)\sin\left(f\right) \\[2mm]
&-\;\overbrace{\frac{1}{\sqrt{g}}\alpha\,i3\sqrt{\frac{\pi}{8}}t x_3^3\sin\left(\frac{k^2}{g}\right)\sin\left(f\right)}
\end{aligned}
\tag{A.6}
$$

$$b3 = -\frac{1}{g^{3/2}}\alpha\, i_3 k\sqrt{\frac{\pi}{8}}x_2^3\cos\left(\frac{k^2}{g}\right)\cos\left(f\right)$$

$$+\ \frac{1}{\sqrt{g}}\alpha\,\sqrt{\frac{\pi}{8}}x_{10}x_3\cos\left(\frac{k^2}{g}\right)\cos\left(f\right)$$

$$+\ \frac{1}{g^{3/2}}\alpha\, i_3 k\sqrt{\frac{\pi}{8}}x_2 x_3^2\cos\left(\frac{k^2}{g}\right)\cos\left(f\right)$$

$$-\ \frac{1}{\sqrt{g}}\alpha\,\sqrt{\frac{\pi}{8}}x_{10}x_2\cos\left(f\right)\sin\left(\frac{k^2}{g}\right)$$

$$-\ \frac{2}{g^{3/2}}\alpha\, i_3 k\sqrt{\frac{\pi}{8}}x_2^2 x_3\cos\left(f\right)\sin\left(\frac{k^2}{g}\right)$$

$$+\ \overbrace{\frac{1}{\sqrt{g}}\alpha\, i3\sqrt{\frac{\pi}{8}}tx_2\cos\left(f\right)}\times$$

$$\left[-x_2^2\cos\left(\frac{k^2}{g}\right)+x_3^2\cos\left(\frac{k^2}{g}\right)-2x_2 x_3\sin\left(\frac{k^2}{g}\right)\right]$$

$$-\ \frac{1}{\sqrt{g}}\alpha\,\sqrt{\frac{\pi}{8}}x_{10}x_2\cos\left(\frac{k^2}{g}\right)\sin\left(f\right)$$

$$+\ \frac{1}{g^{3/2}}\alpha\, i_3 k\sqrt{\frac{\pi}{8}}x_2^2 x_3\cos\left(\frac{k^2}{g}\right)\sin\left(f\right)$$

$$-\ \frac{1}{g^{3/2}}\alpha\, i_3 k\sqrt{\frac{\pi}{8}}x_3^3\cos\left(\frac{k^2}{g}\right)\sin\left(f\right)$$

$$-\ \frac{1}{\sqrt{g}}\alpha\,\sqrt{\frac{\pi}{8}}x_{10}x_3\sin\left(\frac{k^2}{g}\right)\sin\left(f\right)$$

$$+\ \frac{2}{g^{3/2}}\alpha\, i_3 k\sqrt{\frac{\pi}{8}}x_2 x_3^2\sin\left(\frac{k^2}{g}\right)\sin\left(f\right)$$

$$+\ \overbrace{\alpha\, i3\sqrt{\frac{\pi}{8}}tx_3}\times$$

$$\left[x_2^2\cos\left(\frac{k^2}{g}\right)-x_3^2\cos\left(\frac{k^2}{g}\right)+2x_2 x_3\sin\left(\frac{k^2}{g}\right)\right]\sin\left(f\right)\qquad\text{(A.7)}$$

$$b4 = -\frac{1}{\sqrt{g}}\alpha\,\sqrt{\frac{\pi}{8}}x_{10}x_2\cos\left(\frac{k^2}{g}\right)\cos\left(f\right)$$

$$- \frac{2}{g^{3/2}} \alpha\ i_3 k \sqrt{\frac{\pi}{8}} x_2^2 x_3 \cos\left(\frac{k^2}{g}\right) \cos\left(f\right)$$

$$+ \frac{1}{g^{3/2}} \alpha\ i_3 k \sqrt{\frac{\pi}{8}} x_2^3 \cos\left(f\right) \sin\left(\frac{k^2}{g}\right)$$

$$- \frac{1}{\sqrt{g}} \alpha\ \sqrt{\frac{\pi}{8}} x_{10} x_3 \cos\left(f\right) \sin\left(\frac{k^2}{g}\right)$$

$$- \frac{1}{g^{3/2}} \alpha\ i_3 k \sqrt{\frac{\pi}{8}} x_2 x_3^2 \cos\left(f\right) \sin\left(\frac{k^2}{g}\right)$$

$$+ \overbrace{\frac{1}{\sqrt{g}} \alpha\ i 3 \sqrt{\frac{\pi}{8}} t x_2 \cos\left(f\right)} \times$$

$$\left[-2 x_2 x_3 \cos\left(\frac{k^2}{g}\right) + x_2^2 \sin\left(\frac{k^2}{g}\right) - x_3^2 \sin\left(\frac{k^2}{g}\right) \right]$$

$$- \frac{1}{\sqrt{g}} \alpha\ \sqrt{\frac{\pi}{8}} x_{10} x_3 \cos\left(\frac{k^2}{g}\right) \sin\left(f\right)$$

$$+ \frac{2}{g^{3/2}} \alpha\ i_3 k \sqrt{\frac{\pi}{8}} x_2 x_3^2 \cos\left(\frac{k^2}{g}\right) \sin\left(f\right)$$

$$+ \frac{1}{\sqrt{g}} \alpha\ \sqrt{\frac{\pi}{8}} x_{10} x_2 \sin\left(\frac{k^2}{g}\right) \sin\left(f\right)$$

$$- \frac{1}{g^{3/2}} \alpha\ i_3 k \sqrt{\frac{\pi}{8}} x_2^2 x_3 \sin\left(\frac{k^2}{g}\right) \sin\left(f\right)$$

$$+ \frac{1}{g^{3/i}} \alpha\ i_3 k \sqrt{\frac{\pi}{8}} x 3^3 \sin\left(\frac{k^2}{g}\right) \sin\left(f\right)$$

$$+ \overbrace{\frac{1}{\sqrt{g}} \alpha\ i 3 \sqrt{\frac{\pi}{8}} t x_3} \times$$

$$\left[2 x_2 x_3 \cos\left(\frac{k^2}{g}\right) - x_2^2 \sin\left(\frac{k^2}{g}\right) + x_3^2 \sin\left(\frac{k^2}{g}\right) \right] \sin\left(f\right) \qquad (A.8)$$

Appendix B. Fresnel Function Integrals

The majority of equations derived in this thesis were obtained using the symbolic manipulation program, *Mathematica 2.0* for SPARC by Wolfram Research Inc. (15). This program was able to solve some of the integrals that involved the Fresnel Sine and Fresnel Cosine functions. However, in the cylindrical coordinate derivation, the program was not able to solve many of the equations and so they were solved by Lt Col William P. Baker, Associate Professor of Mathematics, United States Air Force Institute of Technology. These derivations are included here in full as a reference.

We begin with the basic definition of Fresnel Sine (S) and Fresnel Cosine (C) functions (1:300)

$$C(x) = \int_0^x \cos\left(\pi \frac{t^2}{2}\right) dt$$

$$S(x) = \int_0^x \sin\left(\pi \frac{t^2}{2}\right) dt$$

1) The first integral is a slightly more complex cosine function.

$$\int_0^t \cos\left(g\sigma^2 + 2k\sigma\right) d\sigma = \int_0^t \cos\left[\left(\sqrt{g}\sigma + \frac{k}{g}\right)^2 - \frac{k^2}{g}\right] d\sigma$$

Using a simple trigonometric identity

$$= \int_0^t \left\{\cos\left[\left(\sqrt{g}\sigma + \frac{k}{g}\right)^2\right]\cos\frac{k^2}{g} + \sin\left[\left(\sqrt{g}\sigma + \frac{k}{g}\right)^2\right]\sin\frac{k^2}{g}\right\} d\sigma$$

We now employ a change of variables. Let

$$\nu = \sqrt{\frac{2}{\pi g}}(g\sigma + k)$$

$$d\nu = \sqrt{\frac{2}{\pi g}}g \, d\sigma$$

The resulting integral is

$$= \int_{\sqrt{\frac{2}{\pi g}}k}^{\sqrt{\frac{2}{\pi g}}(gt+k)} \left[\cos\left(\frac{\pi}{2}\nu^2\right) \cos\frac{k^2}{g} + \sin\left(\frac{\pi}{2}\nu^2\right) \sin\frac{k^2}{g} \right] \sqrt{\frac{\pi}{2g}}\, d\nu$$

which has the solution

$$= \sqrt{\frac{\pi}{2g}} \left[C(\nu)\cos\frac{k^2}{g} + S(\nu)\sin\frac{k^2}{g} \right] \Bigg|_{\sqrt{\frac{2}{\pi g}}k}^{\sqrt{\frac{2}{\pi g}}(gt+k)} \qquad (B.1)$$

Using a similar process we find that

$$\int_0^t \sin\left(g\sigma^2 + 2k\sigma\right) d\sigma = \sqrt{\frac{\pi}{2g}} \left[S(\nu)\cos\frac{k^2}{g} - C(\nu)\sin\frac{k^2}{g} \right] \Bigg|_{\sqrt{\frac{2}{\pi g}}k}^{\sqrt{\frac{2}{\pi g}}(gt+k)} \qquad (B.2)$$

2) The second integral is the product of a Fresnel cosine and a cosine function.

$$\int_0^t C_o\left(f(\sigma)\right) \cos f(\sigma)\, d\sigma \qquad (B.3)$$

As in Chapter 5, we define the following terms

$$C_o(f) = \int_0^t \cos f\, dt$$

$$S_o(f) = \int_0^t \sin f\, dt$$

where

$$f = gt^2 + 2kt + \theta_0 \qquad (B.4)$$

Note:

$$\frac{d}{dt} S_o(f) = \sin f(t)$$

$$\frac{d}{dt} C_o(f) = \cos f(t)$$

To solve the integral we employ the integration by parts technique. let

$$u = C_o(f(t))$$

$$du = \cos f(t)dt$$

$$\implies \int_0^t u\,du = \frac{1}{2}u^2\Big|_0^t = \frac{1}{2}\left[C_o\left(f(t)\right)\right]^2 \qquad (B.5)$$

Using a similar process we find

$$\int_0^t S_o(f(\sigma))\sin f(\sigma)d\sigma = \frac{1}{2}\left[S_o\left(f(t)\right)\right]^2 \qquad (B.6)$$

3) The third integral is a complicated Fresnel cosine function.

$$\int_0^t C_o\left(g\sigma^2 + 2k\sigma\right)d\sigma$$

Using the definition of a Fresnel cosine we have

$$= \int_0^t \int_0^t \cos\left(g\sigma^2 + 2k\sigma\right)d\sigma ds$$

Changing the order of integration results in

$$= \int_0^t \int_\sigma^t \cos\left(g\sigma^2 + 2k\sigma\right)ds\,d\sigma$$

$$= \int_0^t (t-\sigma)\cos\left(g\sigma^2 + 2k\sigma\right)d\sigma$$

Now we add and subtract the same term

$$= t\int_0^t \cos\left(g\sigma^2 + 2k\sigma\right)d\sigma - \frac{1}{2g}\int_0^t (2g\sigma + 2k)\cos\left(g\sigma^2 + 2k\sigma\right)d\sigma$$

$$+ \frac{2k}{2g}\int_0^t \cos\left(g\sigma^2 + 2k\sigma\right)d\sigma$$

The resulting solution is

$$= tC_o\left(gt^2 + 2kt\right) - \frac{1}{2g}\sin\left(gt^2 + 2kt\right) + \frac{k}{g}C_o\left(gt^2 + 2kt\right) \qquad (B.7)$$

Using a similar process we find

$$\int_0^t S_o\left(g\sigma^2 + 2k\sigma\right)d\sigma = tS_o\left(gt^2 + 2kt\right) + \frac{1}{2g}\left[\cos\left(gt^2 + 2kt\right) - 1\right] + \frac{k}{g}S_o\left(gt^2 + 2kt\right)$$
$$(B.8)$$

4) The fourth integral involves the product of the function and the variable of integration.

$$\int_0^t \sigma\cos\left(f(\sigma)\right)d\sigma = \int_0^t \sigma\cos\left(g\sigma^2 + 2k\sigma + \theta_0\right)d\sigma \qquad (B.9)$$

Again, we add and subtract the same term

$$= \frac{1}{2g}\int_0^t (2g\sigma + 2k)\cos\left(g\sigma^2 + 2k\sigma + \theta_0\right)d\sigma$$
$$- \frac{k}{g}\int_0^t \cos\left(g\sigma^2 + 2k\sigma + \theta_0\right)d\sigma$$

The solution to the integral is

$$= \frac{1}{2g}\left[\sin f(t) - \sin\theta_0\right] - \frac{k}{g}C_o\left(f(t)\right) \qquad (B.10)$$

Using a similar process we find

$$\int_0^t \sigma\sin\left(f(\sigma)\right)d\sigma = -\frac{1}{2g}\left[\cos f(t) - \cos\theta_0\right] - \frac{k}{g}S_o\left(f(t)\right) \qquad (B.11)$$

5) The fifth integral is the cosine function squared.

$$\int_0^t \cos^2 f\, d\sigma = \frac{1}{2}\int_0^t \left[1 + \cos 2f\right]d\sigma$$
$$= \frac{t}{2} + \frac{1}{2}C_o(2f) \qquad (B.12)$$

6) The sixth integral is the product of the variable of integration, a Fresnel sine function and a cosine function.

$$\int_0^t \left[(2g\sigma + 2k)\, S_o(f) \cos f \right] d\sigma$$

We employ the integration by parts technique. Let

$$
\begin{aligned}
u &= S_o(f) \\
dv &= (2g\sigma + 2k)\, d\sigma
\end{aligned}
$$

This results in

$$= S_o(f) \sin f \big|_0^t - \int_0^t \sin^2 f \, d\sigma$$

Using a trigonometric relation, we have the solution

$$= S_o(f) \sin f - \frac{1}{2} t + \frac{1}{2} C_o(2f) \tag{B.13}$$

Bibliography

1. Abramowitz, Milto and Irene A. Stegun. *Handbook of Mathematical Functions with Formulas, Graphs, and Mathematical Tables*. Washington D.C.: National Bureau of Standards, Applied Mathematical Series, Ninth Printing, 1970.

2. Beaty, James Ross. *Perturbation Solutions of the Equations of Motion for a Class of Dual-Spin Spacecraft*. PhD dissertation. The Ohio State University, Columbus Ohio, 1986.

3. Gebman, Jean R. and D. Lewis Mingori. "Perturbation Solution for the Flat Spin Recovery of a Dual-Spin Spacecraft," *AIAA Journal*, 14:859-867 (July 1976).

4. Guelman, M. "On Gyrostat Dynamics and Recovery". *Journal of the Astronautical Sciences*, XXXVII(2):109-119, Apr-Jun 1989.

5. Hall, Christopher D. *An Investigation of Spinup Dynamics of Axial Gyrostats Using Elliptic Integrals and the Method of Averaging*. PhD dissertation. Cornell University, Ithaca, NY, January 1992.

6. Hall, Christopher D. and Richard H. Rand. "Spinup Dynamics of Axial Dual-Spin Spacecraft," *Astrodynamics 91*, Vol76, *Advances in the Astronautical Sciences*, Univelt Inc., San Diego, CA 1992, pp. 641-660.

7. Kailath, Thomas. *Linear Systems*. Englewood Cliffs, N.J.: Prentice-Hall, Inc., 1980.

8. Kinney, David L. *An Approximate Solution for the Linearized Spinup Dynamics of a Dual-Spin Spacecraft*, MS Thesis, AFIT/GA/ENY/92D-11. School of Engineering, Air Force Institute of Technology (AU), Wright-Patterson AFB OH, December 1992 (AD-A258903).

9. Likens, P.W. "Spacecraft Attitude Dynamics and Control - A Personal Perspective on Early Developments", *Journal of Guidance, Control and Dynamics*, Vol 9, No. 2, pp. 129-134, March - April, 1986.

10. *Pro-Matlab (Trademark): User's Guide*, The MathWorks, Inc., Version 4.0a, 1992.

11. Nayfeh, Ali Hasan. *Perturbation Methods*. New York: John Wiley & Sons Inc., 1973.

12. Nayfeh, Ali Hasan. *Introduction to Perturbation Techniques*. New York. John Wiley & Sons Inc., 1981.

13. S. Sen and P.M. Bainum. "The Motion and Stability of a Dual-Spin Satellite During the Momentum Wheel spin-up Maneuver". *Journal of Spacecraft and Rockets*, 10(12):760-766, Dec 1973.

14. William E. Wiesel, *Space Flight Dynamics*, McGraw-Hill, New York, 1989.

15. Stephan Wolfram. *Mathematica: A System for Doing Mathematics by Computer*. Addison-Wesley, Reading, MA, second edition, 1991.

Vita

Stewart J. Kowall was born on 29 October 1960 at Bitburg AB West Germany. After moving extensively with his parents, he was finally able to settle down in Glendale Arizona to complete high school. His Air Force career began in 1979 when he entered the Air Force Academy. After Graduation in 1983, then Lt Kowall attended Undergraduate Navigator Training at Mather AFB CA. Capt Kowall flew two tours in the back seat of a McDonald Douglas F-4E at both Tageu AB S.Korea and Seymour Johnson AFB NC before entering pilot training at Laughlin AFB TX in 1988. Capt Kowalls' next assignment took him and his family to Soesterberg AB The Netherlands flying the McDonald Douglas F-15C. After completion of that tour, Capt Kowall entered the Air Force Institute of Technology in pursuit of his Masters Degree in Astronautical Engineering. Capt Kowall is married to the former Janet Ahrens and they have two wonderful sons, Nathan and Nicholas.

Permanent address: 9032 N 48th Ave
Glendale AZ 85302

REPORT DOCUMENTATION PAGE

Form Approved
OMB No. 0704-0188

Public reporting burden for this collection of information is estimated to average 1 hour per response, including the time for reviewing instructions, searching existing data sources, gathering and maintaining the data needed, and completing and reviewing the collection of information. Send comments regarding this burden estimate or any other aspect of this collection of information, including suggestions for reducing this burden, to Washington Headquarters Services, Directorate for Information Operations and Reports, 1215 Jefferson Davis Highway, Suite 1204, Arlington, VA 22202-4302, and to the Office of Management and Budget, Paperwork Reduction Project (0704-0188), Washington, DC 20503.

1. AGENCY USE ONLY (Leave blank)	2. REPORT DATE	3. REPORT TYPE AND DATES COVERED
	December 1993	Master's Thesis

4. TITLE AND SUBTITLE AN APPROXIMATE SOLUTION FOR THE SPINUP DYNAMICS OF NEAR AXISYMMETRIC AXIAL GYROSTATS USING THE METHOD OF MULTIPLE SCALES

5. FUNDING NUMBERS

6. AUTHOR(S)

Stewart J. Kowall

7. PERFORMING ORGANIZATION NAME(S) AND ADDRESS(ES)

Air Force Institute of Technology, WPAFB OH 45433-6583

8. PERFORMING ORGANIZATION REPORT NUMBER

AFIT/GA/ENY/93D-5

9. SPONSORING/MONITORING AGENCY NAME(S) AND ADDRESS(ES)

Dr. Arje Nachman
AFOSR/NM
Bolling AFB DC 20332-6448

10. SPONSORING/MONITORING AGENCY REPORT NUMBER

11. SUPPLEMENTARY NOTES

12a. DISTRIBUTION/AVAILABILITY STATEMENT

Approved for public release; distribution unlimited

12b. DISTRIBUTION CODE

13. ABSTRACT (Maximum 200 words)

Approximate solutions for the spinup of a near axisymmetric gyrostat are derived using the straightforward expansion method and the method of multiple scales. Two method of multiple scale solutions are presented. The first is derived using cartesian coordinates while the second is derived using cylindrical coordinates. The multiple scales solutions are compared to numerically integrated results for oblate and prolate configurations. A comparison for flat spin recovery is also accomplished. Excellent results are obtained for oblate configurations. Trajectory separatrix crossings hindered the results for prolate configurations and flat spin recoveries.

14. SUBJECT TERMS
Spacecraft, Dynamics, Approximation (Mathematics), Multiple Scales, Fresnel Integrals, Dual-spin Spacecraft

15. NUMBER OF PAGES 124

16. PRICE CODE

17. SECURITY CLASSIFICATION OF REPORT	18. SECURITY CLASSIFICATION OF THIS PAGE	19. SECURITY CLASSIFICATION OF ABSTRACT	20. LIMITATION OF ABSTRACT
Unclassified	Unclassified	Unclassified	UL

NSN 7540-01-280-5500

Standard Form 298 (Rev 2-89)
Prescribed by ANSI Std 239-18
298-102